


1. Report No. FHWA-RD-79-32		2. Government Accession No. PB80124621 	
4. Title and Subtitle High Resolution Sensing Techniques for Slope Stability Studies		5. Report Date January 1979	
		6. Performing Organization Code	
7. Author(s) R. L. Jesch, R. B. Johnson, D. R. Belsher, A. D. Yaghjian, M. C. Steppe and R. W. Fleming		8. Performing Organization Report No.	
9. Performing Organization Name and Address U.S. Department of Commerce National Bureau of Standards Electromagnetic Fields Division Boulder, Colorado 80302		10. Work Unit No. (TRAIS) FCP 34E2-142	
		11. Contract or Grant No. FHWA-7-3-0001	
12. Sponsoring Agency Name and Address U.S. Department of Transportation Federal Highway Administration Office of Research Washington, D.C. 20590		13. Type of Report and Period Covered Final Report Oct. 1976-Sept. 1978	
		14. Sponsoring Agency Code M/0532	
15. Supplementary Notes FHWA Contract Manager: James F. Koca, HRS-21			
16. Abstract The National Bureau of Standards (NBS), in conjunction with the U.S. Geological Survey (USGS), conducted a four-phase evaluation of high resolution remote sensing techniques for application to problems of determining slope stability. The first two phases, for which the USGS was chiefly responsible, concentrated on documenting the subsurface features and associated characteristics which determine or influence slope stability. In phase three, the NBS surveyed a variety of electromagnetic and acoustic remote sensing techniques which exhibited the greatest potential for detecting the subsurface features and characteristics and which satisfied the Federal Highway Administration (FHWA) conditions of availability, practicality and portability. Two techniques were chosen for further experimental and developmental pursuit: the existing FM-CW radar system, and the planar near-field reconstruction (PNFR) approach, respectively. In phase four, the existing FM-CW radar system was applied and analysed in a series of field experiments to determine the subsurface structure at a designated test site in the Pike National Forest south of Denver, Colorado. Local and regional subsurface conditions for the test site were mapped and a detailed geologic section of the site was produced from core samples taken from four boreholes drilled into the subsurface granite. The FM-CW system, which has displayed considerable success in the past for locating near-surface anomalies, accurately revealed a joint at a depth of 6.5 meters which was confirmed by the core data. The PNFR technique, which is still in the development stage at NBS and is based on an effective utilization of the exact holographic or near-field equations, was also pursued to the point of running computer simulated experiments. Preliminary results for the detection of small subsurface anomalies by the PNFR technique have been highly encouraging.			
17. Key Words Electromagnetic probing; high resolution sensing techniques; subsurface feature determination; radar soil measurements; void detection; subsurface profiling; geologic features; dielectric constant.		18. Distribution Statement No restrictions. This document is available to the public through the National Technical Information Service, Springfield, Virginia 22161	
19. Security Classif. (of this report) UNCLASSIFIED	20. Security Classif. (of this page) UNCLASSIFIED	21. No. of Pages 142	22. Price \$707.50

PREFACE

This final report on High Resolution Sensing Techniques for Slope Stability Studies terminates a 2-year investigation funded by the U. S. Department of Transportation, Federal Highway Administration, under Federal Highway Administration Order No. 7-3-001. The contract was awarded to the Electromagnetic Fields Division of the National Bureau of Standards for initiation on October 1, 1976. The U. S. Geological Survey has been a subcontractor to the National Bureau of Standards for the performance of geological tasks related to the investigation.

Ramon L. Jesch of the NBS served as project leader for this program. For the NBS, the work reported herein was performed by Ramon L. Jesch, Donald R. Belsher, Arthur D. Yaghjian, and Robert H. McLaughlin. Robert B. Johnson served as project chief for the USGS. For the USGS, the work reported herein was performed by Robert B. Johnson, Michael C. Steppe, and Robert W. Fleming. Laboratory personnel from both the National Bureau of Standards and the Geological Survey have performed some of the electrical and physical testing samples. USGS personnel obtained the core samples in the study. The U. S. Bureau of Reclamation was contracted to run the borehole television of the drill holes. The U. S. Forest Service provided access and permitted drilling at the field site.

The NBS thanks other staff members who contributed in one way or another to this report: Doyle A. Ellerbruch for helpful discussions on measurement techniques and data analysis, Wilbur J. Anson who was instrumental in obtaining and putting together the library of research and reference articles, and the Word Processing Center for providing the typing services.

TABLE OF CONTENTS

	Page
1. INTRODUCTION	1
2. FEATURE DETERMINATION	3
2.1 Background	3
2.2 Geologic Factors that Influence Slope Stability	3
2.3 Slope Stability Analysis and Required Input Data	10
3. CHARACTERISTIC DETERMINATION	17
3.1 Background	17
3.2 Summary of Parameter Measurements from the Literature	17
4. TECHNIQUE DOCUMENTATION	27
4.1 Background	27
4.2 Measurable Characteristics	27
4.3 Applicable Sensing Techniques	28
4.4 The Planar Near-Field Reconstruction (PNFR) Approach to High-Resolution Remote Sensing of Subsurface Anomalies	31
4.4.1 Introduction and Comparison with Alternative Techniques	31
4.4.1.1 A Comparison of PNFR with Holographic, Side-Looking Radar and Computer Aided Tomographic Techniques	34
A. Holographic Techniques	35
B. Side-Looking Radar	37
C. Computer-Aided Tomographic (CAT) Techniques	38
4.4.2 Mathematical Formulation for the PNFR	40
4.4.2.1 Description of the Subsurface Model	40
4.4.2.2 The Plane-Wave Spectrum Representation	42
4.4.3 Some Practical Considerations	45
A. Size of Scan Area	45
B. Horizontal and Vertical Resolution	45

	Page
C. Data Point Spacing Determined by Sampling Theorem	48
D. Sampling Theorem Applied to the Computation of Subsurface Fields	48
E. Application of the Fast Fourier Transform (FFT) Algorithm	49
F. Planarity of Scan Area	49
4.4.4 Preliminary Computer Simulated Results	50
4.4.4.1 Possibilities for Enhancing Vertical Resolution	53
5. TECHNIQUE ANALYSIS	55
5.1 Background	55
5.2 Site Selection	55
5.2.1 Site Documentation	61
5.2.1.1 Mapping of Joints in the Project Area	61
5.2.2 Technical Description of Rock Cores	66
5.2.3 Seismic Refraction Survey Analysis of the Drill Hole Site	70
5.2.4 Borehole TV	72
5.3 FM-CW Technique	72
5.4 Experimental Results	77
5.4.1 Field Tests by NBS	77
5.4.1.1 Evaluation of the FM-CW System	77
5.4.1.2 Experimental Results from the Field Test Site	78
6. CONCLUSIONS	86
7. RECOMMENDATIONS	86
8. REFERENCES	88
APPENDIX	106

LIST OF FIGURES

	Page	
Figure 1	Conceptual View Showing Subsurface Anomalies	1
Figure 2	Schematic of Point Scatterer Buried a Distance "d" Below the Surface of the Earth	41
Figure 3	Simple Method for Estimating Resolution Limits	46
Figure 4	Hypothetical Problem of Point Dipole Scatterer	51
Figure 5	Amplitude of Electric Field	52
Figure 6	Location Map	57
Figure 7	Photo of Weathered Granite Near Site 2	58
Figure 8	Rough Map of Drill Hole Locations Site 2	59
Figure 9	Photo of Granite Blocks Showing High-Angle and Exfoliation Joints	60
Figure 10	Testing the FM-CW System	62
Figure 11	Joint Sampling Sites	63
Figure 12	Joint Histograms	64
Figure 13	Joint Rosettes	65
Figure 14	Contoured Pole Plots for Joint Data	67
Figure 15	Photo of Recirculating Tank	71
Figure 16	Model of Ray Paths for a Two Layer Material	73
Figure 17	Block Diagram of the FM-CW Measurement System	76
Figure 18	Small Broadband Rectangular Aperture-Horns Radiating into Granite Boulder	79
Figure 19	Large Broadband Rectangular Aperture-Horns Radiating into Granite Boulder	80
Figure 20	Photo of Drill Holes 1, 2, and 3 on Site 2	81

	Page	
Figure 21	Test Setup of FM-CW System on Site 2	82
Figure 22	FM-CW System on Site 2	83
Figure 23	Actual Subsurface Feature Responses as Detected by the FM-CW System from the Surface at Site 2	85
Figure 24	Plot of Relative Dielectric Constant as a Function of Frequency	107
Figure 25	Graphic Log of Borehole 1	108
Figure 26	Graphic Log of Borehole 2	109
Figure 27	Graphic Log of Borehole 3	110
Figure 28	Graphic Log of Borehole 4	111
Figure 29	Plot of Unconfined Compressive Strength and Young's Modulus	118
Figure 30	Plot of Unconfined Compressive Strength and Compressional Velocity for 10 Samples	119
Figure 31	Plot of All Compressional Strength and Compressional Velocity Data	121
Figure 32	Plot of Young's Modulus and Compressional Velocity	122
Figure 33	Plot of Young's Modulus and Shear Velocity	123
Figure 34	Plot of Compressional Velocity and Shear Velocity	124
Figure 35	Plot of Unconfined Compressive Strength and Schmidt Rebound Number	125
Figure 36	Plot of Compression Velocity and Schmidt Rebound Number	126

LIST OF TABLES

	Page	
Table 1	Joint Spacings and Lengths for Multiple Sets in Two Rock Masses at Auburn Dam, California	18
Table 2	Ranges in Spacing, Continuity, and Aperture for Three Rock Types in Arizona	19
Table 3	Average Lengths, Spacings, Areas, and Sample Sizes at De Beers Mine, South Africa	19
Table 4	Spacing Data for Rock Types, County Durham, England	20
Table 5	Aperture Widths for Various Rock Types and Depths	20
Table 6	Dielectric Constants Relative to Frequency	22
Table 7	Physical Properties of Pikes Peak Granite	23
Table 8	Comparison of Resistivity of Landslide Mass and Undisturbed Material, Black Sea Coast of Caucasus and Crimea, USSR	24
Table 9	Influence of Depth on Velocity	25
Table 10	Influence of Landslide Disturbance on Velocity	25
Table 11	Descriptive Terminology for Joint Spacing	68
Table 12	Rock Weathering Classification	68
Table 13	Rock Quality Based on RQD Values	69
Table 14	Static Modulus and Poisson's Ratio	113
Table 15	Determination of Density	114
Table 16	Elastic Moduli Expressed in V_p and V_s	115
Table 17	Selected Sonic, Static, and Dynamic Test Data for 10 Test Samples	117
Table 18	Selected Test Data for All Samples	127

		Page
Table 19	Clustered Data Above and Below First Joint	128
Table 20	Tabulation of Selected Data for Zone Above Joint for All Samples	130

1. INTRODUCTION

In response to a request from the Federal Highway Administration (FHWA), the National Bureau of Standards (NBS), in 1976, undertook a program to conduct a study on new and effective approaches to site exploration for slope stability studies. This work was done in conjunction with the United States Geological Survey (USGS) which had the responsibility for identifying and evaluating those geologic features which are pertinent to landslide initiation, and for making test site selection and evaluation.

Landslides have always been a transportation concern. They seem to occur mainly on older roads (more than 10 years old) and on some sections of the Interstate System in difficult terrain. In both situations, the landslide problems can often be traced to a lack of an adequate subsurface exploration program. To date, the availability of applicable sensing techniques for detecting subsurface anomalies (see figure 1) is limited. Most of the existing sensing techniques do not meet requirements necessary to detect slope stability, one of which is to resolve planes ranging in thickness from only about 25 mm to the thickness of the entire mass and its surroundings. Some of the techniques that rely upon taking measurements between boreholes cannot be used in difficult terrain--mainly because of the impracticability of putting down boreholes.

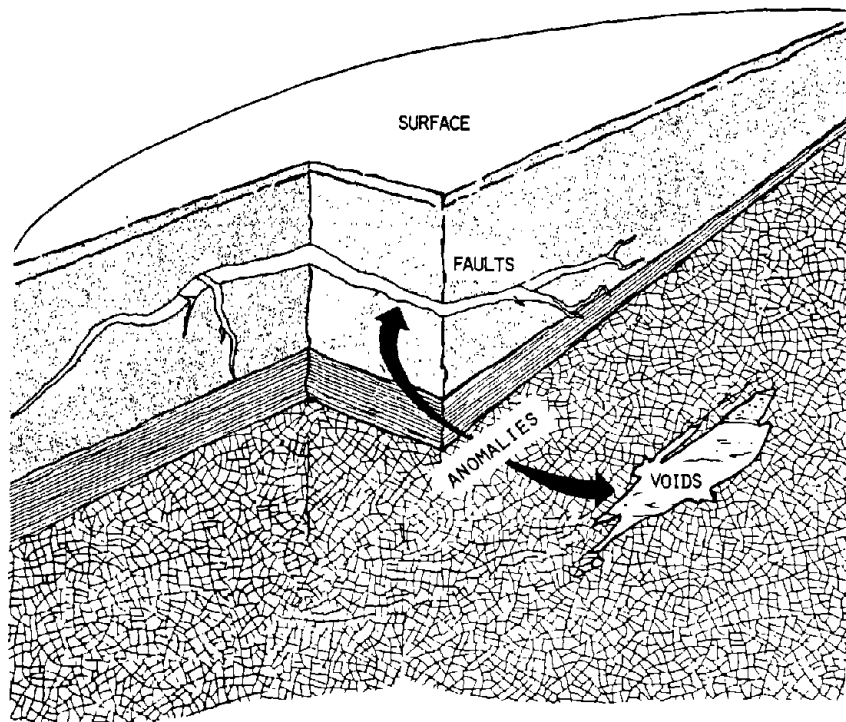


Figure 1. Conceptual view showing subsurface anomalies.

This study investigates the potential of new sensing techniques for subsurface exploration from surface measurements. The objective includes the following specific requirements:

1. To document the types of discontinuities, inhomogeneities, flaws, and boundary conditions relative to the soil/rock fabric which have an influence on the stability of natural and manmade slopes.
2. To document the physical, electrical, chemical, and mechanical characteristics of the features considered in Objective 1 and to relate those characteristics to the surrounding soil/rock mass, emphasizing the range of differences to be expected.
3. To document the capabilities, limitations, and future potential of available techniques for use in the measurement of the characteristics considered in Objective 2.
4. Based on the above documentations, establish the precision and operating ranges of techniques that are feasible for identifying and analyzing different types of discontinuities and inhomogeneities that are important in slope stability problems. This will include laboratory or field evaluation of the techniques to demonstrate the feasibility of using the design or system.

The initial portion of this study is oriented towards identifying and classifying only those features that have potential for detection by high resolution sensing techniques. Major emphasis is finally placed on using existing instruments, equipment, and techniques, especially those that may not have been previously applied to geotechnical studies. However, some promising new techniques and approaches are also evaluated. The experimental phase of the project is limited to one field test to demonstrate a sensing technique suitable for slope stability studies.

To accomplish the requirements, the project was completed in four separate phases designated as follows:

- Phase I - Feature Determination
- Phase II - Characteristic Determination
- Phase III - Technique Documentation
- Phase IV - Technique Analysis

The results of the above phases are documented in sections 2, 3, 4, and 5 respectively in this final report.

2. FEATURE DETERMINATION

2.1 Background

The goal of Phase I was to perform a search of existing methods of slope stability analysis, and to identify those discontinuities that influence slope stability, how they do so, and which lend themselves to mathematical analysis and detection by high resolution sensing techniques.

Traditionally, analysis of slope stability has been divided into empirical and quantitative methods. Systematic use of buried discontinuity data is not made in empirical methods. The quantitative approaches, including the limit equilibrium and stress-strain methods, require such data but a rigorous analysis is prevented by the lack of definitive knowledge concerning the presence, and position and characteristics of potential failure surfaces and subsurface water conditions.

2.2 Geologic Factors That Influence Slope Stability

The geologic factors that influence slope stability include well-defined, anisotropy-producing features such as bedding surfaces, joints, foliation, faults, and slope-failure slip surfaces. The less well-defined anisotropies produced by variations in moisture content, composition, and cementation also were investigated as were surficial factors including slope, slope aspect, and vegetation.

At the onset of this study, emphasis was placed on documenting the more obvious stability-influencing factors such as joints, bedding, and related features that cause a soil or rock mass to be physically discontinuous and anisotropic. This was followed by similar documentation of the influence of the remaining factors listed above. A Phase I interim report (see ref. [176]) titled "Factors that influence the stability of slopes--a literature review" by R. B. Johnson was completed in December 1977.

The information obtained in the early stages of the study has been used to prepare the summary of geologic factors that follows. As a literature review, the interim report contains numerous literature citations and literature-derived illustrations to document the material. These citations and illustrations will not be repeated here for the sake of brevity. The sources of information may be obtained from pertinent sections within the interim report.

Of all of the geologic factors that influence slope stability, the presence of breaks in the physical continuity (discontinuities) of soil and rock was observed to surpass all other factors. While the influence of discontinuities on the stability of soil and rock with soil-like properties has been recognized, failures in soil are not so dependent upon discontinuities because the soil mass is intrinsically weak. By comparison, the stability of a rock mass is more a function of the presence and nature of discontinuities within the mass than of the intact strength of the rock. In addition, it is reasonable to expect that relatively sharp and planar discontinuities may permit more definitive recognition and resolution by geophysical methods than the more diffuse, less planar features.

For these reasons, emphasis was placed on the nature and occurrence of discontinuities present in rock masses. The list of discontinuities occurring in rock is lengthy. It includes joints, bedding, cleavage, foliation, faults, shear zones, failure surfaces, lithologic contacts other than bedding, and unconformities. In the material that follows, the term "joint" will be used as a nongenetic term representative of any of the listed discontinuities. This is in keeping with much of the geotechnical literature and is employed for the sake of simplicity with no attempt to corrupt its genetic geologic meaning or that of any other of the discontinuities.

Regardless of the kind of discontinuity in question, certain measurable parameters are common to all. These are orientation, spacing, continuity, surface roughness, surface separation, and coating or filling material. By identifying and measuring each parameter, the physical characteristics of a discontinuity that influence slope stability will be known without resorting to a classic and perhaps improperly applied geologic name.

Orientation is synonymous with attitude and refers to the position of a joint in three-dimensional space. Orientation is of special importance in the stability of rock slopes. When joints are inclined in the same direction as a natural or cut slope they typically are more susceptible to failure along them than those inclined into a slope or unit. Additionally, joints which are inclined at angles less than that of the slope, intercept or daylight the slope, accentuating the inherent instability. Orientation data consist of dip and strike measurements of the various discontinuities encountered.

Joints occur in sets or groups of subparallel joints in which an average orientation measurement is representative of the set. Sets in turn may intersect giving rise to rock blocks of various geometric form which may be susceptible to downslope movement. An example is the

wedge-failure mode in which joints from two intersecting sets form an intersection which daylights on the slope face.

The spacing, spacing frequency, or intensity of spacing occurrence are synonymous measures of the degree to which a rock mass is subdivided into discrete blocks. Spacing is an important rock-mass strength parameter, especially when combined with multiple intersecting joint sets. Joints seldom are uniformly spaced throughout a rock mass resulting in zones of differing block size and shape.

Discontinuities are themselves discontinuous through a rock mass. Continuity is a measure of this and has been defined as the average length of a discontinuity in a given direction. Thus, it is a two-dimensional measurement of a three-dimensional feature. Continuity greatly affects the stability of a rock slope. A slope with a daylighting joint which is continuous through the rock mass for a considerable distance will be less stable than one where a given joint consists of numerous short sections interrupted by intact rock. Previous failures in a rock mass will have produced continuity along the failure surface which typically supersedes the normally occurring joint lengths within a rock mass. Continuity may interact with spacing. Closely spaced joints may tend to extend the influence of relatively short joints by permitting fracturing across to the adjoining joints propagating the discontinuity to the point where failure may occur in the rock mass.

The roughness of discontinuities, primarily joints, bedding surfaces, and faults (including shear zones), is of considerable importance in providing the frictional resistance to movement along a potential failure surface. For a given orientation and continuity within a rock mass, a smooth surface will be more susceptible to failure than a rough surface. The undulatory or wavy surface (waviness) and finer, projection-caused surface roughness combine to increase the shearing resistance represented by the friction angle. Both result in increased stability. Of the two, roughness is most easily altered by differential movement along a joint, as from faulting. Such movement shears off the small projections, or asperities, causing a reduction in the friction angle, a smoother surface, and reduction in stability. Observation of surface roughness with appropriate measurement of joints oriented in kinematically unstable positions is, therefore, of critical importance.

If some distance separates the adjoining surfaces of a joint (aperture), the influence of waviness and roughness is reduced. Separation also provides for the introduction of surface-coating or space-filling material in the joint. Earlier relative movement of the adjoining blocks may have created the filling material in the form of

gouge, or weathering may have created a clayey filling. In any case, a wide range of stability conditions results. The limiting cases are joint surfaces with no filling in contact with interlocking asperities and widely-spaced surfaces filled with weak material, such as clay, in which the separation distance is greater than the asperity projections. Recognition and mapping of the occurrence of the range of separation and filling conditions, especially along kinematically unstable joints, is of obvious value.

Few rocks are unstable for reasons other than the presence of discontinuities and clay. Some metamorphic rocks have localized low shear strengths from concentrations of talc and mica. The intimate relation of these minerals and their textural orientation within the rock to foliation precludes any consideration of mineralogy as an independent cause of rock-mass failure.

Material or lithologic change present in sections of interbedded high and low shear-strength rock units introduces a form of discontinuity that may be a variation of the bedding surface. However, in such cases failure occurs in the weak unit as well as along contained discontinuities. The most common reference to failure of interbedded rocks involves weak clay-rich rocks, such as shales, in combination with stronger rocks such as siltstone, sandstone, limestone, and dolomite. Interbedded ash or tuff causes similar failures in sections consisting of lava flows.

The critical nature of the foregoing measure of discontinuity characteristics is apparent when the various rock mass quality classifications in use today are examined. In each case, rock-mass quality has been classified so that the strength or stability of a rock mass can be estimated whether the occasion is the construction of a roadcut, tunnel, or open-pit mine. Representative classifications are the Rock Structure Rating (RSR) classification of Wickham, Tiedemann, and Skinner [1], the Council for Scientific and Industrial Research (CSIR) Geomechanics classification of Bieniawski [2], the Norwegian Geotechnical Institute (NGI) classification of Barton, Lien, and Lunde [3], and most recently the description of rock masses for engineering purposes by the Geological Society Engineering Group Working Party (Anonymous, [4]).

The stability of soil masses is dependent primarily on material type and moisture content. An exception is found in the fissured, over-consolidated clays and clay shales. In these materials the presence of the small, slickensided fissures causes mass strength reductions similar to those caused by jointing in rock masses.

Among soils, the presence of clays is a consistent factor among the slopes that are failure susceptible. In general, an increase in clay

content in clay soils and clay shales causes a reduction in shear strength. Variations in strength for a given clay content have been shown to be dependent on the kind of clay or clays present. The presence of swelling clays, typified by montmorillonite, greatly increases the failure susceptibility of a soil in proportion to swelling or nonswelling clay present.

While clays contribute to the low shear strengths of many failure-susceptible soils, noncohesive soils can also have low strength. However, their lack of cohesion makes them susceptible to very thin failures, and they are not typically troublesome. In addition, their good internal drainage reduces the influence that moisture has on soil stability.

Residual soils present unique features that set them apart from transported soils and tend to localize slope failure. These features include lateral and vertical variations in decomposition of parent rock to soil, and relict structures from the preexisting rock. Discontinuities are the controlling factors in nonuniform or localized decomposition of parent rock and the presence of relict structures.

The contact between surficial soils and bedrock provides the necessary material contrast for many slope failures. This too is a variety of discontinuity that includes often considerably different material shear strengths above and below the contact.

Water may interact with material type to influence slope stability or it may act quite independently along a discontinuity. In either case, given near-equilibrium stability conditions in soil and rock slopes, water is an almost universal factor in influencing slope stability. The disturbance in equilibrium may result from loss in shear strength from increased pore pressures in permeable soils, the softening or lubricating of impermeable clays or development of uplift pressures along joints. Additionally, the increased weight from increased moisture content and seepage forces acting in the direction of potential failure upset equilibrium in soil and rock slopes.

From the relationships reviewed above it is not surprising to find that a direct relation exists between landslide activity and rainfall. Rainfall duration and intensity appear to be critical factors. Rainfall influence on stability occurs as it alters moisture content and pore pressures within the material and along discontinuities. Control of water content and related pore pressures is a significant stability maintenance

procedure used in many slide-prone areas. Knowledge of discontinuity orientation, spacing, and continuity may permit evaluation of the intersection of joints and insertion of dewatering drains by drilling or by ditching and tunneling.

The geotechnical literature confirms the obvious conclusion that steep slopes are more unstable than gentle slopes. Moisture content, whether from rainfall or poor drainage, cannot be separated from slope steepness as the two inversely interact. The threshold angle of slope below which failure will not occur is controlled primarily by the shear strength of the slope material with contributions from variables that ultimately relate to moisture content. Regionally, threshold slope angles will correlate with the geographic distribution of different rock types and precipitation amounts and patterns.

Slope aspect or the direction in which a slope faces is complexly related to slope stability. In many areas, those slopes oriented to receive and retain the greatest amount of moisture have the greatest number of failures. The distribution of failure-susceptible materials and the undercutting and resulting steepening of slopes also influence and complicate what appear to be simple relationships.

Vegetation on slopes has been associated with slope stability in preventive as well as causative roles. While not a geologic factor, the interaction of vegetation, slope aspect, and moisture is evident. The ways in which vegetation influences stability include the mechanical reinforcement of slope materials by root systems, the adding of a load to a slope by tree weight and forces transferred from wind stresses on trees, and modification of soil moisture distribution and pore pressure magnitudes.

Loss of vegetative cover from logging practice or overgrazing has been shown to contribute to instability. Decay of root systems following logging reduces the strengthening role of the roots provided by the living trees. Trees also effectively reduce moisture content and pore pressure in comparison with treeless slopes, other factors remaining the same.

The interaction of the various factors that have been referred to in the preceding pages is a pervasive theme in much of the geotechnical literature. The combinations are not consistently the same for many reasons. Among the reasons are the interests of the investigator, the purpose of the investigation, local geologic and topographic conditions, man's activities, climate and vegetation.

Knowledge of local geologic conditions includes having information about rock types and their gross physical properties and local occurrence,

the geologic history of the area. A summary of the geologic history of an area permits estimation of the environments that generated the original rock units and their primary features as well as later tectonic or structural activity that could form predictable joint patterns, differential movements, and metamorphism. Superimposed on this basic crustal data, one needs to know the geomorphic events that have created the topography, released stresses, undercut slopes, and developed transported and residual soils. The next layer of useful information consists of knowledge about seasonal and long-term climatic conditions involving precipitation and temperature data, local vegetation and controls on vegetation distribution, and man's activities over the years.

In conclusion, the results of the Phase I investigation of geologic factors have influenced the direction taken by project investigators in the selection of the type of subsurface feature to be investigated, the choice of method to use, and the set of geologic conditions that were applied to the search for an ideal field site. **As the Phase I work progressed it became evident that there were few features in soil masses sufficiently definitive to permit accurate detection from the surface.** By comparison, the dominant influence of discontinuities on rock-slope stability and the inherent sharpness, planar nature, and spatial orientations of discontinuities, combined to direct research efforts toward the detection of discontinuities.

Discontinuities parallel to the earth's surface were judged to present the fewest problems relating to resolution of return data without the need for dip compensation. Joints were judged to provide the most distinct kind of discontinuity for detection purposes.

Granite was selected as the desired rock type as it would provide relatively good homogeneity in texture and mineralogy between joints. In addition, the joints in granite often are widely spaced, eliminating the potential problem of generating interfering returns from multiple surfaces. Exposed granite typically displays continuous, relatively planar, stress relief joints parallel to the land surface, a condition ideal to the study. A site was located which met this criterion as well as having widely-spaced, high-angle joints leaving a large, uniform, relatively defect-free block intersected at depth by the desired joint. Exposed granite was selected to avoid the change in material physical properties, soil moisture content, and near-surface contact problems that would be present in a soil-covered site. Weathering along the buried joint was expected.

2.3 Slope Stability Analysis and Required Input Data

This section will summarize the state of the art in slope stability analysis, the kinds of site data needed for various analysis methods, and those features which may be measured by remote methods. Although the general concepts of slope stability with respect to movement of a slide mass along a failure or slip surface apply equally to soil and rock masses, there are sufficient differences in mass properties and methods of analysis to justify separate examination.

Basic to the analysis of stability of slopes is the factor of safety concept [5,6,7]. As a generalization, factor of safety is the ratio of the sum of forces resisting failure to the sum of forces that tend to cause failure. Other parameters such as disturbing and restoring moments may be used. A state of equilibrium exists when the ratio is unity. It is assumed that failure is imminent at this value.

The intent of most of the analysis methods for soil slopes is to determine a unique or critical failure surface that produces the lowest factor of safety for a given slope using such site parameters as soil unit weight, water-table height, seepage forces, slope angle, and slope height. Assuming an unfailed slope, the factor of safety should exceed unity. It is assumed further that stability analysis is needed to determine stability conditions following some modification by man or nature of such factors as slope configuration and water table so that potential failure may be avoided. Further assumptions obviously must be made of the two-dimensional geometry of the failure surface, i.e., circular, planar, or some combinations or variations of them. Certain methods are quite restrictive and may require a circular surface, for instance, while others are capable of utilizing a wide range of shapes.

In many cases, uncertainty about stability does not lie in the analysis per se but in the gathering of accurate data concerning subsurface conditions so that the analysis includes potential zones of weakness [8]. Patton and Hendron [9] have cautioned that a circular failure surface should never be considered where the local geology indicates the presence of failure-susceptible discontinuities. They have noted that the shape of relict discontinuities in residual soil may govern the shape of a potential failure surface. Morgenstern [6] considered the factor of safety to act as a factor of ignorance with regard to the reliability of data being used in an analysis. In general, the lower the quality of a site investigation, the higher the design factor of safety needs to be. In addition, the degree of risk relative to the minimum acceptable factor of safety is influenced by the experience of the analyst relative to similar sites. All methods require that some assumptions are made to simplify computation or to conform to the conceptual approach.

Knowledge of the influence of these assumptions on the computed factors of safety for the various methods is an additional factor to be considered [10].

The most widely used stability analysis method for soil slopes involves computation of trial positions and shapes of a potential failure or shear surface. This computation results in a minimum factor of safety for the overlying soil mass. Equilibrium may be calculated with respect to moment or force equilibrium in the mass. The potential slide mass may be treated as a single unit as in the friction-circle method or may be divided into multiple, parallel-sided slices as in the several methods of slices of which six are in common use today. The limit-equilibrium approach as it has developed over the years with emphasis on the various methods of slices has been fully defined [5,6,7,10-22]. Comparisons of the methods based on assumptions made and relative factors of safety given similar site conditions have been prepared [5,15,18,20].

Most limit-equilibrium methods employ a circular failure surface or some modification of it such as a log-spiral curve or composites of curved and planar surfaces based on known subsurface condition. There are representative papers [5,6,11,13,14,17,23,24] dealing with failure or slip surface geometry. Of these, several of the above papers [5,6,23] consider wedge failures which have planar failure surfaces on slopes of assumed infinite height. By comparison, curved failure surfaces are assumed to have slopes of limited height because of their geometry.

Of primary interest to this project is an examination of site parameters required for limit-equilibrium analysis to determine which, if any, can be more accurately measured by the system tested for this study. A composite list of parameters has been prepared from selected papers that list required input to the various methods [7,11-14,17,19,20,24]. They are height of slope, slope angle, bulk density, cohesion, internal angle of friction, pore-water pressure, height of water table, steady-state seepage forces, and estimated geometry of a potential failure surface which is compatible with local subsurface conditions. The analysis methods assume that no failure surface exists. If one does exist then back calculations may be made using a factor of safety equal to unity and post-peak (or residual) cohesion and friction angle values. **Of the factors listed, the improvement that may be expected from this study is an accurate measurement of depth and geometric shape of failure-susceptible subsurface features.** These might take the form of weak clay layers, bedrock surface, or relict discontinuities in residual soil, to cite several possibilities. If failure has occurred previously, the slip-surface discontinuity and any change in physical state such as strain softening in overconsolidated clays or shales might be accurately located and plotted for subsequent stability analyses.

The limit-equilibrium methods of stability analysis are based on factor of safety which describes performance of a slope as being failed or non-failed. The performance of a slope also may be based on analysis of allowable deformation prior to failure. In addition, given both peak and post-peak or residual strength parameters of slope materials, localized zones within a given slope may reach a failure state earlier than others because of slope geometry. Analysis of deformation and locating zones of potential failure may be performed by finite-element analysis using stresses and strains developed in a given slope and adjoining areas [25]. Information concerning the application of finite-element analyses to slope-stability problems is available [25-28]. Wright, Kulhawy, and Duncan [10] have compared such analyses with those performed by the limit equilibrium approach using the methods of slices. Finite-element analyses do not assess the degrees of stability against catastrophic failures as do limit-equilibrium analyses. Results are compared with those of the conventional method of slices for more complete stability evaluation.

In addition to the parameters required for limit-equilibrium analysis, current practice in finite-element analysis requires additional data. These data include peak and post-peak (residual) values of internal friction angle and cohesion, elastic modulus and Poisson's ratio [28]. Duncan and Dunlop [26] have included liquid limit and plastic limit which define material stiffness. In both cases the new data are provided from lab or in situ testing of the materials comprising the slopes under investigation rather than from a geophysical or remotely obtained application. As in the case of the limit equilibrium methods, finite element analyses of slopes would benefit from the accurate measurement of depth and geometry of potential failure-prone surfaces.

The concept that discontinuities in rock masses (bedding surfaces, joints, foliation, etc.) control rock-mass stability so pervades the geotechnical literature that specific references are not needed. The subject of discontinuities has been dealt with in detail in the Phase I Interim Report prepared by the U.S. Geological Survey. It is sufficient here to state that discontinuities in rock are relatively planar features that have measurable orientations in space, differing degrees of continuity along which failure may occur, and friction or surface roughness characteristics that restrict relative block movement.

Discontinuities that are inclined in the same direction as a natural hillslope or which dip into an excavation or cut are of special concern because gravity may move the rock mass along them causing failure. Greatest concern is centered on those discontinuities that intersect, or daylight, a hillslope or cut wall. As a result, rock-mass stability typically deals with potential failure along inclined planes or intersections of multiple planes which daylight naturally or as a result

of construction. Rock masses with very closely spaced discontinuity sets tend to have mass strength characteristics similar to soil masses and are analyzed with the methods discussed earlier [29,30].

As in the analysis of stability of soil slopes, rock slopes may be examined by methods based on limit-equilibrium concepts or by calculation of deformation of the rock mass utilizing stress fields and resulting strains. Because of assumed movement along known planar surfaces, rock-slope stability analyses may include kinematic analyses, i.e., analysis of relative movement of bodies without reference to the forces moving them [31]. Summaries of limit equilibrium and kinematic concepts related to rock slopes may be found in the literature [9,29-34].

Analysis may be directed along several separate paths. These are by the use of physical models, vector analysis, analytical methods, stereographic projections, and finite-element analysis. The first four are limit equilibrium analyses, and the last is a stress analysis. All utilize joint properties such as number and orientation of discontinuities, friction angles along the surfaces and influence of water pressures along the surfaces, as well as volume and bulk density. Finite element analyses and some physical models additionally require rock properties such as shear strength, elastic modulus, Poisson's ratio and measures of rock-mass stiffness, as well as discontinuity spacing. Summaries of these methods have been discussed in the literature [31,35,36].

All methods based on limit equilibrium provide for the calculation of factor of safety as in the analysis of soil slopes. Useful material on factor of safety as it applies to rock slopes is available [9,30,37].

The following parameters [38] are important in obtaining rock-slope factors of safety: orientation of the discontinuities relative to a slope surface, size or continuity, spacing, strength along a surface involving cohesion and friction angle, strength of intact rock if discontinuities are not continuous, and water pressure within the rock slope. The first three have been classed as first-order parameters and the last three as second-order parameters.

The listing above provides insight into the kinds of data required for rock-slope stability analysis. Heuze and Goodman [35] listed the location, orientation, spacing, and character (roughness, for instance) of planar discontinuities as ill-defined site characteristics used as stability analysis input.

Several papers [31,32,39-42] are recommended concerning the use of physical models in stability analysis. Scaling of materials and

discontinuities, and in some cases driving forces (gravity), permits examination in two and three dimensions of critical areas in slopes for various excavation and support designs.

The analysis of slope stability by vector analysis and analytic methods is very similar with vector analysis being a graphical or force diagram solution using the same data employed by the analytic approach. Some variations in terminology exist in the literature. Vector analysis is quite correctly considered [43] to be an analytic method, and the use of stereographic projections to be a graphical approach. Hoek and Bray [30] employ the first-stated terminology. While both techniques are used, the use of force diagrams in conjunction with stereographic projections and the utilizing of the analytical method in solving relatively simple planar failure surface problems are most common.

Hendron, Cording, and Aiyer [43] have provided a comprehensive treatment of the use of vector analysis in slope-stability analysis. A good comparison of the analytic (nongraphical) and vector solutions may be found in **Rock Slope Engineering** by Hoek and Bray [30]. Applications of these similar methods have appeared in other papers [32-34,44-47]. Among the kinds of input data required are discontinuity orientations, block size and weight, uplift water forces, and discontinuity shear strength consisting of cohesion and/or friction angle. Either explicitly or implicitly, the location, orientation, and continuity of discontinuities are of critical importance and are most amenable to determination by the method selected for this study.

The use of stereographic projections [48-51] in stability analysis of rock slopes has grown to the point that it is the most commonly used limit equilibrium method for the solution of three-dimensional stability problems. Very complete and well-illustrated presentations of the basic concepts of stereo net use and stability analysis applications have been published [30,31,43,49,52]. Early stereo-net use dealt only with the kinematics of rock slopes cut by discontinuities with given frictional properties. Later, the use of force or vector diagrams was added to purely stereographic analysis, as stereonets only portray kinematic relations. This permitted the determination of the factor of safety and greatly expanded the utility of the method.

Kinematic applications of stereographic projections appear in the literature [30,51,53-56]. Selected references [31,35,43,49,52,57,58] are listed to describe stability analysis using stereographic projections and vector or force diagrams. Input data for stereographic stability analysis include the orientations of discontinuity planes, surface-slope or cut-slope angle, friction angle for peak and residual strengths along each plane including filling material if applicable, block weight (density and

volume), and water pressures along discontinuities. Dynamic seismic forces and static restraining forces from such items as rock bolts may be included. Daylighted discontinuities and discontinuity intersections with respect to natural or cut slopes are assumed. As in the previous analysis methods, the location, orientation, and continuity of the involved discontinuities are critical to the analysis and in turn are conditions which are detectable by the methods tested during this project. They are among the typically ill-defined quantities involved in rock stability analysis [35]. The more difficult detection and measurement of surface roughness and nature and thickness of filling material have not been assessed to date.

As indicated earlier in the section on stability of soil slopes, finite-element analysis involved examination of the deformation of a slope, which in this case is composed of rock rather than soil. In one of the most comprehensive treatments of the method as applied to rock slope stability, Goodman [31] has noted the method to be an especially powerful tool for cases where rock-type heterogeneity and complex discontinuity conditions preclude the practical use of simpler methods of analysis. He stated that its use is not warranted for many problems typified by wedge failure where the use of stereographic procedures involving limit equilibrium is quite satisfactory. The advantage of the finite-element analysis in more complex geologic situations is that it provides an integrated analysis of natural static conditions, those imposed by man as by excavation or by installation of rock bolts, and dynamic conditions caused by seismic forces [59,60].

The most obvious additional parameter in finite-element analysis in rock masses is the presence of discontinuities. This includes not only the multiple orientations created by bedding, jointing, and foliation, for instance, but also the frequency of spacing in which they occur. These can be modeled by the size and shape of the elements. The geometric factors above, combined with strength and deformation parameters of the rock and associated discontinuities, are all incorporated into the analysis. Selected papers are given [31,35,36,59-63] that provide sufficient details to understand the application of the method to slope-stability analysis, the input data required, and typical results of such analyses. Two- and three-dimensional analyses are treated in these references.

Finite-element analysis involving rock masses requires the greatest amount of input data of all the methods. These include discontinuity orientation and spacing, surface waviness for dilatancy characteristics, discontinuity opening or aperture, compressive and tensile strengths of rock materials, peak and residual shear strengths of discontinuities, initial state of stress in the rock mass and deformation moduli of the

rock such as elastic and shear moduli, and Poisson's ratio. Of these, the location, orientation, and continuity of discontinuities are most likely to be measured by the methods tested in this study. Additionally, it may be possible to obtain information about spacing or frequency of occurrence as the method becomes more refined. The ability of the method to measure waviness along a surface is as yet undetermined.

In summary, of the various parameters which are required for soil-and-rock slope stability analysis, those that are concerned with zones, planes, or intersections of planes along which failure may occur are among the most difficult to assess because they do not lend themselves to laboratory study or direct observations in the field. If there can be any improvement in the three-dimensional location and orientation of these features by new applications of sensing techniques, there would in turn be an improvement in the analysis of stability in soil and rock slopes. These parameters include location, orientation, continuity, spacing or frequency, surface roughness, separation or aperture, and presence and character of filling material of discontinuities. The success of the method chosen and applied in this study in better defining any of these parameters is addressed in a later section of this report.

3. CHARACTERISTIC DETERMINATION

3.1 Background

In this phase, an effort was devoted to determine those physical measures or indicators which are measurable by potential remote sensing techniques as: electromagnetic, seismic and acoustical. Some of the parameters of interest include: elastic moduli, density, resistivity, dielectric constant and moisture content. The expected ranges of values for the various parameters are identified and discussed in the context that differences might be detectable.

3.2. Summary of Parameter Measurements from the Literature

The physical changes that are present across material boundaries in the subsurface provide the opportunity to detect the boundaries, given appropriate measurement systems. This measurement capability is of concern to this project as the boundaries may define surfaces along which slope failure may occur in the future or may have occurred in the past. Remote detection of such surfaces without dependence upon drilling would greatly facilitate the design of relatively failure-free slopes along transportation routes.

Physical changes may range from slip surfaces within a soil mass to discontinuities such as joints within a rock mass. Included within this range are the bedrock-soil interface and a wide variety of discontinuity conditions such as open to clay-filled apertures, tightly closed surfaces, and dissimilar opposing materials.

A search of the literature is not as rewarding as one might hope when attempting to gather data on the many possible conditions that might exist. This is especially true of actual measurements of rock discontinuity such as continuity, surface area, aperture or separation between adjoining blocks, nature of filling material if present, and degrees of surface roughness or waviness. These and other factors are described in detail in the Phase I Interim Report (see ref. [176]). Where data are available, they can serve only as guides as each site is quite unique, relative to quantitative measurements. As an example, the varying depth and degree of weathering in a particular granite exposure superimposes physical changes on a rock type that in itself may have enough compositional and textural variation to be dissimilar from another granite. In addition, variations in moisture content from time to time and even place to place at one site further complicate some of the physical properties that might be measured let alone predicted. Much information appears as averages and ranges of values.

With these problems forming a backdrop, selected data from the literature will be summarized or referenced as appropriate to the subject. The data have been extracted from material which in turn was copied from numerous literature sources during the various Phase I and II tasks. The information is grouped according to discontinuity measurements and physical properties. The latter include elastic moduli, electrical parameters, and seismic velocities.

Joint length (continuity), spacing, and surface area have been reported by several investigators. Heuze and Goodman [35] measured joint length and spacing for multiple joint sets at Auburn Dam, California. Their averaged data for sets from two selected rock masses are reproduced in table 1 to illustrate the variability of such features.

Table 1. Joint Spacings and Lengths for Multiple Sets in Two Rock Masses at Auburn Dam, California (Adapted from Heuze and Goodman, 1972) [35]

	Average joint spacing (mm)		Average joint length (m)	
	<u>Rock mass 1</u>	<u>Rock mass 2</u>	<u>Rock mass 1</u>	<u>Rock mass 2</u>
	488	244	2.44	2.90
	457	274	2.29	1.49
	518	335	1.10	4.57
Rock	518	152	2.29	4.33
joint	274	213	2.13	1.22
sets	488		1.43	
	396		2.90	

Similarly, Mahtab, Bolstad, and Kendorski [64] reported fracture spacing, continuity, and aperture (see section 2.2) in a mine in Arizona for three rock types as shown in table 2. Rock type appears to exert control over all three measurements.

Table 2. Ranges in Spacing, Continuity, and Aperture
for Three Rock Types in Arizona
(Adapted from Mahtab, Bolstad, and Kendorski, 1973) [64]

	Spacing (mm)	Continuity (m)	Aperture (mm)
Quartz monzonite	168-222	0.76-2.13	0.8-2.3
Monzonite prophyry	143-177	0.58-1.10	1.3-1.8
Rhyolite	55-58	0.58-0.64	0.3-0.5

Average joint lengths, spacings, and surface areas for multiple joint sets in several structural rock masses or regions at the De Beers Mine, South Africa have been measured by Robertson [65]. One group of measurements is tabulated in table 3, further documenting the variability of such features. The sample sizes were given by Robertson, and they illustrate the differing degrees of exposure of discontinuities relative to exposed surfaces. Measurements of joint waviness were also made by Robertson. Most fell within a 5°-10° range from a plane surface.

Table 3. Average Lengths, Spacings, Areas, and
Sample Sizes at De Beers Mine, South Africa
(Adapted from Robertson, 1971) [65]

Length (m)	Spacing (m)	Area (m)	Sample size *
0.41	0.31	0.56	241
0.42	0.73	0.58	25
1.35	1.10	5.97	41
0.35	2.44	0.40	8
0.34	0.73	0.38	4
0.41	0.55	0.54	13

* individual joints measured

Mean distributions of joint spacings have been measured and calculated for several sedimentary rock types [66]. All data indicate a negative exponential curve of frequency plotted versus spacing width, indicating the greatest frequency at the smaller spacings. Data for sandstone and mudstone are shown in table 4. Lithologic control over spacing width is indicated.

Table 4. Spacing Data for Rock Types, County Durham, England
(Adapted from Priest and Hudson, 1976) [66]

	Sandstone	Mudstone
Mean spacing (mm)	129	33
Standard dev. (mm)	116	32
Sample size*	249	1828

* individual joints measured

Aperture widths of joints in several rock types have been calculated by Snow [67] from pressure tests. These are of value for the ranges in aperture obtained, as well as documenting the decrease in aperture with increasing depth. Selected average values are reproduced in table 5. Of importance to this project are measured apertures in Pikes Peak granite exposures in the general area of this project's test site. The apertures ranged from 0.12 to 5.4 mm with an average width of 2.00 mm.

Table 5. Aperture Widths for Various Rock Types and Depths
(Adapted from Snow, 1970) [67]

<u>Material</u>	<u>Avg. aperture width (mm)</u>	<u>Depth range (m)</u>
Granite	0.16	2.4-4.3
	0.15	6.1-7.6
Granite gneiss	0.17	0.0-11.6
	0.07	13.1-36.6
Gneiss	0.19	0.0-6.1
	0.14	30.8-62.2
Sandstone and shale	0.23	0.0-4.6
	0.13	15.2-25.0

As seen in the field, failure surfaces exhibit a wide range of thicknesses. Oliveira [68] reported a well-defined slickensided surface in a plastic, organic clay layer. Failure surfaces in a clay-rich glacial till were described [69] to be from several millimeters to 25 mm thick. Reported thicknesses of failure surfaces in clay-rich colluvium range up to 50 mm [70,71]. The failure-prone sensitive clays in Quebec have exhibited surfaces from several millimeters to no more than 25 mm thick [72,73]. The measured thicknesses of failure surfaces in the stiff, fissured clays range from a few microns to several millimeters [74,75]. Similar measured thicknesses in failed glacial lake clays range from sharp interfaces to failure zones up to 1.8 m thick [76].

In rock masses the slip or failure surface may become a zone of failure. Failures in southern California range from paper-thin seams to shear zones "many meters thick" [77]. Shear-zone thicknesses in sedimentary rocks have been measured from several millimeters to about a meter thick [78,79]. The material in the zone is composed of crushed rock material, with composition and size range depending on the rock types involved and the magnitude of the movement. Crushing of the rock will occur to a much greater extent between walls of rough joints or faults than where there are smooth, planar surfaces [80]. A failure zone in schist 100-240 mm thick, consisting of clay, mica, and crushed schist has been reported [81]. The importance of recognizing the presence of crushed or mylonitic zones from earlier failures when examining an area has been emphasized [82]. It is not uncommon to observe the failure zone along or parallel to the bedding or foliation surfaces in sedimentary and metamorphic rocks [77,81,83].

Minerals and rock fragments may exhibit a high degree of orientation in and adjacent to a failure surface. It has been noted [70] that platy claystone and shale fragments are commonly aligned parallel with the failure movement. The same orientation in clay shales has been reported [84]. In a silty clay shear zone, bands have been described [74] of strongly oriented shear material bounding the 15 mm wide shear. The same bounding bands of oriented clay have been optically observed and measured to be 20-30 μm thick [85]. The orientation of clays and micas in a failure zone in schist has been described [81].

Both physical and chemical changes may occur in conjunction with a failure surface or zone. A 25 mm wide zone of softened clay on either side of a slip surface in the London Clay has been described [86]. In association with a failure surface in clay-rich colluvium, water-induced chemical changes have been observed [85] which have oxidized the normally gray clay into several millimeter-thick zones of yellow-brown clay.

The geometry of failure surfaces may be quite complex, even though published generalizations would indicate otherwise [75]. The greatest complexity arises when failures occur in rock masses where they are controlled by discontinuity orientations. "S"-shaped failure surfaces in profile have been described in sedimentary rocks [87,88]. While it is normally assumed that a failure surface is continuous regardless of its geometry, several authors [78,79,89] have described failure surfaces that are multiple discontinuous surfaces. The nature of the material in which failure has occurred may preclude identification of the slip surface. An example is the Parson's Landing slide on Santa Catalina Island off the California coast. The slip surface could not be located in the intimately sheared and foliated rocks of the Franciscan Formation in which the slide had occurred [90].

Masses of data too voluminous to reproduce here are available in the literature concerning elastic modulus, shear modulus, Poisson's ratio, density, porosity, and compressive and tensile strengths. Less numerous, but nevertheless in sizeable quantities, are lists of dielectric constants, longitudinal- and shear-wave velocities, resistivities, friction angles, and cohesion values. Since these data have been available to the research team, only the sources and selected specific data will be listed here because of space. The most comprehensive listing of density, porosity, elastic constants, dielectric constants, resistivities, and seismic velocities for mineral, rock, and soil types worldwide appears in the **Handbook of Physical Constants**, edited by Clark [91]. Dielectric constant data for clayey soil versus granite illustrating the electrical contrasts that may exist across a clay-filled joint are given in table 6 as functions of frequency.

Table 6. Dielectric Constants Relative to Frequency
(Adapted from Clark, 1966) [91]

<u>Material</u>	<u>100Hz</u>	<u>1KHz</u>	<u>10KHz</u>	<u>100KHz</u>	<u>1MHz</u>	<u>10MHz</u>
Clayey soil (dry)	4.72	3.93	3.26	2.79	2.56	2.44
Granite (dry)	9.05	7.78	7.01	6.57	6.22	5.96

In 1956, Wuerker [92] published a literature compilation of specific gravity, porosity, static and dynamic elastic moduli, and seismic velocities for a wide variety of rock types of worldwide occurrence. In a similar, more recent literature compilation, Kulhawy [93] has concentrated more on engineering parameters; namely, density, specific gravity, modulus of elasticity, Poisson's ratio, and compressive and tensile strengths for plutonic, foliated, volcanic, chemical sedimentary and clastic sedimentary rocks. Data for the Pikes Peak granite are summarized in table 7. The influence of weathering on all but density is apparent. Similar engineering data with the addition of seismic velocities and Schmidt rebound hardness data have been collected by Coulson [94].

Table 7. Physical Properties of Pikes Peak Granite
(Adapted from Kulhawy, 1975) [93]

	Density (g/cm ³)	Elastic modulus (GN/m ²)	Poisson's ratio	Compressive strength (MN/m ²)	Tensile strength (MN/m ²)
Coarse- grained weathered granite	2.67	33.4	0.37	88.9	3.93
Dense, medium- to fine- grained granite	2.64	70.6	0.18	226.0	11.9

Densities, compressive strengths, and elastic modulus values for 23 different igneous, sedimentary, and metamorphic rocks have been published [95]. Tabulation and correlation of strengths, velocities, and elastic moduli for 49 rock types have been prepared [96]. A summary table was prepared [71] of dry unit weight, compressive strength, Atterberg limits, friction angle, and cohesion values for cyclic sedimentary rocks occurring in the Northern Appalachian Plateau.

Moisture content influences electrical and seismic parameters. Representative moisture contents for a variety of soils and sedimentary rocks have been listed [97-101]. Moisture changes at a landslide failure surface were documented [100].

In addition to the sources given earlier, representative resistivity values in soils and rocks have been tabulated [102-103]. Of special interest to this project are the differences in resistivity of landslide materials versus underlying material. Such resistivity differences for several material types have been measured [104] and are summarized in table 8. Moisture content in the slide mass may alter the resistivity values obtained. A decrease of 11-15 ohm-meters from surficial, dry landslide material to more moist, underlying slide material has been noted [104]. Similar resistivity responses to both landslide disturbance of bedrock material and moisture content have been reported [105].

Table 8. Comparison of Resistivity of Landslide Mass and Undisturbed Material, Black Sea Coast of Caucasus and Crimea, USSR.
(Modified from Bogoslovsky and Ogilvy, 1977) [104]

Material	Resistivity (ohm-meters)	
	Undisturbed material	Landslide mass
Argillite	60-100	30-45
Clayey sandstone	30-80	20-30
Shale	30-80	10-20
Clay	6-10	4-6

Differences between resistivity values measured horizontally and vertically in tunnel walls have been tabulated [106]. This electrical anisotropy may be expected to be present in other physical measurements because of the inherent anisotropic nature of most soils and rocks.

Seismic refraction and reflection methods have been used for years to obtain depths to material changes. Texts [103,107] in geophysics attest to this as well as providing representative velocities for various soil and rock types. The use of both methods for the shallow exploration required by this project is well covered [108,109a,b].

The presence and frequency of discontinuities in rock masses reduce the velocity of shock waves that pass through them. For the same material, a decrease in velocity was recorded [110] from 5250 m/sec to 4750 m/sec as the frequency of fractures increased from 0 to 4 per meter. The occurrence frequency of discontinuities decreases with increasing depth with an accompanying increase in velocity which is documented [111] in table 9. Material disturbance [104,105,112] within a landslide mass would be expected to cause a decrease in velocity. The data provided [104] are of special interest as they pertain to failures within soils rather than along a soil-rock interface. Selected velocities are reproduced in table 10.

Table 9. Influence of Depth on Velocity
(Adapted from Knill, 1968) [111]

Material	Velocity - m/sec	
	Near-surface	30 m deep
Argillite and slate	1524	4420
Cleaved volcanic ash	1524	3962
Sandstone and shale	762-1371	3505-3962

Table 10. Influence of Landslide Disturbance on Velocity
(Adapted from Bogoslovsky and Ogilvy, 1977) [104]

Material	Velocity - m/sec	
	Undisturbed material	Landslide mass
Medium loam	490-580	240-390
Loamy sand	310-370	250-270
Silty clay	340-880	530-690
Sandy clay	890-950	600-740
Clay	1600-1750	830-980

The influence of fracturing on velocity has been utilized to measure rock quality which is decreased by increased frequency of fractures. The measure used is the velocity index, $(V_F/V_L)^2$, where V_F = rock-mass velocity measured in the field and V_L = intact-rock velocity with no discontinuities. The velocity ratio in turn has been related to Rock Quality Designation (RQD), a measure of rock quality based in part on the frequency of fracture occurrence in a rock core [82,113].

4. TECHNIQUE DOCUMENTATION

4.1 Background

The thrust of this phase was to review existing sensing techniques and recommend those which have the greatest potential to measure those features outlined below in section 4.2 which are important in determining slope stability. Moreover, a new theoretical approach developed by the NBS has the potential for determining most of the same requirements described in section 4.2 but in addition has other features which make it even more attractive. This new approach is described in section 4.4.

4.2 Measurable Characteristics

The geologic features and their characteristics having an influence on slope stability have been evaluated in sections 2 and 3 of this report. It should be noted that in this section the terminology, while consistent with the previous sections, is used in a different format to bring out relationships of importance to a microwave measurement system. Microwave is a term used rather loosely to signify electromagnetic waves in the frequency range from about 1 GHz upwards. The term joint as defined earlier in section 2, while quite useful in considering physical parameters of rocks, cannot easily be used here. In this section a joint will be considered to be a crack of relatively small width compared to its lateral extent with little or no relative movement of the rock. (See table 11.) As before, the term joint will be used in a nongenetic sense.

Of those geologic features which have been determined to be of importance in slope stability, the following appear to have a reasonable chance of being detected using microwave measurement techniques [114].

1. Boundaries of compositional change (sedimentary stratification, schistosity, weathering depth, contacts, veins and seams, previous failure surfaces, voids, etc.)
2. Joints.
3. Shear zones.
4. Relative water content.

In addition to the detection of these features it is highly desirable to be able to measure some of the parameters of these features in order to make reasonable decisions regarding their significance. Fortunately, it appears that microwave measurement techniques can give additional information about the detected feature such as:

1. Orientation of boundaries, joints, and shear zones.
2. Continuity of boundaries, joints, and shear zones.

3. Surface roughness and waviness of boundaries, joints, and shear zones.
4. Thickness of shear zones, layers, veins, seams, and widely spaced joints.
5. The dielectric constant and loss of the filling material for a joint, layer, vein, seam or shear zone. This can give information about the filling material.
6. Water content variations with position and time.

4.3 Applicable Sensing Techniques

In this work we have considered primarily only those methods which would, from the surface, allow us to get a measure of the potential stability and which could be used to economically monitor a site to predict incipient slope failure. Because of economic considerations, any equipment used will have to be portable and cannot be permanently attached to any one site. Also it is imperative that a non-contacting method be used if possible.

Acoustic systems have been attempted for obtaining engineering information and might, with further development, give some usable results for slope stability. The largest drawbacks appear to be associated with the high acoustic loss in soils and the need, as in seismic techniques, to physically couple to the ground [103,115]. Acoustic techniques for monitoring bulk changes have had some limited success, but these do not provide engineering information [116].

Acoustic and seismic velocity measurements have provided some good information about the soundness of rock, but these measurements usually require boreholes or special attachments to the rock surface. These are of limited use for the present work [117,118].

The abilities of seismic techniques for the relatively shallow exploration required in slope stability determination are well covered by several references [108,109]. It does not appear that the details of the features having major importance in slope stability can be obtained well enough in this way, except in very special cases. Here we are looking for details of joints such as spacing, size, slope and fill material, if any, at very short ranges. Seismic techniques tend to give good results on larger features at somewhat greater ranges. We are primarily interested in a range of 10 meters or less, but in as much detail as may reasonably be obtained. In a slope stability investigation of an existing site it does not appear desirable, either in a new investigation or a monitoring check, to induce any significant vibration into the ground which could precipitate a slope movement itself.

The low frequency inductive systems in use today do not appear to have sufficient resolution to detect and measure the prominent geologic features involved in slope stability [119,120]. This is in spite of the fact that they are employed productively in geophysical mineral survey work.

The direct current and low frequency resistivity techniques in use today do not provide the detection sensitivity or resolution needed for measurement of the prominent slope stability features [103,121,122]. Resistivity measurements have shown differences in the before and after slide conditions but do not appear to hold much promise as a predictive or diagnostic technique [123].

A literature search reveals that there are at least four different potential microwave systems which might be developed for detection and analysis of some of the prominent features involved in slope stability. These general system approaches are:

- 1) The pulse-time domain or baseband pulse systems;
- 2) FM-CW systems;
- 3) Synthetic pulse systems; and
- 4) Holographic and related systems.

1) A pulse-time domain or baseband pulse system is dependent upon transmitting a pulse whose waveform is known and looking for return signals whose amplitude, time delay, relative phase, polarization, and propagation directions give information about the target [124]. The return signals are usually displayed in real time as amplitude with respect to delay time. In order to obtain sufficient penetration of most rocks, the frequencies used must be less than about 2.0 GHz [125,126].

2) An FM-CW (Frequency Modulated-Continuous Wave) system sweeps through a band of frequencies and compares the instantaneous output frequency with the frequency returning from a target. The difference frequency is a function of the distance to the target and the dielectric constant of the intervening material. These target difference frequencies are displayed as amplitude with respect to frequency, which is equivalent to distance to the target [127-130].

3) Synthetic pulse systems transmit a single frequency at a time and measure the amplitude and phase of the return. The returns at all frequencies are summed and converted by an inverse Fourier transform into a resultant time domain series of signals which are the same as would be obtained if a pulse were transmitted and returned signals were exhibited, as in the pulse-time domain system [131,132]. As is the case with the other systems this information may be displayed in the frequency domain.

4) Microwave holographic systems, as presently attempted, are single or multiple frequency, physically scanned, and depend on considerable data storage and manipulation [133]. There is a large amount of literature on acoustic holography which may be applicable to underground detection problems using microwaves [134]. Microwave holography appears to have considerable potential for the measurement of slope stability geologic features. It has potentially very good resolution. However, the results to date have been insufficient for slope stability work. As a result of microwave antenna calibration efforts carried out by the Electromagnetic Fields Division at the National Bureau of Standards, a potentially very useful holographic related technique has been found. This new technique will be discussed more fully in section 4.4.1.1.

A microwave measurement system potentially has the ability to provide useful information without having to make a direct physical contact to the rock. For this reason a microwave measurement system should be repeatable, relatively easy and economical to use, and provide no ground disturbance.

The FM-CW system was favored over the pulse systems because at the present state-of-the-art one can obtain better resolution at useful ranges (approximately 0-10 m) in the rock, higher transmitter power if required, and components which are commercially available.

A comparison of the FM-CW system with the synthetic pulse system shows that both systems have certain advantages but that the synthetic pulse system as now used is considerably more expensive. However, in recent work conducted at the NBS, the synthetic pulse system would probably have been considered as the second choice for the experimental work.

Upon consideration of all the techniques outlined above, the FM-CW system was chosen for the field experimental effort of this project. An introduction to this system and its operation is given in section 5 of this report.

4.4. The Planar Near-Field Reconstruction (PNFR) Approach to High-Resolution Remote Sensing of Subsurface Anomalies

4.4.1 Introduction and Comparison with Alternative Techniques

The primary and explicit objective of this section is to explain, formulate, and present preliminary computer results of the plane-wave spectrum approach to near-field reconstruction, hereafter referred to as planar near-field reconstruction and abbreviated PNFR. A secondary objective is to compare the PNFR technique with other high-resolution methodologies which appear to have similar remote sensing capabilities.

The PNFR technique has been proposed by the NBS as a possible high resolution, remote measurement scheme to help predict subsurface anomalies and slope stability. The technique, which requires measurements at a single frequency only, is based on the plane-wave spectrum description of radiators and scatterers, a description which has been utilized extensively at the NBS during the past 20 years for the near-field measurement of antennas and acoustic transducers [135]. For antenna measurement applications where the NBS is most experienced, the near field of an antenna is measured and usually the far-field radiation pattern is computed from the near-field measurements. For the present subsurface remote sensing applications, however, the requirement is to extrapolate in the opposite direction toward the scatterers of radiation, i.e., to measure scattered fields on or just above the surface of the earth and determine by mathematical transformation the scattered fields beneath the earth from the measured data. The scattered fields are produced by a source of radiation also located on or just above the earth's surface.

We do not specify *a priori* whether scattering emanates from local or stratified discontinuities, nor do we ask in advance what propagation parameters display the inhomogeneities responsible for the scattering. Of course, such physical features and propagation characteristics, which have been discussed in sections 2 and 3 of this report, are of primary importance in predicting slope stability, and their determination or estimation represents an ultimate goal of the project. However, our initial approach here is to simply assume there exists detectable scattering from an applied incident field and ask how we can best determine the location of the subsurface discontinuities by measuring the scattered field at the surface. A high resolution mapping of the major discontinuities would yield information on the localized inhomogeneities and joints important to highway construction and slope stability. The resolved discontinuities would represent valuable clues to the experienced geologist to help further decipher the local subsurface structure. In addition, the resolved inhomogeneities could be examined with complementary systems such as the FM-CW radar to possibly determine the values of the subsurface physical parameters more precisely.

Complementary usage of more than one method has long been espoused as a reasonable and effective approach to geophysical investigation [136].

The FM-CW system and the closely related baseband pulse and Fourier-synthetic pulse systems for remote subsurface probing are described and evaluated in sections 4.3 and 5.3. These systems, which have been developed and applied successfully in the past to detecting snow pack characteristics, water tables, oil well casings, coal thicknesses, water-filled voids, and other near-surface anomalies [128,137-140], are expected to also prove valuable in resolving subsurface features pertinent to road construction and landslides. To date, the three systems have been most useful for investigating discontinuities in the vicinity and lying perpendicular to the main-beam axis of the source of radiation. In this section we are concentrating on alternative techniques and especially those which show potential to resolve a more detailed, complex conglomeration of inhomogeneities over a more extensive area.

Certainly the PNFR technique is not the only alternative remote sensing method which shows potential for the high-resolution investigation of complex media. Even a superficial survey of the literature on remote sensing suggests a seemingly unlimited number of approaches and systems which have been or could be utilized for subsurface probing. However, when the dual stipulations of **remote sensing** and **high resolution** at relatively shallow depths are invoked, many of the techniques are eliminated.

In landslide prone areas, as well as being expensive, it can be too difficult, dangerous, or both to introduce large, heavy drilling and impact equipment, or to detonate explosives. Thus, for example, the classical seismic exploration methods which require boreholes, impact devices, or explosives could not be applied safely to sensing slope stability [141]. Furthermore, the classical, low-frequency seismic reflection and refraction techniques do not have the capability of resolving the comparatively small, shallow discontinuities important in highway planning, construction and maintenance. Local stratifications and joints a few centimeters thick, a few meters beneath the surface, and a few tens of meters across typically determine local landslide conditions.

This high-resolution requirement immediately eliminates a number of other available remote sensing possibilities, including gravity and magnetic profiling [142], infrared scanning [143] and radiometry in general [144], electromagnetic wave tilt and induction methods [145], nuclear detection [146], and subaudible acoustic listening [117]. (A report by Stanford Research Institute conveniently reviews, tests, and summarizes a number of these available techniques [147].) This is not to suggest that each of these remote sensing schemes could not be utilized for detecting slope instabilities in certain regions under specialized

subsurface conditions, only that these methodologies inherently lack the capability of resolving the centimeter size anomalies a few meters beneath the earth's surface necessary for accurate slope stability predictions.

The high-resolution criterion at shallow depths also directs our attention away from earth resistivity profiling as a viable method for the present highway subsurface applications. The resistivity techniques have proven useful for locating large ore bodies and sinkholes with a resolving power of a few meters [148]. Very near the surface, resolving increments as small as several centimeters have been attained [148c]. Unfortunately, experience indicates that this very high resolution with resistance methods deteriorates rapidly when detecting and mapping scatterers located a few meters or more beneath the earth's surface [147]. Other disadvantages of resistivity methods are that poor contact with the surface often prevents adequate current distributions, and too conductive a layer will mask the resistivity profile beneath it.

Thus far we have briefly noted several probing methods which do not "measure up" to the remote and/or high-resolution criterion necessary for the subsurface investigations related to highway construction and maintenance. A number of different techniques still remain which show promise for high-resolution remote sensing. The FM-CW, baseband pulse, and Fourier-synthetic pulse radars, as mentioned above and reported upon in sections 4.3 and 5.3, are presently being refined at the NBS to address the subsurface probing problem [137]. Also, the extension of sophisticated seismic reflection techniques used in geophysical exploration to higher (kHz) frequencies and shallower depths could prove fruitful to the FHWA problem of slope stability determination [109a].

A major difficulty encountered when going to high-frequency seismic reflection is the poor coupling between the air-earth interface, and the higher losses in the earth at the higher frequencies. In order to reduce the coupling problems, microwave antennas could conceivably replace the acoustic sources of vibration. Moreover, presently available antennas several wavelengths across could be used to direct the beam and resolve discontinuities without the need for the vast amount of data and sophisticated computer processing intimately involved with existing state-of-the-art reflection seismology. (The mass of measured data and computer processing associated with accurate low-frequency, seismic reflection exploration at great depths is required in large part because of the unavailability of controlled, highly directive, penetrable sources of radiation at the low frequencies). In other words, if the explosive seismic source can be replaced by a directive antenna, subsurface probing can be accomplished in a less complicated fashion by using, for example, the conventional pulsed rf or chirp (electrically synthesized pulse) radar scanning techniques, possibly enhanced by deconvolution processes to normalize to the source antenna pattern and to reduce reverberations. And

indeed, conventional sector scanning and linear scanning radar, like the FM-CW, baseband pulse, and Fourier-synthetic pulse radars, show promise as feasible high-resolution remote sensing techniques [147,149]. The analogous "sonographic scanning" with directed ultrasonic beams has achieved considerable success and refinement for the remote medical examination and diagnosis of the human body [150]. Other high-frequency acoustic pulse-echo (sonar) techniques have been used within boreholes where sufficient coupling can evidently be attained [151], although serious mode conversion and data analysis problems have been encountered.

We have refrained from conventional sector scanning radar as a means of subsurface investigation chiefly because of the large, complex phased array antennas which would be required to scan conveniently with a sufficiently directive beam. As for linear scanning radar, the system we have emphasized to date has been the FM-CW rather than the alternative pulsed (rf, baseband, or synthetic) radars; although the emphasis has been due in part to the availability of expertise, experience, and equipment within the NBS.

4.4.1.1 A Comparison of PNFR with Holographic, Side-Looking Radar, and Computer Aided Tomographic Techniques

Similarly, part of the reason we have emphasized and chosen to pursue the PNFR remote sensing technique is our previous familiarity and success with applying the plane-wave spectrum approach to measuring antennas and acoustic transducers [135]. Fortunately, a fairly extensive literature search has supported our initial prejudice. The results of this literature search, along with exchanges between the NBS and the USGS personnel and information gleaned from recent professional meetings involved with remote sensing and inverse scattering, continually point to three high resolution surface techniques (holography, side-looking radar, and computer-aided tomography) which should be seriously considered in addition to PNFR and the radar systems discussed in the previous section and section 4.3. Although their application to shallow subsurface exploration has been rather limited, the remarkable success of holography, side-looking radar, and computerized tomography in optical processing, airborne microwave photography of the earth's surface, and medical radiology, respectively, dictates their serious consideration to underground remote sensing as well.

A comparative analysis of these three techniques with the PNFR technique was undertaken to ascertain if the foundational theory on which each technique was based had the potential for resolving small subsurface anomalies and discontinuities. The main conclusions of this analysis are summarized in the following subsections.

A. Holographic Techniques

Holographic and the PNFR techniques are very closely related. The mathematical formulation on which both techniques rest is the same, namely the Fourier transform or plane-wave spectrum representation of the wave equation [135,152]. Both methods effectively require the recording of the amplitude and phase of the scattered field, usually on a planar surface in front of the sources of scattering. The field from behind the measurement plane is then reconstructed from the recorded data. The difference between the two techniques lies in the way the amplitude and phase of the field is recorded and in the way the field behind the measurement plane is reconstructed.

For optical holography the amplitude and phase of the scattered light is usually recorded on photographic data film through interference with a reference light beam, and 3-D images of the scattered light behind the recording plane are usually reconstructed by directing a similar reference beam of the same wavelength through the developed transparency or hologram [152].

In the case of microwave or acoustic (including ultrasonic) holography, interference patterns usually cannot be recorded directly on "film." At microwave and acoustic frequencies, however, the longer wavelengths allow direct measurement of the amplitude and phase by scanning with a probe across the measurement plane. The measured amplitude and phase voltages can, for example, be superimposed with a phase-locked reference wave and the resulting interference pattern displayed on a cathode-ray tube. The cathode-ray display can then be photographed to create the hologram, which will visually reconstruct the microwave or acoustic images when illuminated with a beam of coherent light [133,134,153,154].

The PNFR technique always requires the amplitude and phase of the scattered field data to be recorded numerically, usually by scanning the measurement plane with a probe phase-locked to the incident source of radiation [135]. The data is mathematically transformed with the aid of the fast Fourier transform (FFT) computer algorithms to yield the numerical values of the scattered field, anywhere between the measurement plane and the scatterers. (Actually, the fields can be computed anywhere in front of the scatterers, but for subsurface probing applications, only the fields behind the measurement plane (underground) are of interest.) At optical wavelengths, computer reconstructed or simulated holography, or backward propagated reconstruction [155], three alternatively used names for methods similar to the method we refer to as the PNFR technique, is presently impossible because existing technology is unable to measure directly the phase across a light beam. Thus, PNFR is especially suited

to microwave and acoustic wavelengths where it is possible to make direct phase measurements routinely.

One may well ask why computer reconstruction of the scattered fields should even be considered as an alternative to visual 3-D holographic images. Should not one picture be worth a thousand numbers? Even if the numbers are used to plot contour curves of the scattered fields, it would seem like an unnecessarily tedious procedure to obtain no more information than that which is contained on a single hologram. This valid inquiry can best be answered by looking into the three main limitations of microwave and acoustic holography for subsurface investigation, namely severe image distortion, masking of images by surface reflections and background noise, and poor resolution. A lesser fourth disadvantage is also identified.

In microwave and acoustic holography, the holograms are recorded using wavelengths much longer than the optical wavelength used for visual reconstruction. This leads to a distortion in vertical (longitudinal) magnification of the images proportional to the ratio of the recording to reconstructing wavelength. Typically, this means that even at ultrasonic frequencies the vertical distortion ratio would be on the order of 1000 to 1. This primary distortion problem has been reduced but apparently not to a satisfactory extent [153b]. In addition to the primary distortion, the visual hologram inherently records the interference data under the paraxial ray approximation. That is, scattered fields impinging on the holographic film from a wide angle will be reconstructed under spherical aberrations [156, section 6.3]. The PNFR method does not encounter either this primary or secondary distortion because its computer reconstruction of the scattered fields uses the exact equations (no paraxial approximation) at the frequency of the measured data (no wavelength scaling distortion).

Holographic images like conventional photographs also suffer from the shading of the distant images by the nearer images. For subsurface probing, the large reflections from the air-earth interface strongly mask the subsurface images of interest [133,154]. To date no simple, realistic procedure has been found for subtracting these overlying reflections. Again, the PNFR technique has the distinct advantage of being able to compute the scattered fields at arbitrary distances below the measurement plane and thus can selectively avoid the masking of the nearer reflections and scattering.

The third main limitation of holographic images is that the absolute resolution in both the horizontal and vertical directions becomes poorer with increasing depth, i.e., vertical distance from the recording or measurement plane. Specifically, as the depth of interrogation grows larger than the breadth of the recording plane, the horizontal and vertical resolutions decrease in proportion to the first and second power,

respectively, of the distance from the recording plane [157, section 2.10]. This degradation, especially severe for the vertical resolution, is also present in the PNFR technique (see section 4.4.3b). However, if necessary, possibilities exist for enhancing vertical resolution within the PNFR method, and these will be discussed below in section 4.4.4.1.

One final advantage which PNFR has over microwave and acoustic holographic techniques should be mentioned. In measuring with a finite size probe, amplitude and phase of the scattered field are always somewhat averaged or distorted. A hologram developed from this data will also contain these probe distortions. For the PNFR technique, however, the distorting effects of the probe can be removed in a surprisingly simple manner, and the field can be extracted exactly (including both polarizations for EM fields) to the accuracy of the scanning facility and receivers [135].

In brief summary, four distinct advantages of the computer PNFR technique over microwave and acoustic holography have been identified:

- 1) Wavelength ratio and paraxial distortions are not encountered.
- 2) Masking of distant images by overlying reflections and scattering from nearer images can be selectively avoided.
- 3) Possibilities exist for enhancing vertical resolution (if necessary).
- 4) The distorting effects of the finite size measuring probe can be readily removed, and both polarizations of EM fields are computed.

B. Side-Looking Radar

Airborne side-looking radar and its acoustic counterpart, shipboard side-looking sonar, have produced strikingly detailed photographs of the earth's surface and the ocean bottom [158,159]. It is only natural to consider these techniques for subsurface probing as well. (To avoid redundancy, we will discuss side-looking radar only.) As previous authors have pointed out [158a], side-looking radar consists essentially of a microwave holographic technique in which reflected signals from a radar antenna mounted on the belly of an aircraft (or satellite) and aimed to the side are recorded to form the hologram. The along-track dimension of the hologram is produced by the forward travel of the aircraft and the side-track dimension is recorded by monitoring in time the return arrival of the reflected radar pulse. The technique is ingenious and yields impressive mappings of the earth's surface, but there are two main reasons why it would not be feasible to adapt the technique for subsurface investigation.

First, because it is essentially a holographic technique, it would exhibit the limitations of holography mentioned in the previous section A if applied to subsurface probing. Secondly, because the across-track hologram dimension of the side-looking radar is formed by recording the variations in the reflected pulse across the pulse width, accurate horizontal resolution depends strongly on the fact that the earth's surface in the vicinity of the aircraft is relatively flat compared to the height of the aircraft. In other words, the side-looking radar techniques are especially designed for resolving surface features and do not have the capability of distinguishing buried anomalies at equal radii from the antenna. Furthermore, modifications necessary to give side-looking radar significant depth resolving capabilities would probably involve narrow beam, electronically scanning phased arrays [158c] inappropriate for shallow subsurface exploration conducted on the ground.

C. Computer-Aided Tomographic (CAT) Techniques

To quote a recent article by a respected authority on the subject, "Computer aided tomography (CAT) is causing a revolution in the medical field of radiology. By combining "ordinary" x-ray technology with sophisticated computer signal processing, it is possible to generate a display of the tissues of the body which is unencumbered by the shadows of other organs" [160a]. Our interest in these CAT techniques once again centered around the question of whether or not they had application to subsurface remote sensing.

Electromagnetic tomography has recently been applied at Lawrence Livermore Laboratories (LLL) to cross-borehole surveying [160c]. The initial results appear quite encouraging, and work is being continued in this area [160d]. The basic limitations of this cross-borehole tomography are that the theoretical model assumes only isotropic absorption and transmission of rays (reflection or scattering is ignored), multipath effects are not considered, and, of course, boreholes are required. Implicitly, gradual rather than abrupt changes in electromagnetic parameters are assumed. In regard to the present NBS project (which wishes to avoid boreholes), we ask the question of whether tomographic techniques depending on the surface measurement of scattered rays rather than transmitted rays between boreholes can be formulated to effectively profile the subsurface structure.

We can begin to address this question by first gaining an understanding of the fundamental result, commonly known as the projection theorem, on which most modern tomographic systems are based (implicitly or explicitly) [160a,b]. The theorem is exact, and it simply states that the Fourier transform of the measured "projection" of an absorbing body is the center-cross-section of the Fourier transform of the image. Physically, this means if we can describe the transmission of radiation by a body

completely in terms of a spatial absorbtivity function, the value of the absorbtivity function can be computed by measuring the transmitted radiation or projection of the body at various view angles.

Now, if the scattered radiation from buried anomalies is expressed in terms of their equivalent sources, an equation in a form which appears solvable by the tomographic projection theorem can be extracted. Thus, at first sight it appears that CAT techniques can be adapted with very little alteration to determine the sources of subsurface scattering and their location from measurements on the surface.

Unfortunately, a more careful analysis reveals that the scattering function (replacing the absorbtivity function) to be determined does not possess the spatially invariant property of x-ray absorbtivity functions. This lack of invariance of the scattering function with rotations of the reference coordinate system means that the projection theorem and thus the CAT schemes do not strictly apply.

For this reason, which as far as we are aware has not been previously pointed out, computerized tomography, so useful with x-ray transmission in medical radiology, does not generally apply to the inverse scattering problem and, in particular, to the problem of subsurface investigation from the surface. However, we do not exclude the possibility that under certain restrictions, surface tomographic techniques could complement other scattered field reconstruction techniques such as microwave holography [161] or PNFR, and that further research into this subject could prove fruitful.

Finally, we conjecture that the LLL cross-borehole tomography, which is especially suited for detecting gradual inhomogeneities, and the PNFR technique, which appears to be especially suited for detecting more abrupt inhomogeneities, could be utilized as complementary techniques to enhance delineation of subsurface features.

4.4.2 Mathematical Formulation for the PNFR

In the previous section a comparative review of holographic, side-looking radar, and computer-aided tomographic techniques with planar near-field reconstruction (PNFR) revealed that the PNFR had the potential for overcoming a number of the serious limitations of the other three techniques. In this section we formulate the basic mathematical theory necessary to apply the PNFR technique to remote subsurface probing and to predict its limitations. Although the theory may at first appear quite removed from practical application, it will finally determine specific answers to such practical concerns as measured data point spacing, size of scan area, accuracy of the scanning equipment, required planarity of the scan plane, and expected resolution.

4.4.2.1 Description of the Subsurface Model

For initial simplicity, consider a perfectly flat homogeneous earth, as depicted in Fig. 2, with a single point anomaly or scatterer located a distance d below the surface of the earth along the z -axis. The x - y plane at $z = 0$ will be chosen as the air-earth interface. The point scatterer is illuminated by a source of radiation incident from the surface. By measuring the scattered field on the surface of the earth we want to compute the scattered fields below the surface and locate the point scatterer by determining the position of the maximum computed fields. The assumption that the point anomalies or scatterers will be located at the position of the local maxima of the computed scattered field (see section 4.4.4) is basic to the success of the PNFR. As an inverse scattering technique, this assumption represents the extra **a priori** information or condition sufficient to convert the generally nonunique, single frequency inverse scattering problem into a problem in which the sources can be uniquely located [162]*. In practice, this assumption which holds perfectly for point scatterers, will hold only approximately for finite sized scatterers and will become completely invalid for reflection from interfaces of stratified media. However, stratified media

* It should be mentioned that Bojarski [163] has proven that the shape and location of a perfectly reflecting body in an otherwise homogeneous medium can be fully recovered from far-field information measured at all frequencies and at all aspect angles with respect to the scattering target. Bleistein and Cohen [164] and Tsien and Chen [165] also present a "pulse-spectrum technique" for inverse scattering to determining small variations in propagation speed in inhomogeneous media. These and similar techniques in the mathematical development stage do not appear to be presently feasible to general subsurface investigation because of the large number of measurements which would be required in practice, the lack of efficient inversion algorithms, and the restrictive assumptions necessary to yield a solvable model.

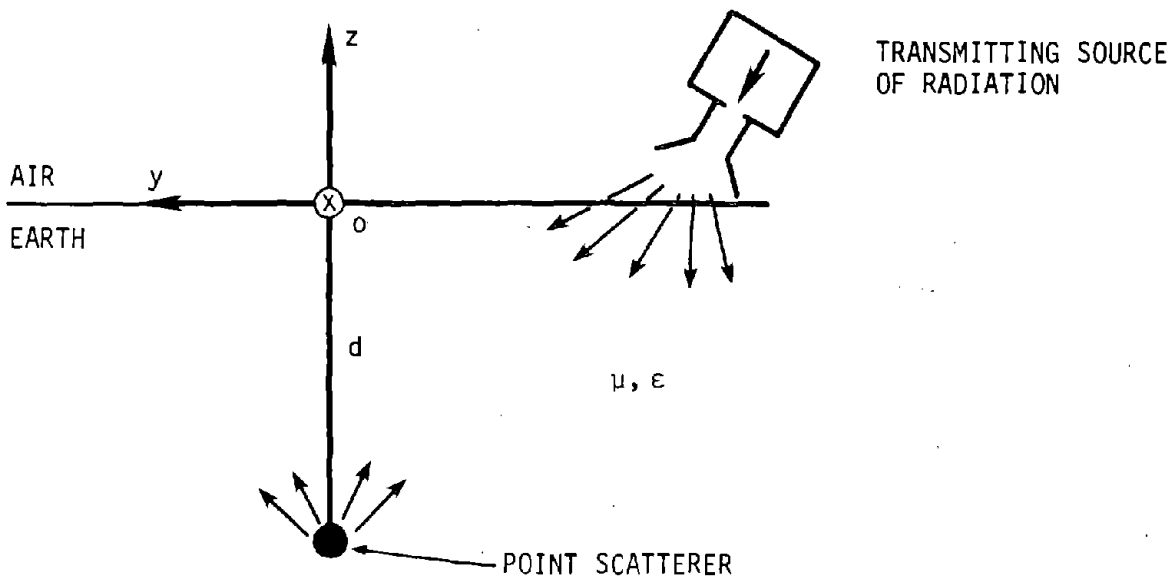


Figure 2. Schematic of point scatterer buried a distance "d" below the surface of the earth.

will produce images of the source radiator, and these image sources can be distinguished from localized scatterers by seeing if the images relocate when the source radiator is relocated.

In this initial year of work, the details of applying PNFR to finite scatterers and stratified media were not developed, but the simpler point scatterer problem was chosen for study in order to determine feasibility of the technique. In Fig. 2 a single point scatterer is located along the z-axis as a matter of descriptive convenience rather than necessity. The following formulation applies equally well to any number of discrete point scatterers located arbitrarily within an otherwise homogeneous earth.

4.4.2.2 The Plane-Wave Spectrum Representation

Let the source of radiation at the surface be an antenna illuminating the earth which, except for the point scatterer, is a homogeneous, lossless medium of permittivity (dielectric constant) ϵ and permeability μ . (Although ϵ and μ are here assumed real, generalization to lossy media can be made by merely allowing ϵ to be complex.) Between the surface of the earth and the scatterer, the scattered electric and magnetic field can be written as a superposition of plane waves traveling toward the surface [135b] (to keep the number of necessary equations at a minimum we shall concentrate on the electric field):

$$\bar{E}(x,y,z) = \frac{1}{2\pi} \int_{-\infty}^{\infty} \bar{b}(\bar{K}) e^{i\gamma z} e^{i\bar{K}\cdot\bar{R}} d\bar{K}. \quad (1)$$

where $\bar{b}(\bar{K})$ is the electric field (divided by 2π) in the plane wave propagating in the $\bar{k} = \bar{K} + \gamma\hat{e}_z$ direction for $\exp(-i\omega t)$ time dependence, and thus $\bar{b}(\bar{K})$ is perpendicular to \bar{k} , i.e.,

$$\bar{b}(\bar{K}) \cdot \bar{k} = 0. \quad (2)$$

The z-component, γ , of the propagation vector \bar{k} ($k = \omega/c = 2\pi/\lambda$) is given simply by

$$\gamma = (k^2 - K^2)^{1/2}, \quad (3)$$

where the square root is taken positive real or positive imaginary. Here c is the speed of light and λ the wavelength in the earth. In eq (1) $\bar{K} = k_x \hat{e}_x + k_y \hat{e}_y$, $\bar{R} = x \hat{e}_x + y \hat{e}_y$, and $d\bar{K}$ is shorthand notation for the double differential $dk_x dk_y$. As indicated, the range of integration covers the real k_x and k_y line from $-\infty$ to $+\infty$. Although it takes some effort to explain the notation in eq (1), it is helpful to remember that eq (1) is merely an integration or superposition of the weighted spectrum of plane waves which can propagate upward from the scatterer.

Equation (1) neglects the scattered field which is reflected from the earth-air interface. Since measurements are to be taken above the earth's surface, at first thought this neglect would appear to introduce serious errors. Fortunately, however, it can be shown that the plane-wave fields just above the earth's surface have the same phase as the scattered fields incident from below provided the angle of incidence is less than the critical angle of total reflection [166, p. 495]. In addition, the plane-wave amplitude just above the surface is related to the incident amplitude just beneath the surface by a proportionality factor which varies slowly with angle of incidence. Thus, away from the critical angle the field measured just above the surface of the earth will be nearly proportional to the incident fields from below and as a first approximation the reflected fields from the interface can be neglected. Of course, if necessary, the plane-wave spectrum of the incident fields can be recovered (exactly, in principle) from the measured transmitted fields by simply applying Fresnel's equations which describe plane-wave refractions ([166], sec. 9.5).

When γ becomes imaginary the z dependence of the plane waves becomes exponentially decaying or evanescent. In a practical measurement scheme these evanescent modes usually contribute negligibly compared to the radiated fields and thus the integration in (1) need extend only over $K < k$.

Equation (1) says that if we know $\bar{b}(\bar{K})$ for the scattered field we can compute the scattered field everywhere between the scatterer and the surface of the earth. Thus we need to perform measurements which allow the evaluation of $\bar{b}(\bar{K})$. This can be accomplished by measuring the electric field at the surface of the earth, i.e., $\bar{E}(x,y,0)$, and taking the inverse double Fourier transform of (1). Specifically,

$$\bar{b}(\bar{K}) = \frac{1}{2\pi} \iint_{-\infty}^{\infty} \bar{E}(x,y,0) e^{-i\bar{K} \cdot \bar{R}} d\bar{R}, \quad (4)$$

where $d\bar{R}$ is shorthand notation for $dx dy$. Since we know that $\bar{b}(\bar{K})$ is perpendicular to \bar{k} we need only two components, say b_x and b_y to determine \bar{b} uniquely. Consequently, only the x and y (transverse) components of the electric field (\bar{E}_t) at the surface need be measured to yield the transverse components (\bar{b}_t) of the spectrum:

$$\bar{b}_t(\bar{K}) = \frac{1}{2\pi} \iint_{-\infty}^{\infty} \bar{E}_t(x,y,0) e^{-i\bar{K}\cdot\bar{R}} d\bar{R} . \quad (5)$$

Simple vector algebra also yields an explicit expression for the complete spectrum in terms of the transverse spectrum:

$$\bar{b}(\bar{K}) = \frac{1}{2\pi} \bar{b}_t(\bar{K}) - \left(\frac{\bar{K}}{Y} \cdot \bar{b}_t(\bar{K}) \right) \hat{e}_z . \quad (6)$$

In brief, the PNFR technique can be explained in principle as follows. Measure the transverse electric field on a planar surface just above the surface of the earth and compute the transverse spectrum $\bar{b}_t(\bar{K})$ from eq (5), and the complete spectrum from eq (6). From eq (1) compute the electric field at increasing depths beneath the surface of the earth. Determine the location of the subsurface scatterers by determining where the magnitude of the computed electric field reaches local maxima.

As we have stated above, eq (1) holds only in the region above the scatterer. However, if it is applied blindly below a point or localized scatterer, it can be shown that the amplitude of the field reaches a maximum regardless of the direction of approach. Although the phase of the fields beneath the localized scatterer will not necessarily be correct the magnitude will become less with increasing distance from the scatterer, and this is sufficient behavior to determine the approximate location of the source of scattered power.

Important practical questions involving resolution, data point spacing, size and planarity of scan area, and methods of computation are addressed in the following section.

4.4.3 Some Practical Considerations

A. Size of Scan Area

In principle, eq (5) requires the transverse electric field to be measured on the infinite plane ($z = 0$) at the surface of the earth. In practice, we can only measure on a finite scan area, and this reduction in scan area introduces errors into the calculation of $\bar{b}(K)$ from eqs (5) and (6). The effect of the finite scan area on $\bar{b}(K)$ has been determined analytically [135e] and verified experimentally [135f]. Essentially, these reports conclude that the spectrum $\bar{b}(K)$ will be determined accurately only within the solid angular regions defined by the scatterer and the edges of the scan area.

Furthermore, when this partial spectrum is inserted into eq (1) in order to compute the scattered fields, poorer resolution in both the vertical and horizontal direction results. In other words, the smaller the scan area the poorer the resolution.

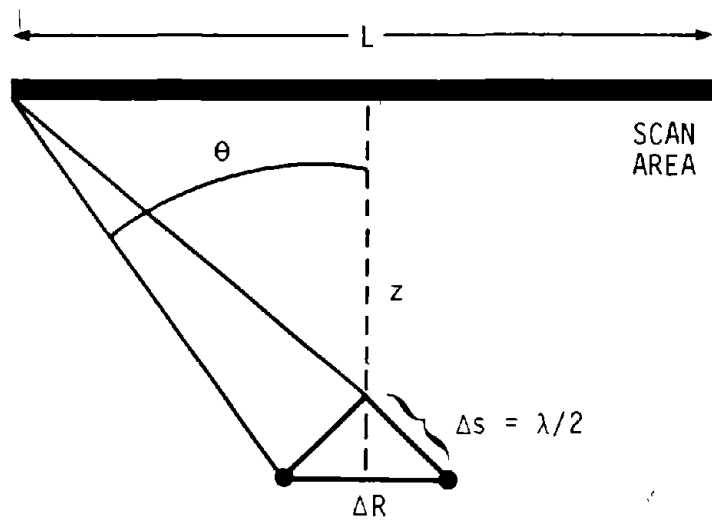
B. Horizontal and Vertical Resolution

An estimate of the horizontal and vertical resolution as a function of scan area can be obtained by viewing the scan area as a large receiving antenna. Consider the circular scan area of diameter L with a point source situated a distance z below as shown in Fig. 3. We ask how far can the point source be moved horizontally before there will be an appreciable change in the phase difference between the received field at the edge and center of the scan area. Specifically, when will Δs in Fig. 3a change about one-half wavelength.* Applying simple trigonometry to Fig. 3a, one obtains the horizontal resolution distance of

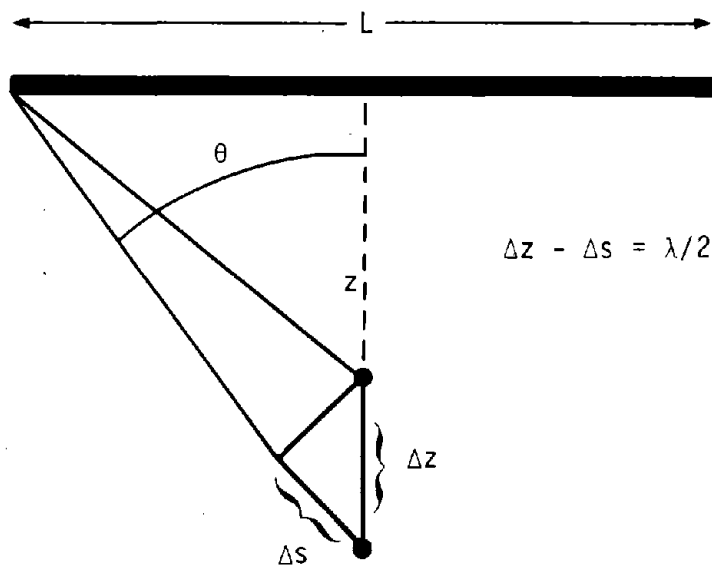
$$\Delta R = \frac{\lambda}{2 \sin \theta} = \frac{\lambda \sqrt{z^2 + \left(\frac{L}{2}\right)^2}}{L} \quad (7)$$

For a depth z less than the scan area radius, the horizontal resolution distance is about one-half wavelength. As z grows larger than the radius of the scan area the horizontal resolution begins to degrade linearly with z .

* Although the point scatterer is shown directly below the center of the scan area in Fig. 3, the estimates of horizontal and vertical resolution distances derived here remain valid for any point beneath the scan area.



a) HORIZONTAL RESOLUTION



b) VERTICAL RESOLUTION

Figure 3. Simple method for estimating resolution limits.

Looking at Fig. 3(b) we can estimate the vertical resolution distance Δz by the same criterion, which in this case amounts to letting $\Delta z - \Delta s = \lambda/2$. So doing yields,

$$\Delta z = \frac{\lambda}{2(1 - \cos \theta)} = \frac{\lambda \sqrt{z^2 + \left(\frac{L}{2}\right)^2}}{2 \sqrt{z^2 + \left(\frac{L}{2}\right)^2} - z} \quad (8)$$

For a depth z less than half the radius of the scan area, the vertical resolution distance is about one-half wavelength. As z grows larger than the radius of the scan area the expression for the vertical resolution distance becomes approximately

$$\Delta z \approx \frac{4\lambda z^2}{L^2} \quad (9)$$

which shows that the vertical resolution grows poorer as the square of the depth. This quadratic degradation in vertical resolution with depth is much greater than the corresponding linear degradation of the horizontal resolution with depth, and represents a major limitation of the PNFR as well as holographic techniques. In section 4.4.4.1, suggestions are made which may overcome the severe loss of vertical resolution as the depth increases beyond the radius of the scan area. Of course, if the subsurface structure is required to only a few meters below the surface, a scan area just a few meters across would practically yield the maximum resolution without additional enhancement procedures or measurements. The degradation in resolution with depth becomes a serious problem only when information appreciably deeper than the feasible scan radius is required.

Finally, it should be mentioned that the vertical and horizontal resolution distances expressed in eqs (7), (8), and (9) agree (except for a factor of 2 in eqs (8) and (9)) with those derived by Hildebrand and Brenden [157, sec. 2.10] for holograms when the depth z becomes much larger than the scan area radius. Moreover, our eqs (7) and (8) are more general in that they give resolution limits for arbitrary depth, not just greater than the scan area radius.

C. Data Point Spacing Determined by Sampling Theorem

The electric field measured at the surface forms the integrand of eq (5) from which the spectrum $\bar{b}(K)$ is evaluated. From a measurement as well as a computational standpoint we would like to determine the spacing in x and y required to compute $\bar{b}(K)$ from (5) accurately. Fortunately, and rather surprisingly, the required spacing can be obtained directly and immediately from the Whittaker-Shannon sampling theorem [152,sec. 2.3]. Since it can be shown that $\bar{b}(K)$ is a function bandlimited essentially at $K \approx k$, the sampling theorem says that the double integral in eq (5) can be converted to a double summation with spacing Δx and Δy given by

$$\Delta x = \Delta y = \frac{\pi}{k} = \frac{\lambda}{2} . \quad (10)$$

That is, $\bar{E}(x,y,0)$ need only be measured on a square grid of points separated by half a wavelength. If larger data spacing is taken, the higher spatial frequencies of $\bar{b}(K)$ will be in error through the "aliasing" which is introduced. Usually, however, for finite scan areas the data point spacing can be increased to a wavelength or so without the aliasing greatly changing the subsurface fields computed from eq (1).

D. Sampling Theorem Applied to the Computation of Subsurface Fields

Once the spectrum $\bar{b}(K)$ is computed by inserting the required data into eq (5), as explained in the previous subsection, the subsurface field must be computed from eq (1). The sampling theorem can also be applied to facilitate the computation of these integrals as well. Here it turns out that the spacing in Δk_x and Δk_y required by the sampling theorem depends on the range of x and y over which $\bar{E}(x,y,z)$ is computed. The details of this more involved application of the sampling theorem will not be included in this report but can be found in another recently prepared NBS manuscript [167]. The results of this study show that the increments in Δk_x and Δk_y needed to sum eq (1) accurately are

$$\Delta k_x = \Delta k_y = \frac{\pi}{2R_0} , \quad (11)$$

where R_0 equals 2λ plus the maximum range of $R = \sqrt{x^2 + y^2}$ over which the electric field is required to be computed accurately.

E. Application of the Fast Fourier Transform (FFT) Algorithm

Although the double integrals in eqs (1) and (5) can be converted to double summations via the Whittaker-Shannon sampling theorem, we are still faced with the problem of computing the double summations efficiently. Again, it is fortunate that eqs (1) and (5), when converted to summations, are in a form in which the fast Fourier transform (FFT) algorithm can be applied to perform the summation much more rapidly than a straightforward term by term addition to evaluate the summations. The FFT algorithm we use called FOURT, written by Norman Brenner of MIT Lincoln Laboratories, reduces typical computation times for the evaluation for eqs (1) and (5) from many minutes to a few seconds. The FFT computer algorithm developed in the mid-sixties coupled with the results of the sampling theorem has literally transformed near-field techniques from the realm of the possible to that of the practical.

F. Planarity of Scan Area

In 1975, an extensive error analysis of planar near-field techniques was undertaken to determine the measurement accuracy required to compute the spectrum from eq (5). In particular, it addressed the question of how accurate does one need to measure $\bar{E}(x,y,0)$ in eq (5) to compute a reasonably accurate spectrum $\bar{b}(K)$.

The results of this error analysis, reported in NBS Technical Note 667 [135e], show that for our purposes the critical errors of concern are phase errors. Phase needs to be measured to within a small fraction of a wavelength in air, λ_a . Actually, $\pm\lambda_a/10$ or $\pm 36^\circ$ will probably suffice for subsurface investigative work. Assuming the receiver which measures phase has an accuracy well within these limits, the major contribution to phase errors will be deviation from planarity of the scan area. Since phase typically changes about 2π radians per wavelength of displacement in the vertical direction, the probe used to measure the electric field must stay in a plane to within about $\pm\lambda_a/10$.

Also, since the wavelength in the earth is shorter, typically by a factor of 2 or 3, than in air, the surface of the earth over which the scan plane is chosen should be flat to within a small fraction of a wavelength in air; $\pm\lambda_a/10$ should suffice in most situations. Alternatively, this stringent flatness requirement could be relaxed if the phase fluctuations caused by the uneven surface either tended to cancel upon computer transformation, or were reduced by a mathematical filtering process.

Finally, because the direction of propagation of a wave changes, in general, upon refraction by the surface of the earth, the measurements should either be made as close to the earth as possible or transformed

mathematically to the earth's surface by eq (1) and its inverse. In practice, since the direction of propagation does not change too greatly until the critical angle is approached, a rule of thumb would be to choose the measurement plane within $\lambda_a/2$ of the surface of the earth if the extra mathematical transformation is to be avoided. (Of course, the rules of thumb stated here are results obtained from the analysis and experience with antenna measurements, but it remains to be seen if they are verified in subsurface applications.) In the event it is desirable to take measurements on a plane on the order of a wavelength or larger distance above the earth's surface, the extra mathematical transformation to the surface of the earth consists of a straightforward application of the FFT.

4.4.4. Preliminary Computer Simulated Results

A hypothetical problem is proposed in Fig. 4. A point dipole scatterer lying in the horizontal direction is buried 5 meters beneath the ground and the amplitude A and phase ϕ of the field are measured on a square scan area at the surface. The frequency is 1 GHz, the data point spacing is $\lambda_a/2 = 15$ cm (assuming for simplicity that $\lambda = \lambda_a$), and the side of the square scan area has length L .

Knowing the analytic form for the spectrum $\bar{b}(\bar{K})$ of a point dipole, the amplitude of the electric field was computed at increasing depths z from eq (1) using the FFT algorithm discussed in section 4.4.3E. As discussed in section 4.4.3A, only that portion of the spectrum subtended by the scan area can be extracted from the data measured on the scan area. Thus only that portion of the spectrum was used to compute $|\bar{E}|$ from eq (1).

Figure 5 displays the results of the computations for a scan area of infinite length (Fig. 5a) and for a realistic scan area of 3 meters in length (Fig. 5b). The horizontal profiles are plotted directly over the point scatterer and only to the approximate depth of the scatterer because the symmetry of the problem makes any further curve plotting redundant.

Figure 5a displays the half-wavelength vertical and horizontal resolution distance predicted by eqs (7) and (8) for large scan areas. That is, an infinite scan area would allow the determination of the position of the scatterer to within about a half-wavelength. Unfortunately, as eqs (7) and (8) also predict, Fig. 5b shows that the resolution distances become larger when the 3 meter scan area is used. The horizontal resolution distance doubled to an acceptable one wavelength (predicted by eq (7)), but the vertical resolution distance increases to about the 5 wavelengths predicted by eq (8). Thus Fig. 5 graphically confirms the large predicted degradation in vertical resolution when the scan length is made smaller than the depth of the scatterer.

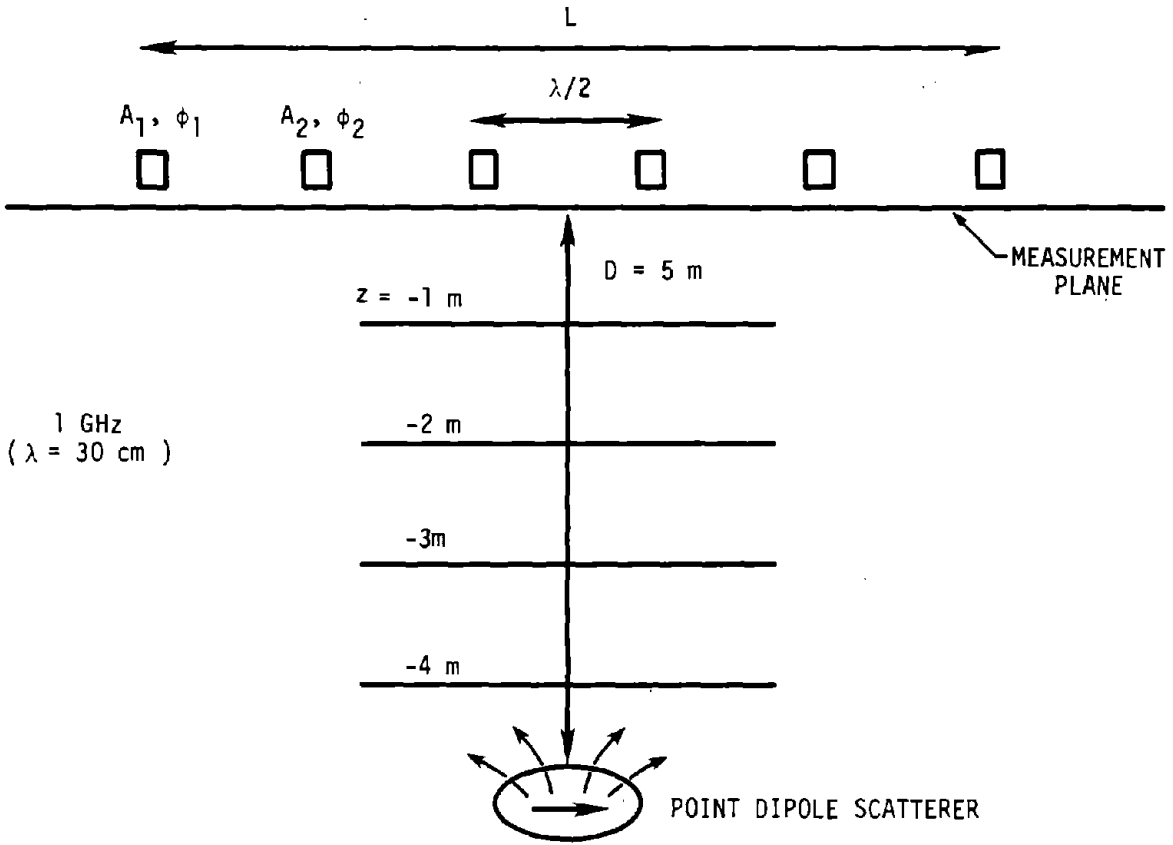


Figure 4. Hypothetical problem of point dipole scatterer.

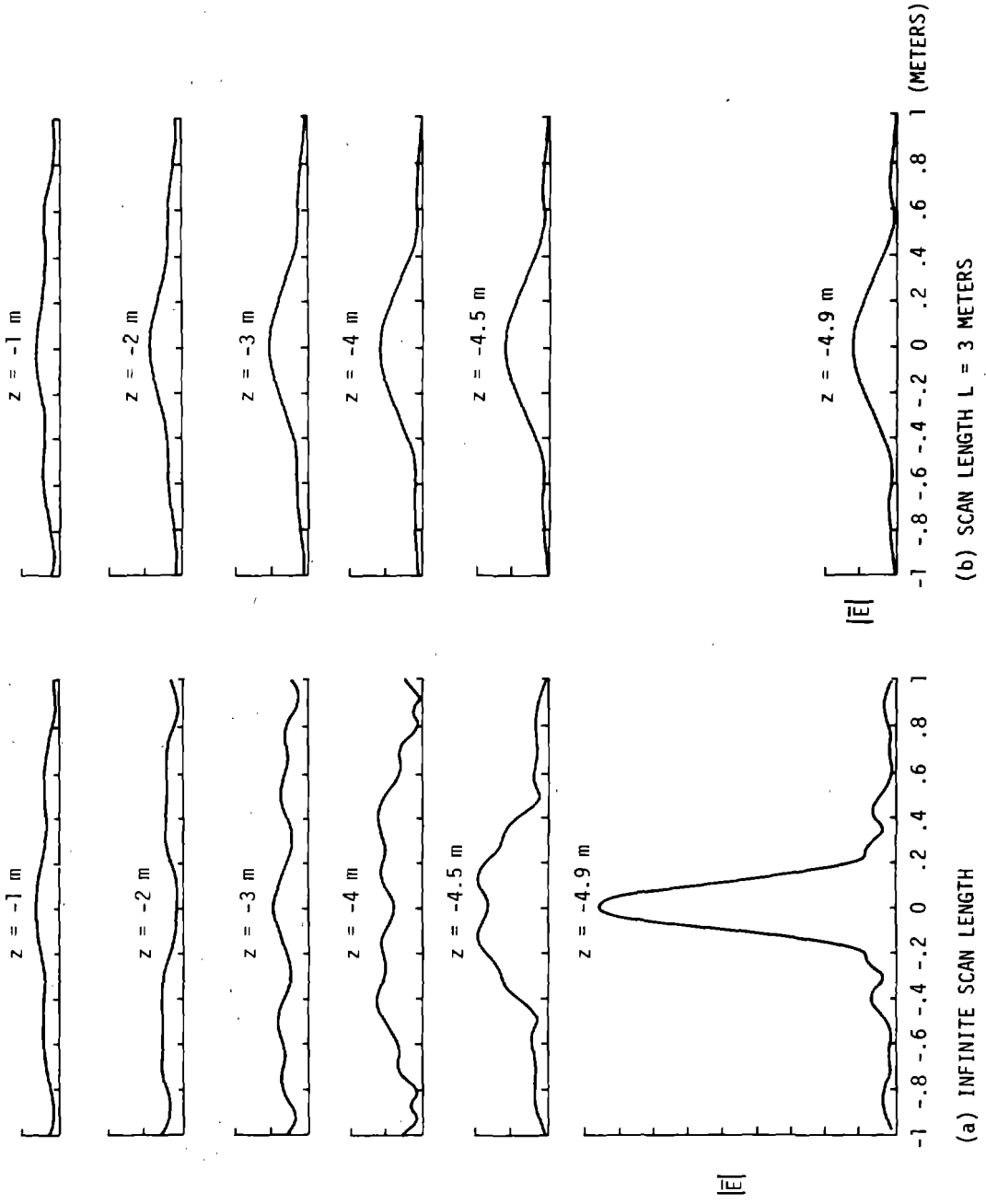


Figure 5. Amplitude of electric field.

However, these preliminary computer simulations have also been very encouraging in that they serve to show above all else that the PNFR technique does have the capability of determining the position of localized scatterers. Whether the encouraging results obtained here with this extremely clean model will be sustained in the more complex subsurface structure remains to be determined, along with methods for enhancing vertical resolution at depths greater than the scan length.

4.4.4.1 Possibilities for Enhancing Vertical Resolution

One way of enhancing vertical resolution distance to a wavelength or so is to increase the scan length to a value at least equal to the depth over which the subsurface structure is required. In the problem of the previous section this would mean increasing the scan area from a 3 meter square to at least a 5 meter square. This would also increase the number of measurement points from 400 to over 1100 (for each polarization). Even if the data point spacing could be increased to one wavelength, the number of measurement points remains in the hundreds. To keep the number of measurement points and associated time required to take the data at a reasonable amount, it may be necessary to find alternative methods for enhancing vertical resolution.

A simple method which could be tried involves plotting the phase of the scattered field as well as amplitude. In Fig. 5 only the amplitude of the scattered field is plotted. However, eq (1) also computes the phase. And hopefully, a plot of constant phase contours would help determine the centers of scattering somewhat more accurately. This phase method, which has not been tried yet, and may provide a beneficial increase in resolution, still suffers from the basic resolution limitations expressed approximately by eqs (7) and (8).

Another suggestion which has been made for enhancing resolution involves the idea of analytic continuation which, in principle, can yield infinitely precise resolution [152,sec. 6.6]. The idea can be explained rather easily by referring to eq (1). If the spectrum $\bar{b}(K)$ were known for all values of K including the evanescent modes (γ imaginary), then the computed electric field at a point source would approach infinity and two point sources could be resolved infinitely precisely. Unfortunately, as previously explained, the measurement of the electric field on the scan area allows $\bar{b}(K)$ to be computed from eq (4) only for the limited range of K subtended by the scan area. This limited determination of $\bar{b}(K)$ resulted in the reduced resolutions represented by eqs (7) and (8). In principle, however, $\bar{b}(K)$ can be shown from eq (1) to be an analytic function of K and thus it should be completely recoverable from a finite range of K by analytic continuation. A number of procedures have been proposed to perform the analytic continuation in practice, but

to date success has been obtained with only the simplest of sources and noise-free measurements [168].

A promising idea for increasing depth resolution is one borrowed from "Mother Nature", in particular the dual eye system for increasing vertical resolution. Two eyes separated by a distance much larger than their pupil diameters can resolve vertical distances to a much higher accuracy than a single eye. The principle involves the enhanced parallax enabled by the larger distance between the eyes. In a similar manner, two or more smaller scan areas should provide two or more spectra which each have maxima in the direction of the scatterers. If the two or more spectra were superimposed so that the intersection of their maxima could be determined, the distance to the intersection or centers of scatterers would be resolved more accurately. Implementation of this parallax idea for enhancing vertical resolution represents a challenging and enticing direction for future PNFR work.

Finally, if measurements are taken at many frequencies, vertical resolution could be enhanced by incorporating synthesized time-delay calculations. Specifically, the FM-CW system could be combined with PNFR to effect this enhancing time-delay capability. Probably, the major drawback to the complementary usage of the FM-CW and PNFR techniques would be the considerably greater amount of data which would have to be recorded and deconvolved.

5. TECHNIQUE ANALYSIS

5.1 Background

The major thrust of this phase was to choose an available technique that had a high potential to detect subsurface features which are pertinent in slope stability analysis. The one measurement technique that seemed to best fit the prerequisites of availability, practicality, portability, required level of user skill, and potential for further development was the FM-CW technique which is detailed below in section 5.3. One field test was to be conducted using this technique and to determine its capability to detect one chosen feature. The actual extent of the field tests depended to a large extent upon the availability of laboratory equipment and the knowledge of the geology and structure of available field sites.

The criteria for selection of a site for one field experiment to check the FM-CW technique was established, and reconnaissance was conducted along the Front Range of the Rocky Mountains in Colorado. Discussions between the USGS and the NBS were held to evaluate the relative importance of the geologic features in rock slope stability that might be effectively detected by electromagnetic measurement techniques. An attempt was made to define the size, orientation, frequency of occurrence, and filling material of joints.

5.2 Site Selection

The field site was selected after a search along the Front Range in Colorado from Estes Park south to Colorado Springs. The difficulty encountered in interpreting complex subsurface geology from surface derived information required the selection of the most geologically simple site as possible. The criteria for the selection of the site included a homogeneous rock mass, simple mineralogically as well as structurally, and with widely spaced fractures summarized from the following list of optimum site requirements set by the National Bureau of Standards:

1. Massive, homogeneous rock without foliation and many fractures.
2. Rock such as limestone or granite with simple jointing.
3. Avoid mafic igneous rocks, metamorphic rocks, and shales, mudstone, and evaporite.
4. Avoid extremely wet rocks.

5. Find rock mass with single joint approximately parallel to surface.
6. A boundary between two rock types can serve same purpose as a joint.
7. The required surface or discontinuity can be filled with water, gouge, breccia, clay, etc.
8. A thick discontinuity is acceptable.
9. Avoid depths to discontinuities greater than 10 m, less would be preferable.
10. Locate a site with a moderate slope with easy access for equipment.
11. Alternate sites would facilitate final site selection. Ready access to the site required that driving distance be kept within reason from the USGS and the NBS offices.

The site finally chosen is a homogeneous block of granite of the Pikes Peak Formation exposed along Rampart Range Road, located in Pike National Forest on the Devils Head, Colo., 7.5' Quadrangle NE1/4, Sec. 3, T.9S., R. 69 W. (site 2, Fig. 6). The site was selected because the granite is simple mineralogically and structurally with high-angle joints spaced approximately 8 m apart. Field evidence indicated the development of nearly horizontal relief joints.

Observation of exposed granite blocks in the area (Fig. 7) revealed a crumbly weathered zone approximately 2 m beneath the surface outcrops. There was a concern that the drill holes would reveal a badly weathered zone at depth. Later drilling indicated this potentially serious problem did not exist within the rock mass.

A rough pace and compass map of the drill hole site at site 2 (Fig. 8) shows the exposed granite blocks along with the strikes and dips of high angle joints. Exfoliation relief jointing noted above is exposed at the site and at nearby outcrops as shown in Fig. 9.

In accordance with the NBS requirements, alternate sites were selected (Fig. 6). At site 1 a large block of granite is exposed bordered by high angle joints. Site 1 meets all the requirements set by the NBS. However, it was determined site 2 was better than site 1 due to the approximately 3 m vertical walls of granite flanking the southern edge of

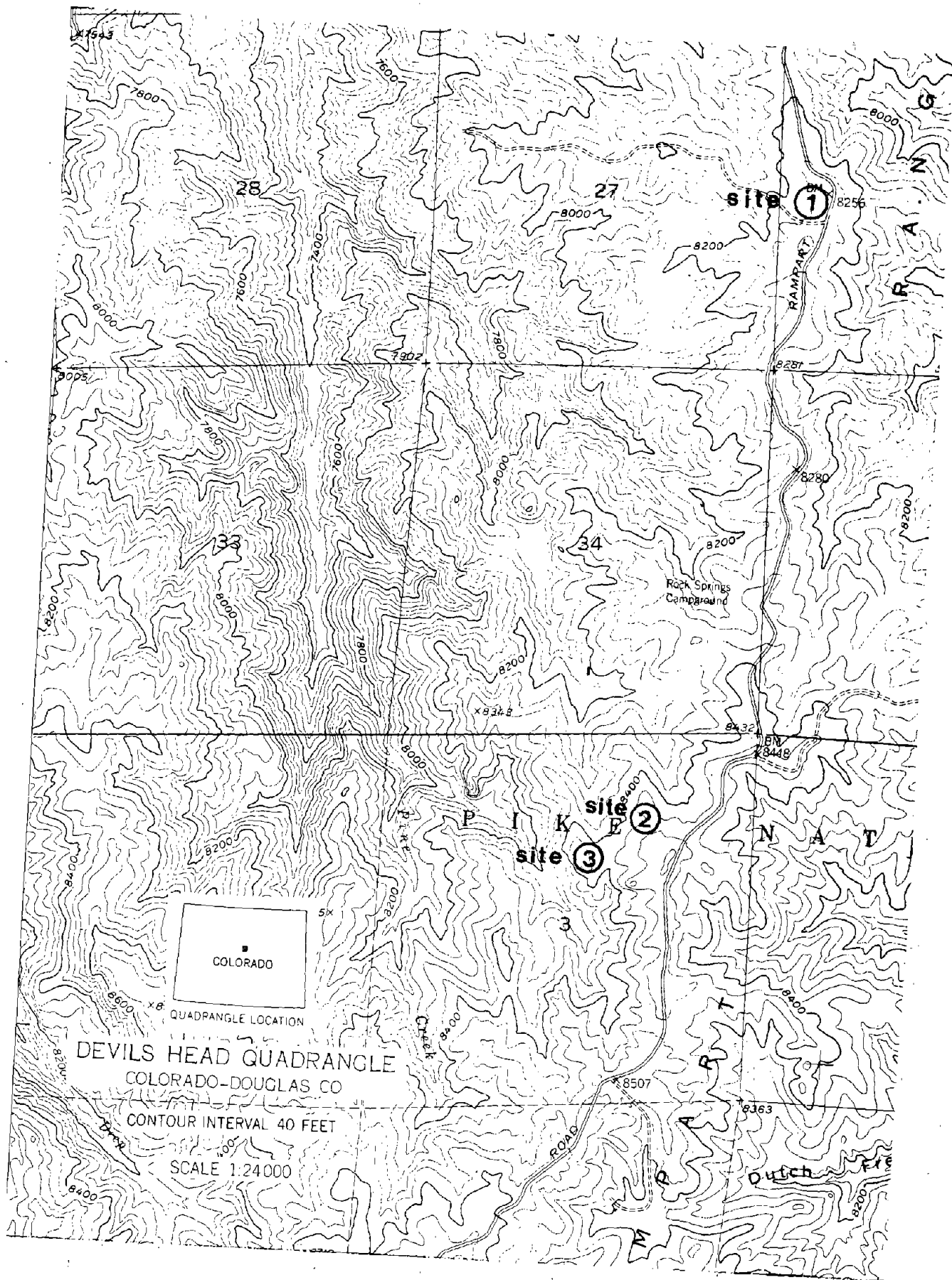


Figure 6. Location map.

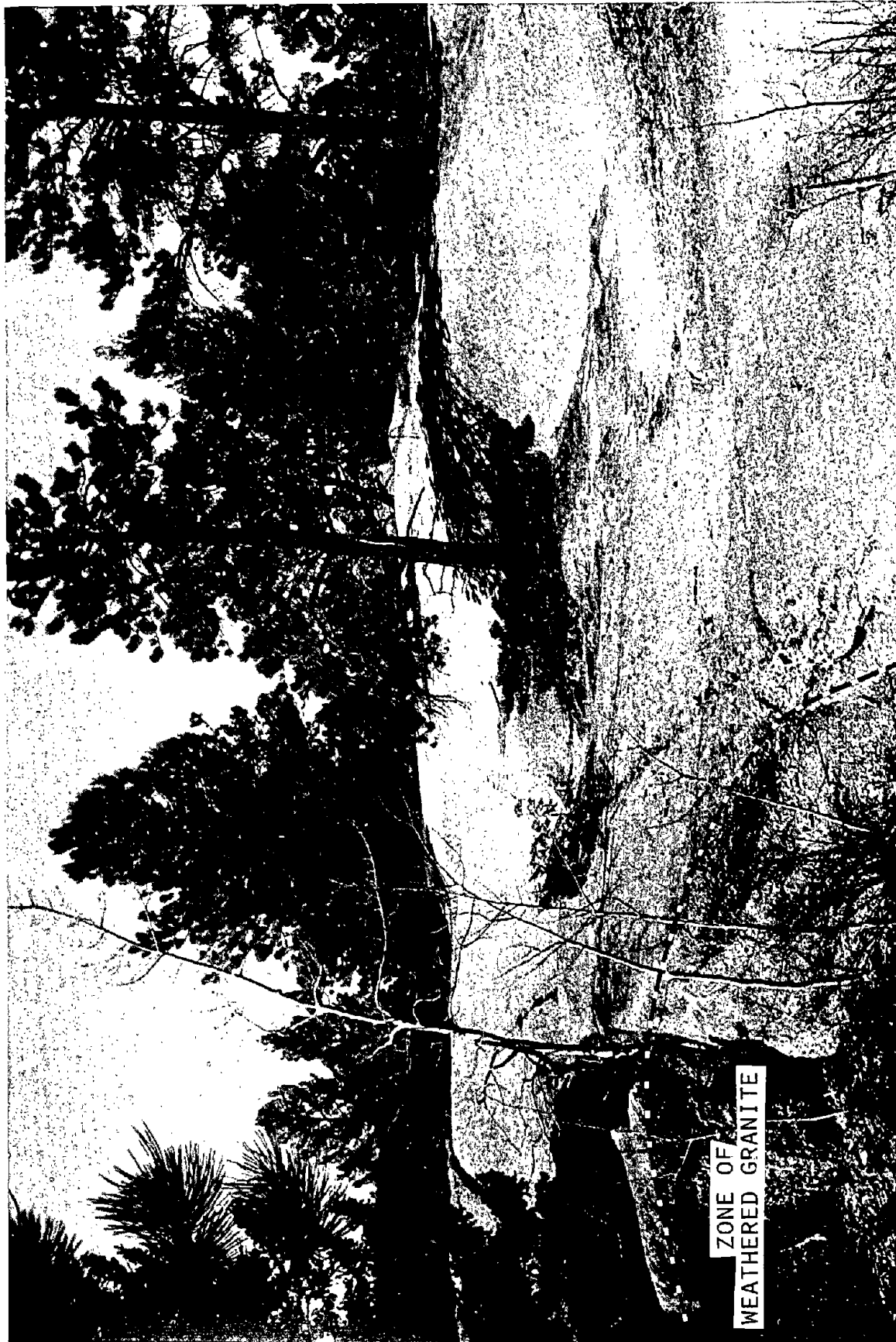


Figure 7. Photo of weathered granite near site 2.

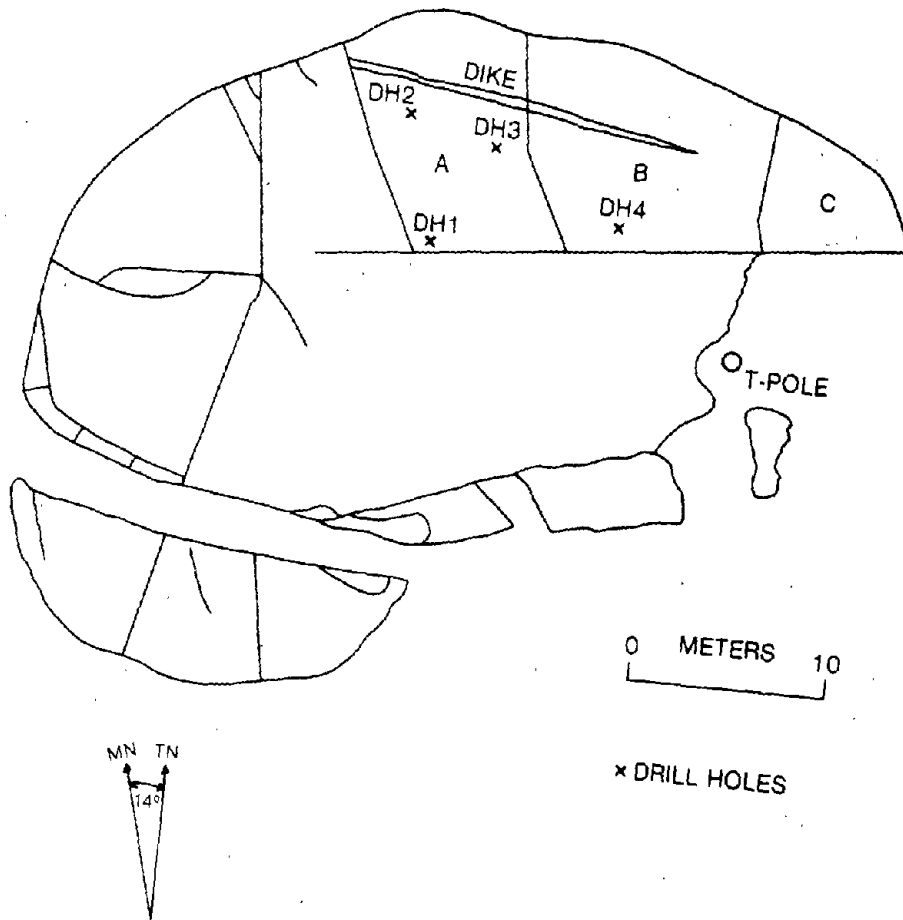


Figure 8. Rough map of drill hole locations site 2.



Figure 9. Photo of granite blocks showing high-angle and exfoliation joints.

blocks A, B, and C (Fig. 9). These walls allowed electromagnetic probing into the blocks from the side, as well as from the top.

Site 3 exposes a large exfoliation mass of granite used by the NBS for testing the FM-CW system (Fig. 10). However, because of the difficulty in moving drilling rigs onto the site, cores could not be obtained for this site.

5.2.1 Site Documentation

Four drill holes were cored in two adjoining blocks with total depths ranging from 8 to 12 m. This was done to accurately locate jointing at depth and to recover intact rock samples for lab determination of physical properties. The boreholes are located in Fig. 8 with a numerical ordering system based on the sequence in which they were drilled. By using a level and a 1.5 m grid system across the site, the elevation differences between the boreholes were obtained for depth correlations between holes. This also permitted contouring of the block surface using 200 mm contour interval. To avoid intersecting the high angle joints cross cutting the site, the drill holes were offset from the edges of the blocks. Boreholes 1, 2, and 3 were located in a triangular pattern approximately 6 m apart on a single block (A) of granite. Borehole 4 was located approximately 11 m from borehole 1 across a high angle joint providing cross joint control for geophysical work.

5.2.1.1 Mapping of Joints in the Project Area

The Pikes Peak Granite has many surface exposures along the Rampart Range Road and in the general area surrounding the field site. In addition to determining the orientation of joints present at the drill site, the nearby area was sampled by the blind method [169] for additional joint readings (Fig. 11). Fifty-seven joint readings were obtained allowing determination of the preferred regional orientations of the joints. However, bias exists when taking joint readings of obvious joints by the blind sampling methods. Tests of this method indicate that this bias was independent of the operator in all except almost randomly jointed rocks. Also, in many regularly jointed rock masses, as few as 50 measurements were found to be adequate.

The data obtained from mapping the joints may be presented in two different statistical plots, histograms and stereographic projections. By the use of statistical plots, a large number of scattered observations can be pooled together about a single origin in a composite diagram. A common method of plotting and presenting a large number of orientation measurements is by means of joint histograms (Fig. 12) and rosettes (Fig. 13).



Figure 10. Testing the FM-CW system.

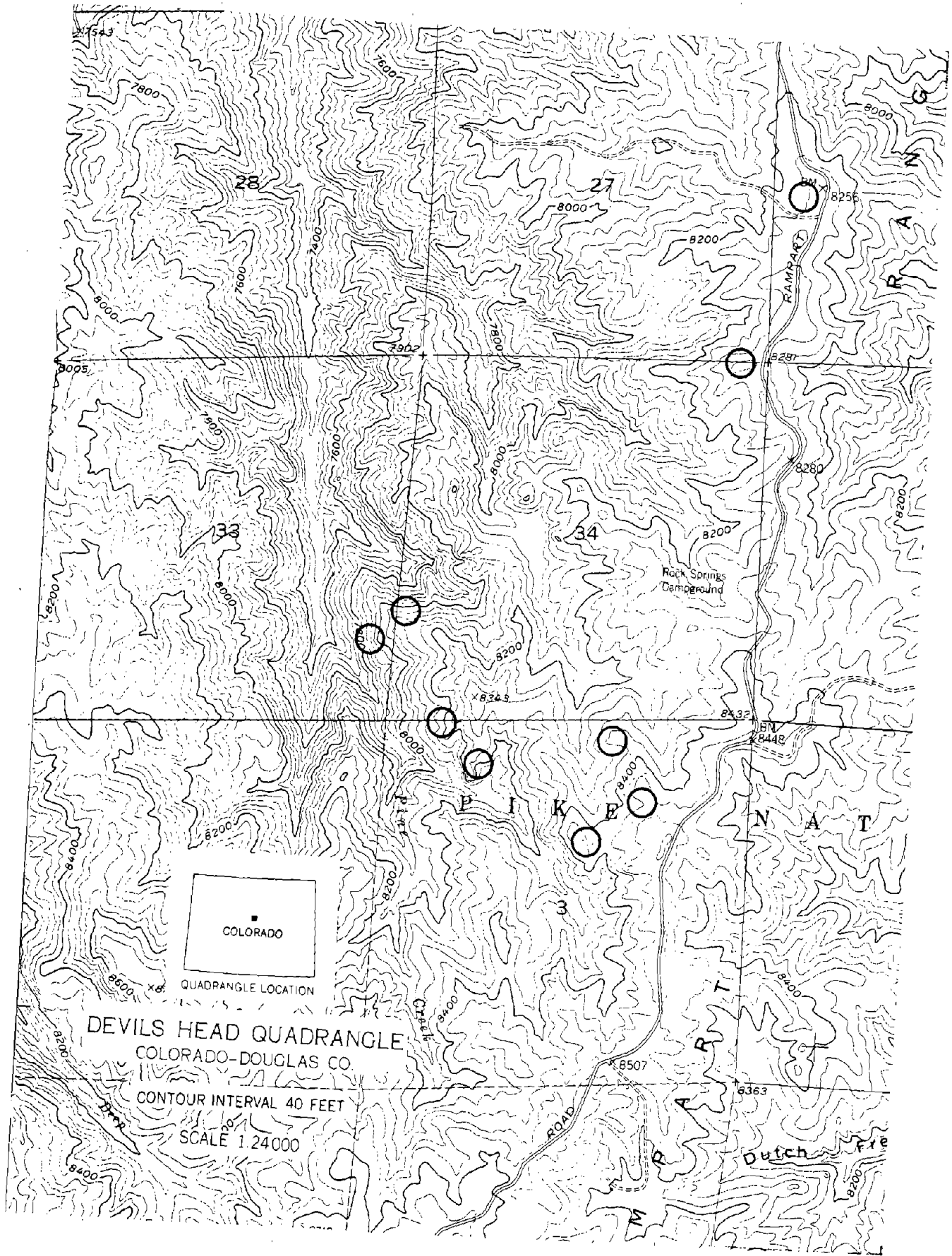


Figure 11. Joint sampling sites.

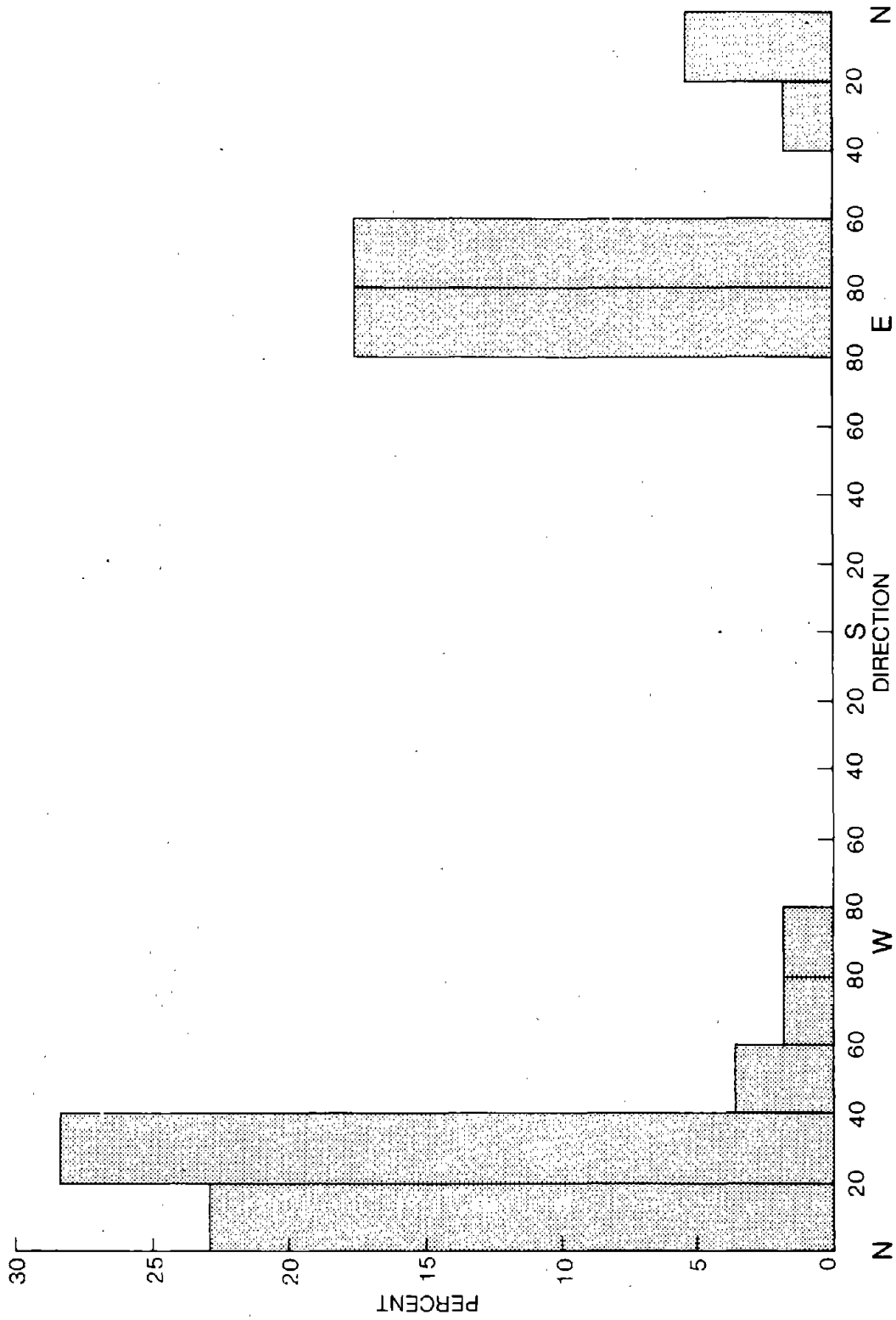


Figure 12. Joint histograms.

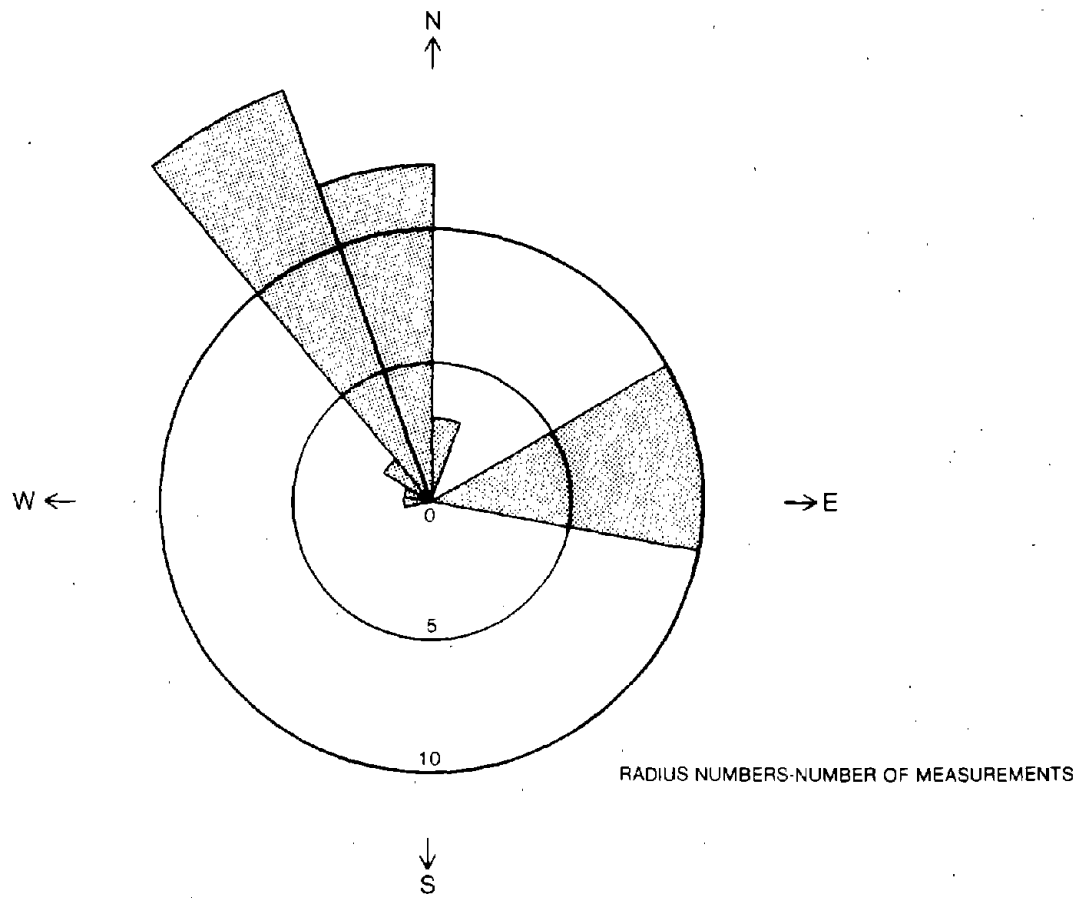


Figure 13. Joint rosettes.

Along the X-axis of the histogram (Fig. 12) dip directions are given in 20 increments while along the Y-axis a percentage of the joints in each increment was plotted. In a histogram, the area of a given class is proportional to the percentage of total values in that class.

On the joint rosette (Fig. 13) measurements are marked from 0°-360° with radial lines at 20° intervals. The grouped observations are represented along the radial lines with the concentric 5 and 10 circles representing the number of observations. However, it should be noted since the area plotted for a class is not proportional to the class abundance, large concentrations of observations are exaggerated and low concentrations are suppressed. The histograms and the rosette indicate two primary sets of high-angle joint strike directions:

N. 60-90 E.
N. 0-40 W.

The attitude of a plane is best described in a spherical coordinate system or a stereographic projection. A Lambert equal-area projection, or Schmidt net, is used in the report for the three-dimensional analysis of joint data. The equal-area method is vastly superior to strike diagrams of the histogram and rosette. Those diagrams cannot show simultaneous variation in both strike and dip; thus, they may give misleading impressions of angular relations and symmetry.

In order to find the preferred regional orientations of the joints, 62 poles of the joint readings taken in the area were plotted (Fig. 14). Then by using a center counter and a peripheral counter on a grid system the pole densities were determined. Pole densities were then contoured and by taking the central value of the highest concentration of poles the mean orientation for the joint sets was found. However, since there is a variance connected with that mean, orientation is a random variable. The mean values for the joints are shown in Fig. 14.

5.2.2 Technical Description of Rock Cores

A large amount of information concerning the in situ rock mass can be determined from the borehole cores. The cores at the site were sectioned in approximately 1.5 m intervals. The only exception is the last segment of borehole 4, which is 2.37 m in length. These closely spaced sample intervals provide a tight control for an accurate location of subsurface features.

Technical descriptions of the cores were prepared at the drill hole site according to Deere [170]. The guidelines for the description of

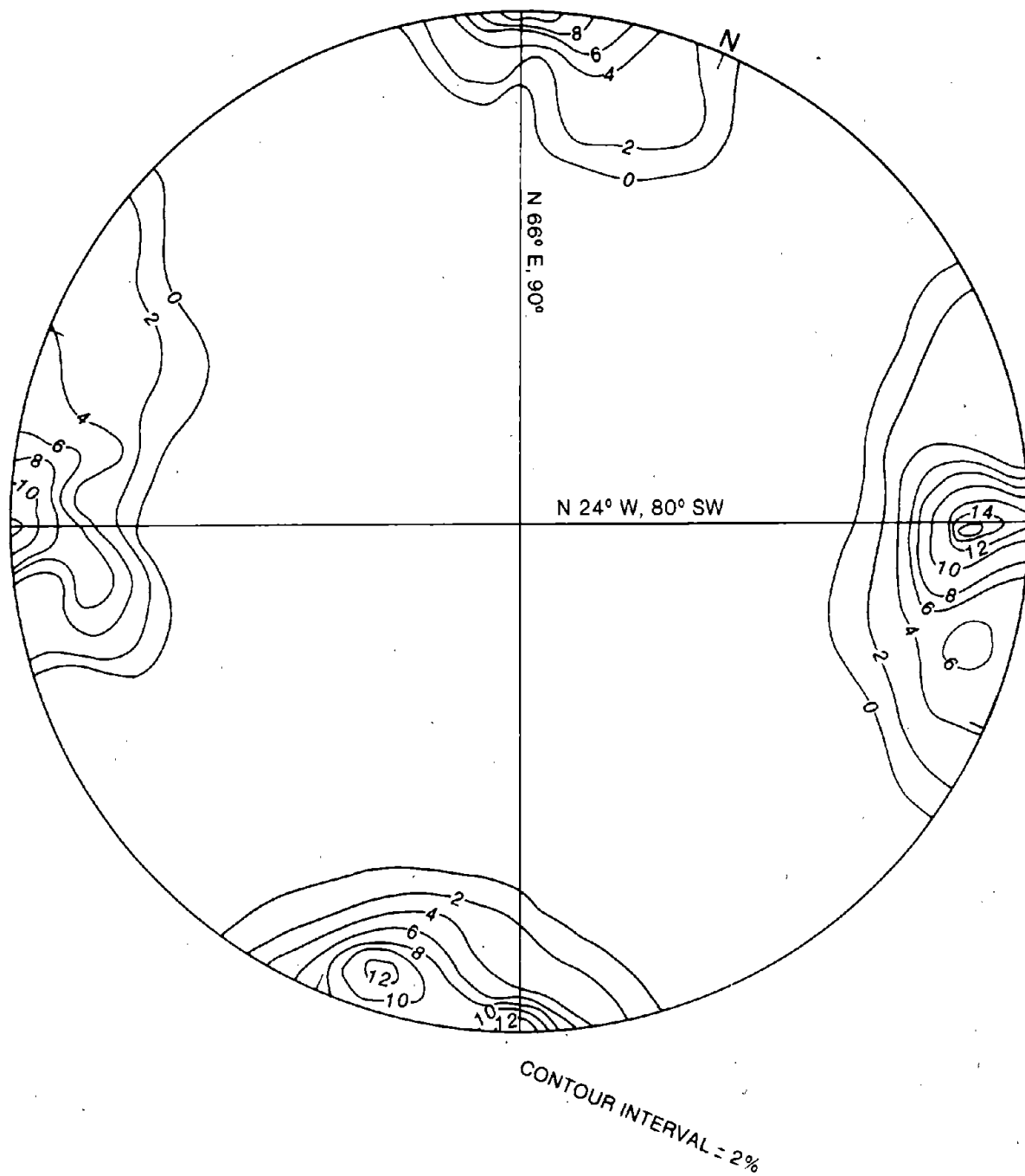


Figure 14. Contoured pole plots for joint data.

joint spacings (table 11) and the degree of weathering [171] (table 12) in granite can be used to qualitatively describe the cored sections.

Along with obtaining an estimate of the core loss per cored section, the RQD (Rock Quality Designation) was determined for each drilled segment. RQD is a measure of rock mass quality derived from recovered core. The RQD value is the sum of the total lengths of recovered core greater than 100 mm divided by the length of the section cored, expressed as a percentage. A description of rock mass quality based on RQD values is shown in table 13.

Table 11. Descriptive Terminology for Joint Spacing
(adopted from Deere, 1964) [170]

Descriptive Term	Spacing of Joints
Very close-----	Less than 50 mm
Close-----	50 - 300 mm
Moderately close-----	300 mm to 1000 mm
Wide-----	1 - 3 m
Very wide-----	greater than 3 m

Table 12. Rock Weathering Classification
(from Clayton and Arnold, 1972) [171]

Class 1, Unweathered Rock.--Unweathered rock will ring from a hammer blow; cannot be dug by the point of a rock hammer; joint sets are the only visible fractures; no iron stains emanate from biotites; joint sets are distinct and angular; biotites are black and compact; feldspars appear to be clear and fresh.

Class 2, Very Weakly Weathered Rock.--Very weakly weathered rock is similar to class 1, except for visible iron stains that emanate from biotites; biotites may also appear "expanded" when viewed through a hand lens; feldspars may show some opacity; joint sets are distinct and angular.

Class 3, Weakly Weathered Rock.--Weakly weathered rock gives a dull ring from a hammer blow; can be broken into "hand-sized" rocks with moderate difficulty using a hammer; feldspars are opaque and milky; no root penetration; joint sets are subangular.

Class 4, Moderately Weathered Rock.--Moderately weathered rock may be weakly spalling. Except for the spall rind, if present, rock cannot be broken by hand; no ring or dull ring from hammer blow; feldspars are opaque and milky; biotites usually have a golden yellow sheen;

Class 5, Moderately Well Weathered Rock.---Moderately well weathered rock will break into small fragments or sheets under moderate pressure from bare hands; usually spalling; root penetration limited to fractures, unlike class 6 rock where roots penetrate through the rock matrix; joint sets are weakly visible and rounded; feldspars are powdery; biotites have a light golden sheen.

Class 6, Well Weathered Rock.--Well weathered rock can be broken by hand into sand-sized particles (grus); usually so weathered that it is difficult to determine if rock is spalling, roots can penetrate between grains; only major joints are preserved and filled with grus; feldspars are preserved and filled with grus; feldspars are powdery; biotites may appear silver or white in thin flakes.

Class 7, Very Well Weathered Rock.--Very well weathered rock has feldspars that have weathered to clay minerals and rock is plastic when wet, no resistance to roots.

Table 13. Rock Quality Based on RQD Values

RQD (percent)	Description of Rock Quality
90-100	Excellent
75-90	Good
50-75	Fair
25-50	Poor
0-25	Very Poor

During the coring operation it was also desirable to estimate the water loss in the joints per coring run as an indication of the magnitude of joint separation and nature of filling material. The water loss was

calculated with the use of a recirculating tank and a meter stick (Fig. 15).

5.2.3 Seismic Refraction Survey Analysis of the Drill Hole Site

The in situ P-wave seismic velocity at the drill-hole site was calculated with the use of a Bison Signal Enhancement Seismograph, and was found to be approximately 3048 m/s for the granite block containing drill holes 1-3. In order to obtain this value, four seismic profiles were patterned across the drill hole site. The profiles were carefully positioned to avoid intersecting any of the high-angle joints bordering the block. The main advantage of calculating field velocity is that it provides a bulk assessment of the properties of the intact rock for comparison with lab testing of intact core samples. Field velocity is affected by the number and type of joints present in the rock mass. In this case no joints were visibly intersected and the field velocities were obtained to provide comparative data for lab data.

The effect of mass weathering in the rock mass is determined by comparing the field velocity (V_F) with the sonic P-wave velocity (V_L) obtained on intact samples in the laboratory. The field velocity is a mass measure of the total mass whereas the lab samples were selectively chosen from the cores. As the velocity ratio (V_F/V_L) approaches one, the quality of the rock mass increases. Using a calculated V_F value of 3048 m/s, and a V_L value of 3246 m/s, the mean value from 11 samples, the velocity ratio is 0.939. As expected, the velocity ratio at the drill site is less than one due to the presence of slight mass weathering in the rock mass. The closeness to 1.0 indicates the absence of any undetected joints or similar velocity reducing features within the rock mass.

The ratio of the shear wave velocity in the field to the shear-wave velocity measured in core samples may also be calculated, but due to difficulties in generating, recording, and interpreting shear-wave velocities in the field, this has not been determined at this site.

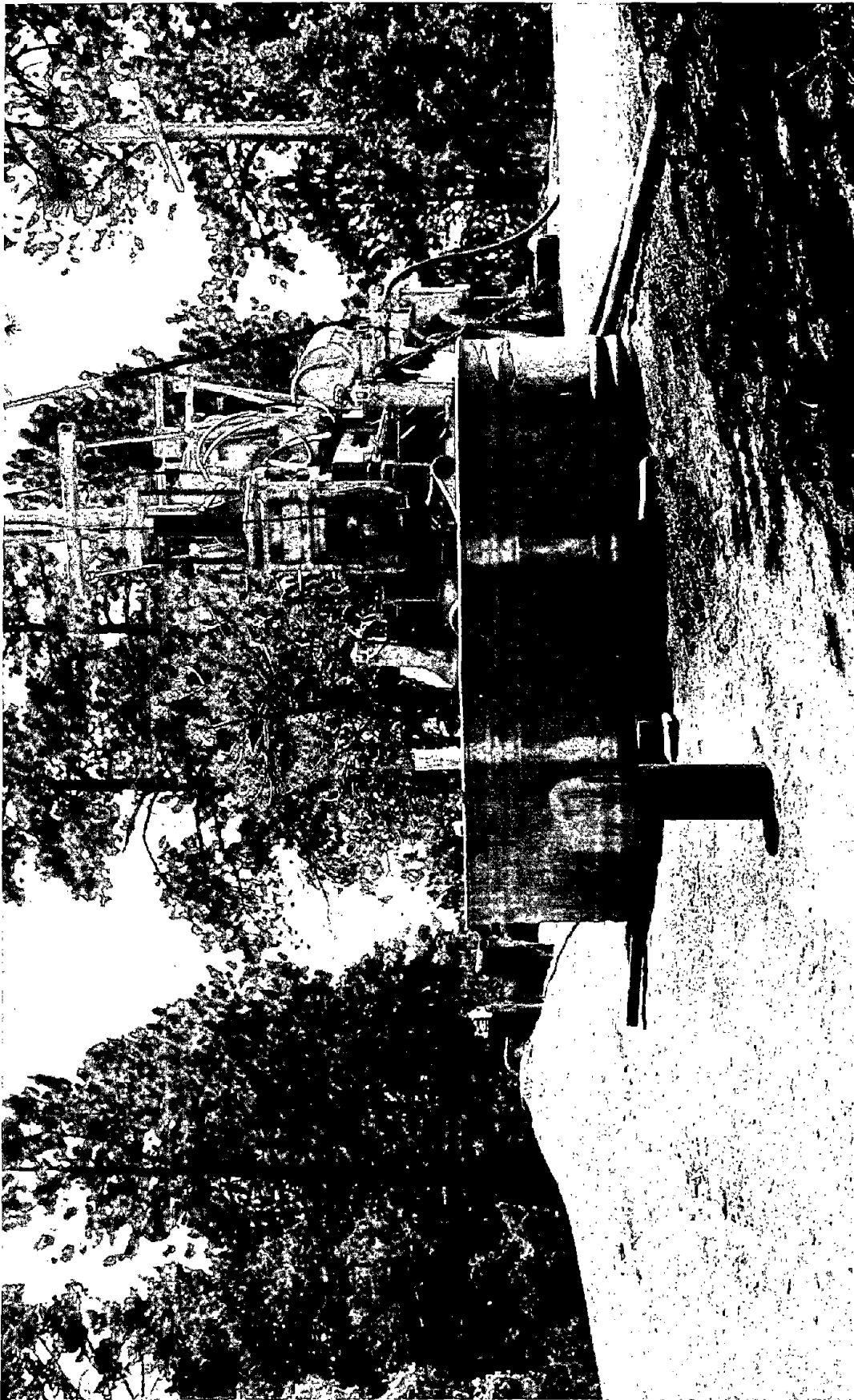


Figure 15. Photo of recirculating tank.

5.2.4 Borehole TV

A borehole TV camera was used to accurately locate joints in the boreholes. The borehole TV camera takes continuous oriented pictures from the inside of the drill hole. The use of the TV allows for the location of joints in remarkable detail. Not only are the depths of the joints located, but also their number, thickness, surface roughness, and orientation can be determined. A complete description of the joint system was obtained, which can be stored on video tape and be studied at a later time. Cross sections using the data obtained from the cores were modified with data obtained from the TV record.

5.3 FM-CW Technique

The use of microwaves for the evaluation of material properties is becoming increasingly important because they can propagate through many materials. The velocity of propagation and the attenuation that the signal undergoes as it propagates are dependent upon the properties of the medium through which it is propagating.

The FM-CW measurement technique [127,128,129] is based upon electromagnetic theory that assumes that each medium, i.e., free space, air, granite, etc. can be described as linear, homogeneous, and isotropic. Linearity implies that the electromagnetic response or output voltage from the medium is directly proportional to the input voltage. Homogeneity implies that the electromagnetic properties of a medium are constant from point to point. Isotropy implies that the electromagnetic properties of a body in the neighborhood of some interior point are the same in all directions. Moreover, it is assumed that the medium has parallel plane boundaries and can be divided into small linear, homogeneous, isotropic layers as shown in Fig. 16.

The propagation through each layer can be calculated and each contribution mathematically added to the previous one, thereby generating a total result. Electromagnetic properties of each layer can be described by permeability μ , permittivity ϵ , and conductivity σ . All layers are assumed non-magnetic, i.e., $\mu = \mu_0$, where $\mu_0 = 4\pi \times 10^{-7}$ h/m. Additionally, ϵ is assumed to be independent of frequency over the measurement bandwidth. It should also be noted that the relative dielectric constant ϵ' is equal to ϵ/ϵ_0 where ϵ_0 is the permittivity of free space equal to 8.854×10^{-12} f/m.

Optical ray paths for the electromagnetic energy radiated from the transmitting antenna or horn are also assumed. In general, electromagnetic waves propagating in a material undergo an attenuation

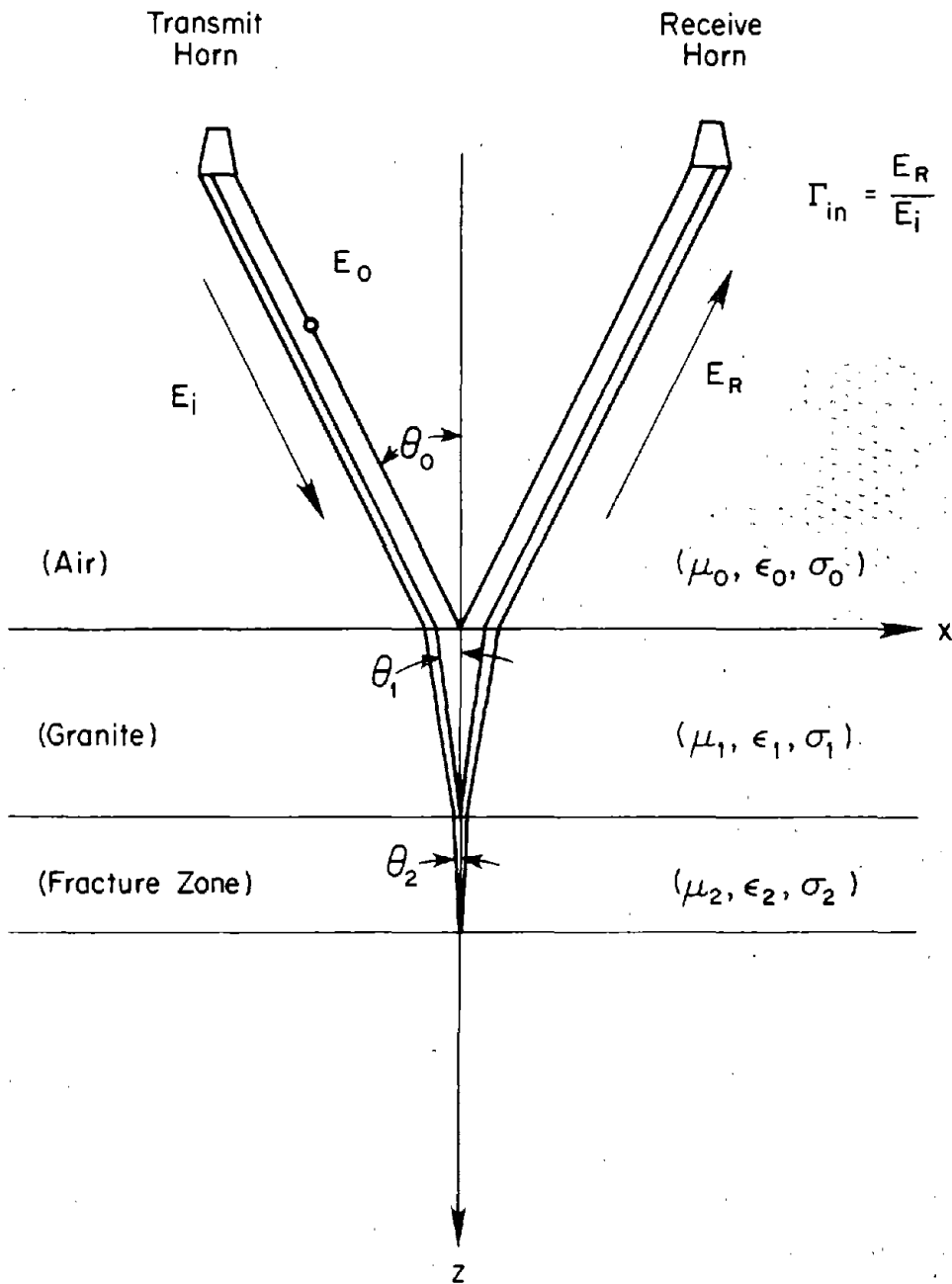


Figure 16. Model of ray paths for a two layer material.

with an attenuation constant α as well as a phase change with a phase constant β . Therefore, it is useful to determine the real and imaginary parts of the complex propagation constant [172]. Thus, if

$$\gamma = \alpha + j\beta = j\omega \sqrt{\mu\epsilon} \left[1 - j\frac{\sigma}{\omega\epsilon} \right]^{1/2} \quad (12)$$

then

$$\alpha = \omega \left(\frac{\mu\epsilon}{2} \right)^{1/2} \left[\left(1 + \frac{\sigma^2}{\omega^2 \epsilon^2} \right)^{1/2} - 1 \right]^{1/2} \quad (13)$$

and

$$\beta = \omega \left(\frac{\mu\epsilon}{2} \right)^{1/2} \left[\left(1 + \frac{\sigma^2}{\omega^2 \epsilon^2} \right)^{1/2} + 1 \right]^{1/2} \quad (14)$$

The intrinsic impedance η of the material in each layer is given by

$$\eta = \left[\frac{\mu}{\epsilon \left(1 + \frac{\sigma}{j\omega\epsilon} \right)} \right]^{1/2} \quad (15)$$

If the antenna orientation is chosen so that the electric field vector E_0 in Fig. 16 is normal to the plane of incidence (xz plane), then the input reflection Γ_{in} at a material surface can be written in terms of the impedance Z [172] in region 0 and 1 as

$$Z_0 = \eta_0 \sec \theta_0 \quad (16)$$

$$Z_1 = \eta_1 \sec \theta_1 \quad (17)$$

and

$$\Gamma_{in} = \frac{Z_1 - Z_0}{Z_1 + Z_0} = \frac{\eta_1 \sec \theta_1 - \eta_0 \sec \theta_0}{\eta_1 \sec \theta_1 + \eta_0 \sec \theta_0} \quad (18)$$

For small losses where $\frac{\sigma}{\omega \epsilon} \ll 1$, eq (18) can be reduced to

$$\Gamma_{in} \cong \frac{\sqrt{\epsilon'_0} \cos \theta_0 - \sqrt{\epsilon'_1 - \epsilon'_0 \sin^2 \theta_0}}{\sqrt{\epsilon'_0} \cos \theta_0 + \sqrt{\epsilon'_1 - \epsilon'_0 \sin^2 \theta_0}} \quad (19)$$

Figure 17 is a block diagram of the FM-CW microwave measurement system [128]. In principle, the microwave signal generator is swept through a band of frequencies so that a linear frequency vs. time output signal is produced. The governing factors that have to be considered for frequency range of sweep, f_1 to f_2 , include: the material thickness and its attenuation constant and the return loss of the second and succeeding interfaces. Normally, the lowest band of frequencies is chosen to achieve maximum penetration. However, there are tradeoffs since lower frequencies tend to limit bandwidth, thereby limiting target resolution.

The microwave signal travels from the generator to the mixer via more than one path. If the electrical lengths of the paths are identical, the reference and test signals going into the mixer would arrive at the same time, and the instantaneous rf frequencies would be identical at all times. However, the test signal will arrive at a later time because that signal goes through the antennas via the granite sample. A portion of the test signal is reflected at the air-granite interface, and another portion is reflected at the granite-fracture zone interface. These reflected signals will arrive at the mixer at times t_2 and t_3 respectively, as shown on Fig. 17 and for the actual data as shown in Fig. 23. Since all inputs to the mixer arrive at different times, the instantaneous microwave frequencies differ. The mixer is a product demodulator and has an output that is a function of the product of the inputs. Only the lowest frequency components in the output are preserved; the higher frequencies are filtered out. The lower frequency components are displayed on a spectrum analyzer. The location of the first peak is a function of the distance from the antennas to the granite surface. The location of the next peak is a function of that distance plus the granite layer depth and its dielectric constant.

The reference signal arriving at the mixer is

$$e_1 = E_1 \cos \omega(t) t, \quad (20)$$

while the test signal reflected from the granite surface is,

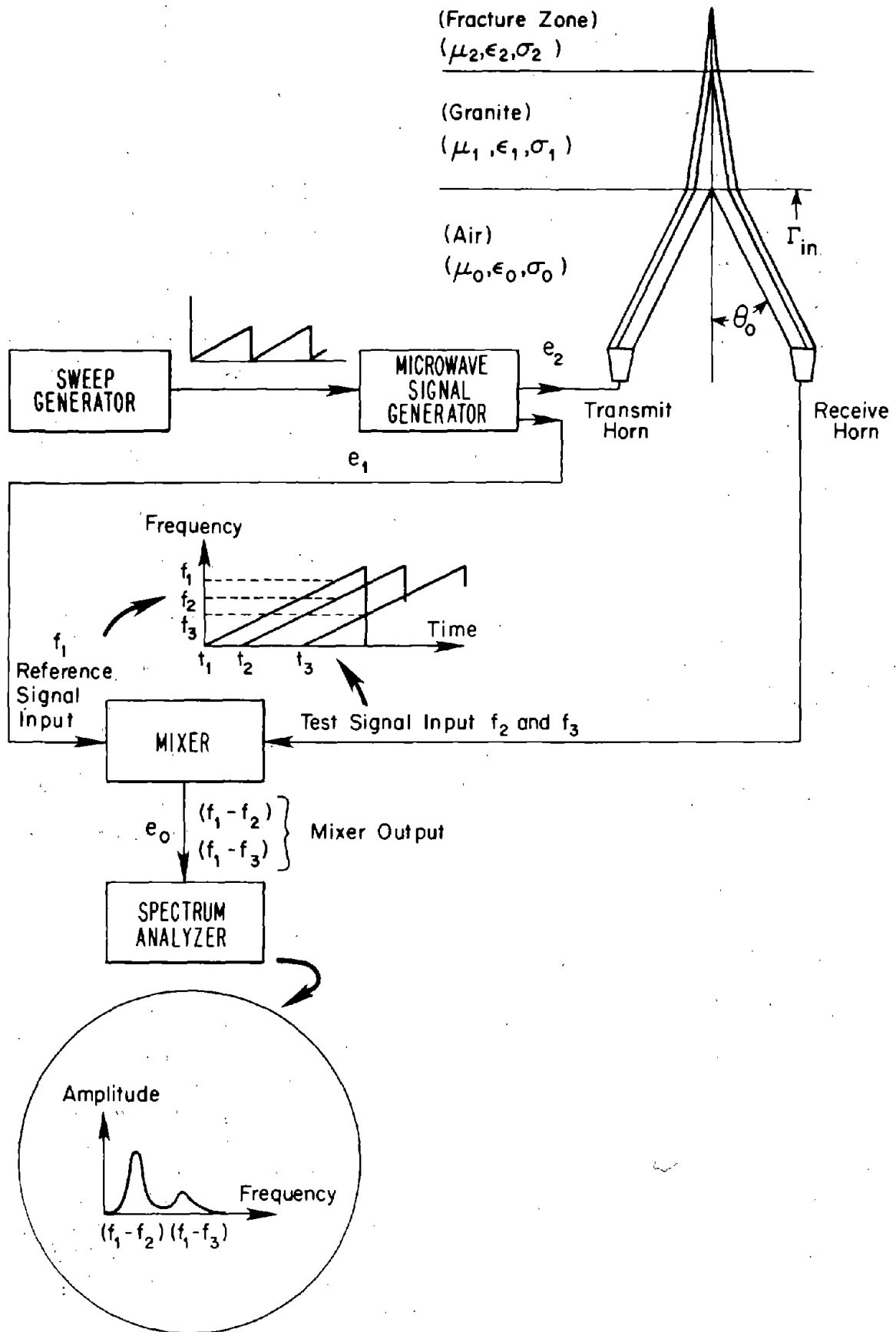


Figure 17. Block diagram of the FM-CW measurement system.

$$e_2 = \Gamma_1 E_2 \cos \left[\omega(t) \left(t + \frac{2R}{c} \right) \right], \quad (21)$$

where $2R/c$ is the time required for the signal to travel a distance R from the transmitting antenna to the granite surface and back to the receiving antenna.

The received waveform has been analyzed by Ellerbruch and Belsher [128] which in practice compares the instantaneous output frequency with the frequency returning from the granite surface. The difference frequency fd is related to the distance to the granite surface and the dielectric constant of the intervening material by

$$d = \frac{c \, fd}{2 \sqrt{\epsilon_1} (f_2 - f_1)/t_s} \quad (22)$$

These difference frequencies for granite surfaces are displayed as amplitude with respect to frequency (see Fig. 17) which is equivalent to time or distance to the granite surface. Equation (22) can be used to determine the material thickness d or the dielectric constant ϵ_1 . The dielectric constant ϵ_1 can be obtained for granite by several techniques discussed in [127]. The value for bandwidth $(f_2 - f_1)$ is read from the frequency scale from the microwave generator while the value for sweep time t_s is chosen after bandwidth selection to provide sufficient spectrum bandwidth out of the mixer for frequency processing.

5.4 Experimental Results

5.4.1 Field Tests by NBS

5.4.1.1 Evaluation of the FM-CW System

The theories developed for all microwave measurements on the granite test site assumed ray paths for the electromagnetic energy radiated from the horn antenna (Fig. 16). Modern day antennas are designed as closely as possible to approximate the single ray model. In practice, the antennas are not 100 percent directive leaving a certain degree of uncertainty in the single ray model. The single ray model approximation can be helped by proper antenna placement and polarization. In addition, improvements in antenna directivity and in providing better isolation between them greatly decreases the susceptibility of the measurement system to spurious reflections from surrounding obstacles.

Two different sizes of antennas were used in the preliminary testing of the FM-CW system. The antennas were broadband rectangular aperture

horns which utilize double ridged waveguide techniques [173]. The smaller horns (Fig. 18) are suited to high frequency applications between approximately 1 to 10 GHz, while the larger horns (Fig. 19) are used for lower frequency applications between approximately 200 to 2000 MHz. Typically, both types of antennas exhibit better beam width characteristics toward the upper end of their frequency ranges. The larger horns were ultimately used for the on site experiments mainly because of better range of penetration into the granite. For maximum penetration and resolution, different frequency bands were tried between 200 and 2000 MHz. Subsequent tests showed that the best test results using available equipment were obtained for the frequency band between 1 and 2 GHz.

Initial evaluation of the FM-CW system using both antenna types was demonstrated on a granite boulder (Figs. 18 and 19) approximately 17 feet thick (5.2 m) located near test site 3. The experimental results were successful in demonstrating that a reflected electromagnetic wave from the back surface of the granite boulder could be detected through 17 feet (5.2 m) of granite at the front surface. Also, a measured value for the dielectric constant ϵ' of approximately 5.3 was obtained for the granite boulder by transmission techniques [127]. This value was later used in eq 22 to determine the distance to subsurface responses from FM-CW measurements taken from the surface at test site 2. Additional testing with the FM-CW system was conducted on test site 3 (Fig. 10) using the smaller antennas. This concluded the preliminary testing and evaluation of the FM-CW system. The final test results showed the potential of the FM-CW system to detect subsurface features in granite.

5.4.1.2 Experimental Results From the Field Test Site

The field test was conducted at test site 2 using the FM-CW technique. Figure 20 is a photo of drill holes 1, 2, and 3 on site 2. Figures 21 and 22 show the setup of the FM-CW system on site 2. To achieve proper antenna height and orientation, the large horn antennas were mounted inside a rectangular metal frame on adjustable legs. The rectangular blocks situated next and between the antennas are absorbent material used to eliminate interference and reflections between antennas. For convenience and additional shielding, a large rectangular metal plate was placed on top of the metal frame between the antennas.

A number of measurements were taken near each drill hole (1-4) to determine if differences in subsurface features could be detected. Some differences were noted and were compared with data from the core samples. Based upon data from the core samples, it appeared that the most comprehensive test results could be obtained from the area bounded by drill holes 1, 2, and 3 with antenna placement closer to drill hole 3.

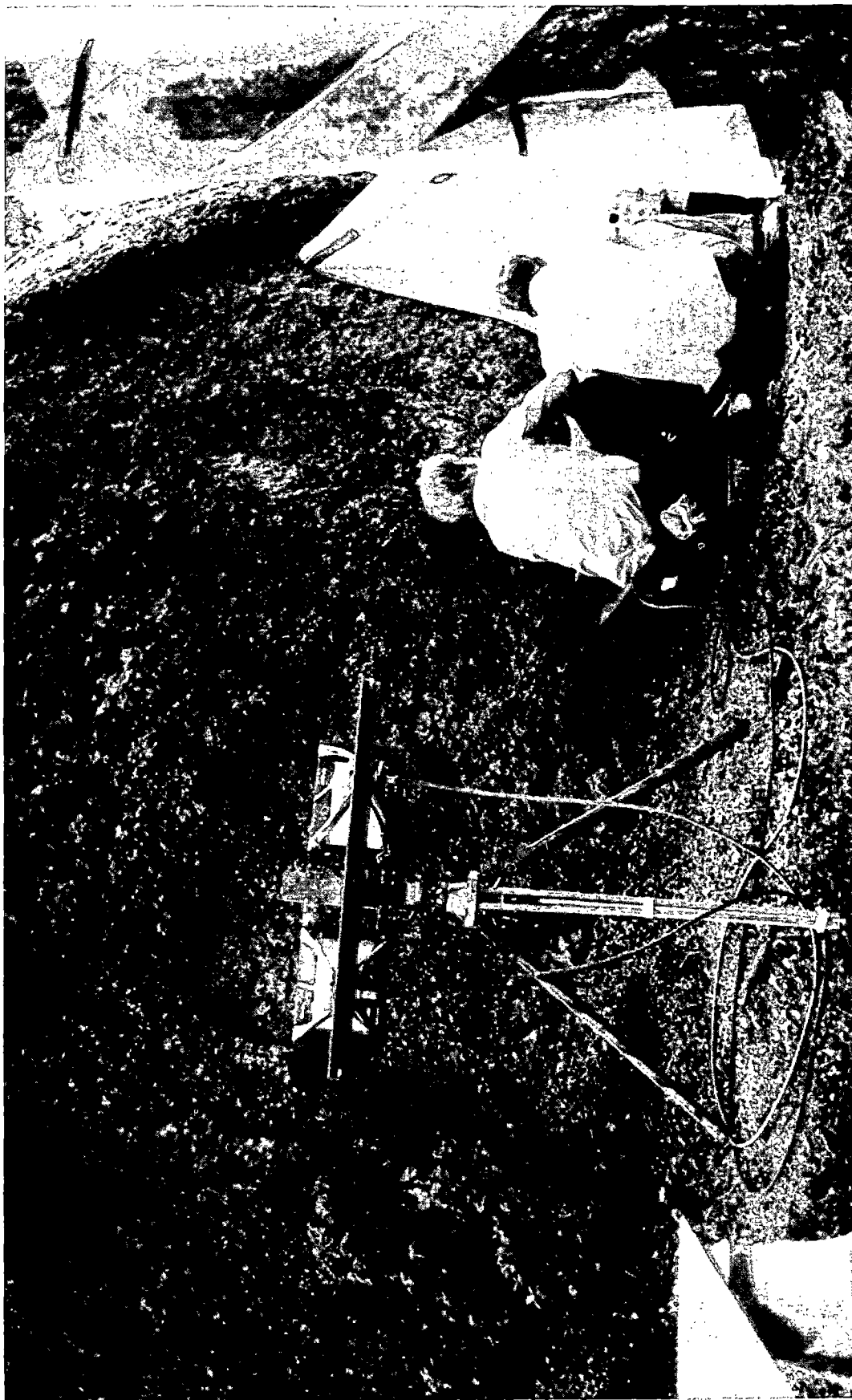


Figure 18. Small broadband rectangular aperture-horns radiating into granite boulder.

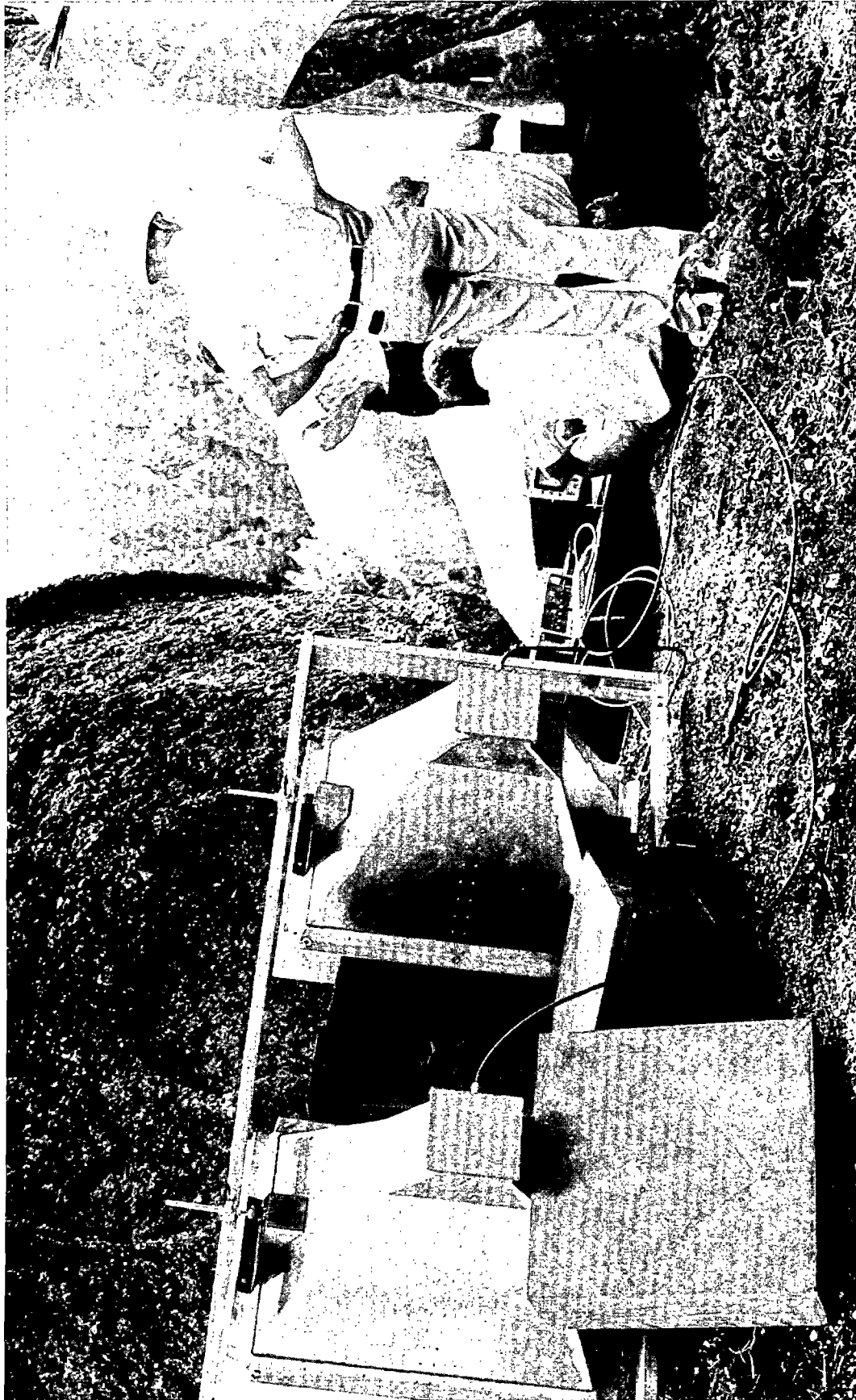


Figure 19. Large broadband rectangular aperture-horns radiating into granite boulder.



Figure 20. Photo of drill holes 1, 2, and 3 on site 2.



Figure 21. Test setup of FM-CW system on site 2.

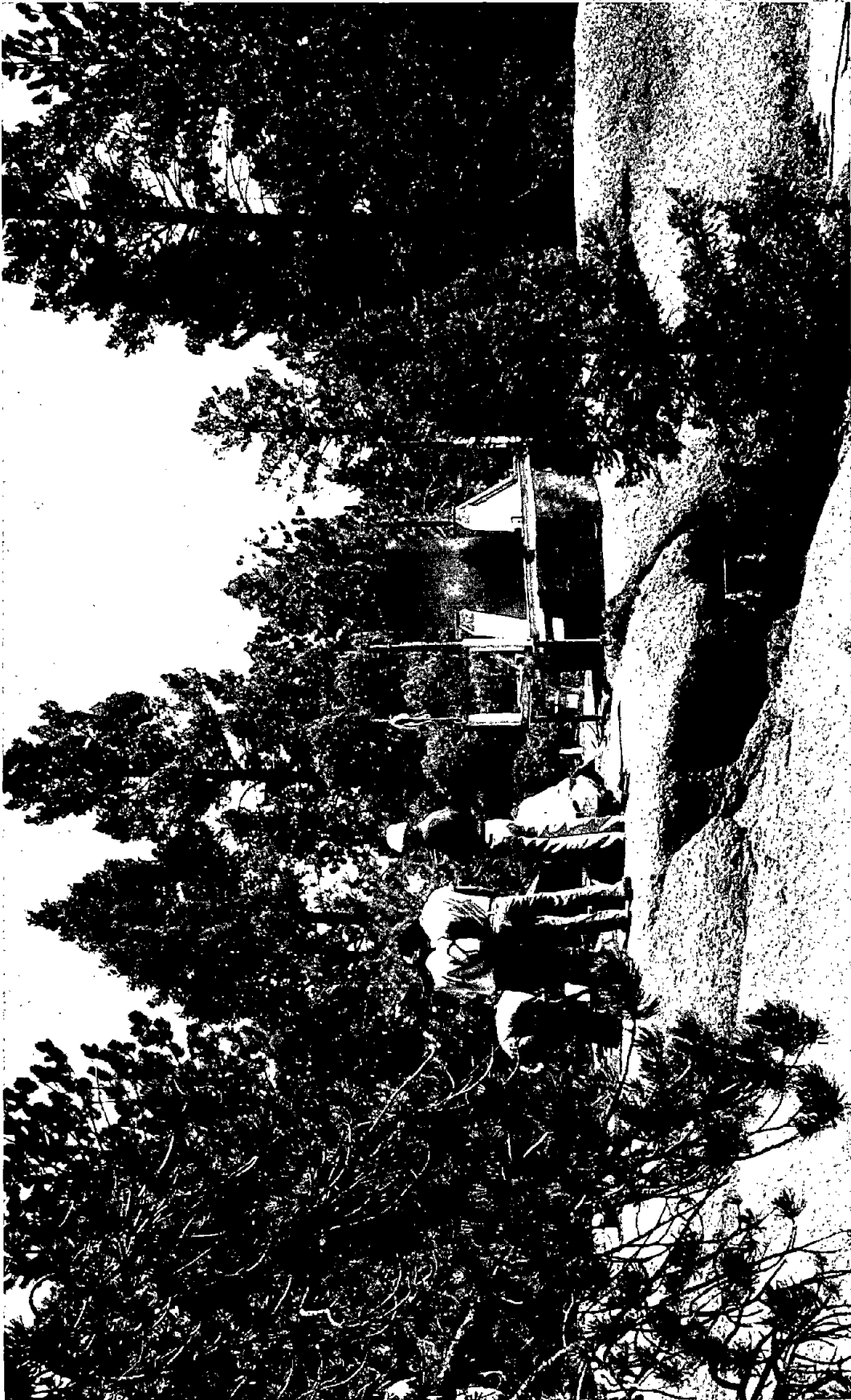


Figure 22. FM-CW system on site 2.

Figure 23 shows the actual subsurface feature responses as detected by the FM-CW system from the surface at site 2. The signal amplitude responses are detected and displayed on an oscilloscope of a spectrum analyzer and then plotted on a x-y recorder. The main trace shows signal amplitude responses from subsurface features occurring at approximately 8.5, 9.3, 12.6 and 13.6 kHz. The other minor responses on the main trace are systematic. The return from the air-granite surface interface is plotted separately in Fig. 23 at 6.7 kHz at a different amplitude level.

Referring to Fig. 23 and using eq 22, the distances from the surface to subsurface feature responses are calculated. Taking one example, the difference frequency f_d between the surface response (6700 Hz) and the first subsurface feature response (8500 Hz) is 1800 Hz. The distance d to the first subsurface feature response is 1.80 meter. Accordingly, the other values are calculated at 9250, 12650 and 13550 Hz yielding distances of 2.55, 5.96 and 6.86 meters respectively.

In analyzing the values obtained for the distances with those of the core data from drill hole 3 (Fig. 27), a direct correlation is seen with the pegmatite layer at 1.85 m and the series of open fractures between 5.91 and 6.75 meters. Direct correlation does not exist for the return response obtained at 2.55 m even though a return is being detected from some source. This was later thought to be a system reflection based upon additional measurements that were taken.

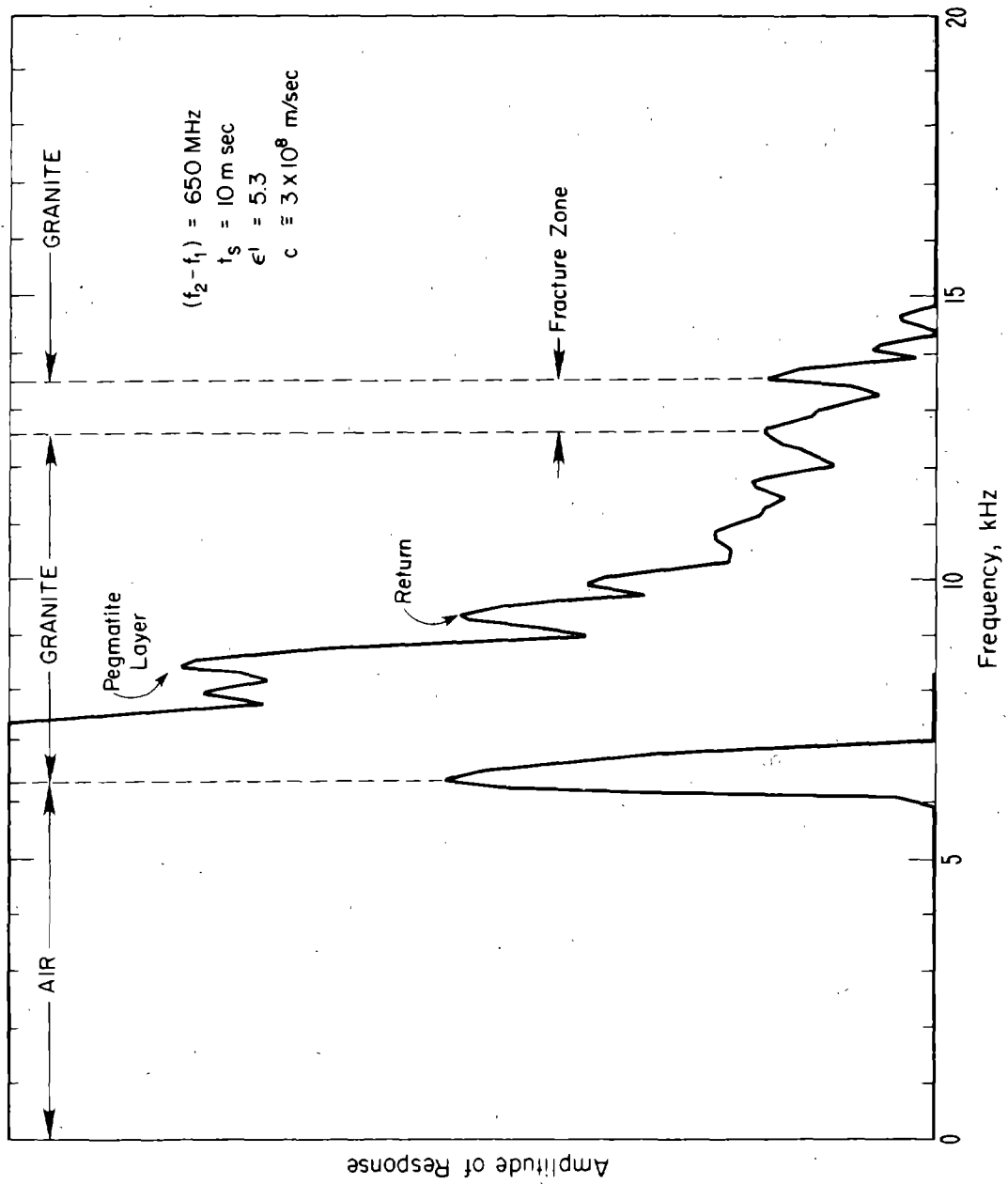


Figure 23. Actual subsurface feature responses as detected by the FM-CW system from the surface at site 2.

6. CONCLUSIONS

A test site has been located near Denver, Colorado, which provides ideal conditions for testing high-resolution sensing equipment in a simple field situation. The physical characteristics of the site have been documented, and the site is available for future experiments.

Two measurement techniques have been described that potentially offer high-resolution methods of determining features in the subsurface from the surface. Experimental results using the FM-CW technique at the field test site accurately located a series of open fractures in granite between a depth of 5.96 and 6.86 meters. Further, the test results were confirmed by the core data which indicated a maximum measurement uncertainty of less than 2%. The PNFR technique, in computer simulations and theoretical analyses, also appears to have excellent potential in detecting and resolving small subsurface anomalies.

Because this initial study has produced encouraging results, further research on this topic appears warranted. A suggested program to extend this study is outlined in the following section.

7. RECOMMENDATIONS

A program should be undertaken on high resolution sensing techniques for slope stability studies to further develop and apply the PNFR technique and to combine it, if appropriate, with other techniques such as the FM-CW. The following specific efforts are recommended for advancing the technology toward developing a practical, reliable system capable of detecting small subsurface anomalies from the surface. Consideration should be given to estimating the cost effectiveness and reliability of a remote sensing technique relative to conventional slope stability studies. Design considerations would be given for fabricating a remote measurement system from existing commercially available equipment.

This proposed program would be accomplished in three major phases over a period of approximately three years as follows:

- Phase 1--Technique Development and Evaluation
- Phase 2--Site Selection, Characterization and Evaluation
- Phase 3--Slope Instability Monitoring and Documentation

The phase 1 work would be concentrated on completing both the theoretical and experimental development of the PNFR system. Both the PNFR and FM-CW techniques would be considered as possibilities, along with other techniques currently in the research and development stage in a complementary system that would have the potential for measuring

subsurface strata and joints. A sensing system would be recommended that has the greatest potential to determine those features as required by FHWA.

The phase 2 work would include the joint efforts of both the NBS and the USGS. The USGS would be called upon to provide selection and geologic description of a site or sites needed for continued method documentation under typical field conditions in soil and/or rock, i.e., greater heterogeneity, thin water-bearing seams, multiple discontinuity sets, and closer discontinuity spacing. The task to fulfill the obligations will include mutual NBS-USGS agreement with FHWA on needed site characteristics and resulting site selections. Geologic mapping and detailing of site or sites would be required to describe and/or identify soil or rock mass characteristics needed for the NBS activities and those pertinent to potential short or long term slope instability monitoring.

In completing the work in phase 2, the NBS would use the remote sensing system from phase 1 considered best suited for locating subsurface features from surface measurements. The data from more complex test sites would have to be thoroughly analyzed to determine precision and accuracy.

The phase 3 work would concentrate on deploying remote measurement systems in potential slide areas as designated by the FHWA, the USGS, or both for slope instability monitoring. Periodic measurements would be taken over a one to two year interval to determine what activity can be detected electromagnetically. Some of the sites selected could very well be those chosen in phase 2, and part of the monitoring could begin towards the end of the phase 2 activities.

8. REFERENCES

- [1] Wickham, G. E., Tiedemann, H. R., and Skinner, E. H., Support determination based on geologic predictions (Proc. North Am. Rapid Excavation Tunneling Conf. 1, 43-64, 1972).
- [2] Bieniawski, Z. T., Engineering classification of jointed rock masses, South African Inst. Civil Eng. 15, No. 12, 335-343 (1973).
- [3] Barton, N., Lien, R., and Lunde, J., Engineering classification of rock masses for the design of tunnel support, Rock Mechanics 6, No. 4, 189-236 (1974).
- [4] Anonymous, The description of rock masses for engineering purposes, Quart. Jour. Eng. Geol. 10, No. 4, 355-388 (1977).
- [5] Lambe, T. W., and Whitman, R. V., Soil Mechanics, p. 553 (John Wiley and Sons, New York, 1969).
- [6] Morgenstern, N. R., Methods of slope stability analysis, Computer Application in Foundation Engineering and Construction, Chicago Soil Mechanics Lectures: Am. Soc. Civil Engineers, Geotech. Eng. Div., Illinois section, 44-68 (1974).
- [7] Attewell, P. B., and Farmer, I. W., Principles of Engineering Geology, p. 1045 (John Wiley, Halsted Press Div., New York, 1976).
- [8] Wu, T. H., Investigation into slope movements (Proc. Ohio Highway Engineering Conf., 24th Ann., 36-39, 1970).
- [9] Patton, F. D., and Hendron, A. J., Jr., General report on mass movements (Proc. Internat. Assoc. Eng. Geology Cong., 2d, Sao Paulo, 2, paper V-GR1-57, 1974).
- [10] Wright, S. G., Kulhawy, F. H., and Duncan, J. M., Accuracy of equilibrium slope stability analysis (Proc. Am. Soc. Civil Engineers, Jour. Soil Mechanics and Found. Div., 99, No. SM10, 783-791, 1973).
- [11] Bishop, A. W., The use of the slip circle in the stability analysis of slopes, Geotechnique 5, No. 1, 7-17 (1955).
- [12] Bishop, A. W., and Morgenstern, N. R., Stability coefficients for earth slopes, Geotechnique 10, No. 4, 129-150 (1960).

- [13] Morgenstern, N. R., and Price, V. E., The analysis of the stability of general slip surfaces, *Geotechnique* 15, No. 1, 79-93 (1965).
- [14] Spencer, E., A method of analysis of the stability of embankments assuming parallel inter-slice forces, *Geotechnique* 17, No. 1, 11-26 (1967).
- [15] Wright, S. G., A study of slope stability and the undrained shear strength of clay shales, Berkeley, University of California, Ph.D. dissertation (1969).
- [16] Chen, W. F., and Giger, M. W., Limit analysis of stability of slopes (Proc. Am. Soc. Civil Engineers, Jour. Soil Mechanics and Found. Div. 97, No. SM1, 19-26, 1971).
- [17] Janbu, N., Slope Stability Computations, Embankment-Dam Engineering, Casagrande Volume, pp. 47-86 (John Wiley and Sons, New York, 1973).
- [18] Siegel, R. A., Computer analysis of general slope stability problems, Joint Highway Research Project, Engineering Experiment Station, Purdue University, Rept. JHRP-75-8, 113 (1975).
- [19] Fredlund, D. G., Usage, requirements, and features of slope stability computer software (Canada 1977), *Canadian Geotech. Jour.* 15, No. 1, 83-95 (1978).
- [20] Fredlund, D. G., and Krahn, J., Comparison of slope stability methods of analysis, *Canadian Geotech. Jour.* 14, No. 3, 429-439 (1977).
- [21] Revilla, J., and Castillo, E., The calculus of variations applied to stability of slopes, *Geotechnique* 27, No. 1, 1-11 (1977).
- [22] Law, K. T., and Lumb, P., A limit equilibrium analysis of progressive failure in the stability of slopes, *Canadian Geotech. Jour.* 15, No. 1, 113-122 (1978).
- [23] Seed, H. B., and Sultan, H. A., Stability analysis for a sloping core embankment (Proc. Am. Soc. Civil Engineers, Jour. Soil Mechanics and Found. Div. 93, No. SM4, 69-83, 1967).

- [24] Bell, J. M., Noncircular sliding surfaces (Proc. Am. Soc. Civil Engineers, Jour. Soil Mechanics and Found. Div. 95, No. SM3, 829-844, 1969).
- [25] Dunlop, P., and Duncan, J. M., Development of failure around excavated slopes (Proc. Am. Soc. Civil Engineers, Jour. Soil Mechanics and Found. Div. 96, No. SM2, 471-493, 1970).
- [26] Duncan, J. M., and Dunlop, P., Slopes in stiff fissured clays and shales (Proc. Am. Soc. Civil Engineers, Jour. Soil Mechanics and Found. Div. 95, No. SM2, 467-492, 1964).
- [27] Wang, F-D., and Sun, M. C., Slope stability analysis by the finite element stress analysis and limiting equilibrium method, U.S. Bur. Mines Rept. Inv. 7341 (1970).
- [28] Lo, K. Y., and Lee, C. F., Stress analysis and slope stability in strain-softening materials, Geotechnique 23, No. 1, 1-11 (1973).
- [29] Jaeger, J. C., Friction of rocks and stability of rock slopes, Geotechnique 21, No. 2, 97-134 (1971).
- [30] Hoek, E., and Bray, J. W., Rock Slope Engineering, 2d ed. (London Inst. Mining and Metall., 1977).
- [31] Goodman, R. E., Methods of Geological Engineering in Discontinuous Rocks, (West Publishing Co., St. Paul, Minn., 1976).
- [32] Hoek, E., and Boyd, J. M., Stability of slopes in jointed rocks, Inst. Hwy. Engineers Jour., London 18, No. 12, 16-19 (1971).
- [33] Jennings, J. E., A mathematical theory for the calculation of the stability of slopes in open cast mines (Symposium on Planning Open-Pit Mines, South Africa Inst. Mining and Metall., 87-102, 1971).
- [34] Jennings, J. E., An approach to the stability of rock slopes based on the theory of limiting equilibrium with a material exhibiting anisotropic shear strength (Stability of Rock Slopes, Symposium on Rock Mechanics, 13th, Urbana, Ill., 1971, Proc. Am. Soc. Civil Engineers, 269-302, 1972).

- [35] Heuze, F. E., and Goodman, R. E., Three-dimensional approach for design of cuts in jointed rock (Stability of Rock Slopes, Symposium on Rock Mechanics, 13th, Urbana, Ill., 1971, Proc. Am. Soc. Civil Engineers, 397-441, 1972).
- [36] Goodman, R. E., Geotechnical practice for stability in open pit mining (Internat. Conf. on Stability in Open Pit Mining, 2d, Vancouver, B.C., Canada, 1971, Proc. Am. Inst. Mining, Metall., and Petroleum Engineers, pp. 125-132) Book, Geological Investigations to Evaluate Stability, chap. 9, Brawner, C.O., and Milligan, V., eds. (1972).
- [37] Calder, P. N., Slope stability in jointed rocks, Canadian Mining and Metall. Bull. 63, No. 697, 586-590 (1970).
- [38] Steffen, O. K. H., and Jennings, J. E., Definition of design joints for two-dimensional rock-slope analyses, Advances in Rock Mechanics (Internat. Soc. Rock Mechanics Cong., 3d, Denver, Colo., 1974, Proc. 2, pt. B, 827-832, 1974).
- [39] Brown, E. T., and Trollope, D. H., Strength of a model of jointed rock (Am. Soc. Civil Engineers Proc., Jour. Soil Mech. and Found. Div., Proc. 96, No. SM2, 685-704, 1970).
- [40] Barton, N., Rock slope performance as revealed by a physical joint model, Advances in Rock Mechanics (Internat. Cong. Rock Mechanics, 3d Denver, 1974 2, pt. B, 765-773, 1974).
- [41] Stacey, T. R., The behavior of two-and three-dimensional model rock slopes, Quart. Jour. Eng. Geology 8, No. 1, 67-72 (1975).
- [42] Reik, G., and Teutsch, C., The use of equivalent models in slope stability investigation, Internat. Jour. Rock Mechanics and Mining Science and Geomech. Abstracts 13, No. 12, 321-330 (1976).
- [43] Hendron, A. J., Jr., Cording, E. J., and Aiyer, A. K., Analytical and graphical methods for the analysis of slopes in rock masses, U.S. Army Engineer Nuclear Cratering Group Tech. Rept. 36 (1971).
- [44] Londe, P., Vigier, G., and Vormeringer, R., Stability of rock slopes, a three-dimensional study (Am. Soc. Civil Engineers Proc., Jour. Soil Mechanics and Found. Div. 95, No. SM1, 235-262, 1969).
- [45] Londe, P., Vigier, G., and Vormeringer, R., Stability of rock slopes--graphical methods (Am. Soc. Civil Engineers Proc., Jour. Soil Mechanics and Found. Div. 96, No. SM4, 1411-1434, 1970).

- [46] Wang, F-D., Analysis of slopes in a discontinuous rock mass (Symposium on Rock Mechanics, 10th, Austin, Texas, 1968, Proc. Am. Inst. Mining, Metall. and Petroleum Engineers, pp. 599-620) Book, Basic and Applied Mechanics, Gray, K. E., Ed., (1972).
- [47] Londe, P., Analysis of the stability of rock slopes, Quart. Jour. Eng. Geology 6, No. 1, 93-124 (1973).
- [48] John, K. W., An approach to rock mechanics, Am. Soc. Civil Engineers Proc., Jour. Soil Mechanics and Found. Div. 88, No. SM4, pt. 1, 1-30 (1962).
- [49] John, K. W., Graphical stability analysis of slopes in jointed rock (Am. Soc. Civil Engineers Proc., Jour. Soil Mechanics and Found. Div. 94, No. SM2, 497-526, 1968).
- [50] John, K. W., An engineering approach to evaluate the strength and deformability of regularly jointed rock systems, Rock Mechanics 1, No. 4, 183-197 (1969).
- [51] Goodman, R. E., The resolution of stresses in rock using stereographic projection, Internat. Jour. Rock Mechanics and Mining Science 1, 93-103 (1963).
- [52] Hoek, E., Bray, J. W., and Boyd, J. M., The stability of a rock slope containing a wedge resting on two intersecting discontinuities, Quart. Jour. Eng. Geology 6, No. 1, 1-55 (1973).
- [53] Taylor, C. L., Geometric analysis of geological separation for slope stability investigations, Assoc. Eng. Geologists Bull. 7, No. 1-2, 67-85 (1970).
- [54] Hoek, E., Methods for the rapid assessment of the stability of three-dimensional rock slopes, Quart. Jour. Eng. Geology 6, No. 3/4, 243-255 (1973).
- [55] Heuze, F. E., Analysis of geological data for the design of rock cuts, Advances in Rock Mechanics (Internat. Soc. Rock Mechanics Cong., 3d, Denver, Colo., 1974, Proc. 2, pt. B, 798-802, 1974).
- [56] Cruden, D. M., A composite net for the rapid analysis of rock slope stability, Quart. Jour. Eng. Geology 9, No. 2, 119-124 (1976).
- [57] John, K. W., Engineering analyses of three-dimensional stability problems utilizing the reference hemisphere (Internat. Soc. Rock Mechanics Cong., 2d, Belgrade, Proc. 7, No. 6, 385-391, 1970).

- [58] John, K. W., Three-dimensional stability analyses of slopes in jointed rock (Symposium on Open Pit Mines, 1970, Proc. South African Inst. Mining and Metallurgy, 209-214, 1971).
- [59] Finn, W. D. L., Static and seismic analysis of slopes, *Felsmechanik U. Ingenieurgeologie* 4, No. 3, 268-277 (1966).
- [60] Goodman, R. E., Taylor, R. L., and Brekke, T. L., A model for mechanics of jointed rocks (Am. Soc. Civil Engineers Proc., Jour. Soil Mechanics and Found. Div. 94, No. SM3, 637-659, 1968).
- [61] Brekke, T. L., and Howard, T. R., Stability problems caused by seams and faults (North Am. Rapid Excavation and Tunneling Conf., Proc. 1, 25-41, 1972).
- [62] St. John, C. M., Three dimensional analysis of jointed rock slopes, Rock Fracture (Internat. Symposium on Rock Mechanics, Nancy, France, 1971, Proc. 2, 1971).
- [63] Ghaboussi, J., Wilson, E. L., and Isenberg, J., Finite element for rock joints and interfaces (Am. Soc. Civil Engineers Proc., Jour. Soil Mechanics and Found, Div. 99, No. SM 10, 833-848, 1973).
- [64] Mahtab, M. A., Bolstad, D. D., and Kendorski, F. S., Analysis of the geometry of fractures in San Manuel copper mine, Arizona; U. S. Bur. Mines Rept. Inv. 7715 (1973).
- [65] Robertson, A. M., The interpretation of geological factors for use in slope theory (Symposium on Open Pit Mines, 1970, Proc. South African Inst. Mining and Metallurgy, 55-71, 1971).
- [66] Priest, S. D., and Hudson, J. A., Discontinuity spacings in rock, *Internat. Jour. Rock Mechanics and Mining Sci. and Geomechanics Abs.* 13, 135-148 (1976).
- [67] Snow, D. T., The frequency and apertures of fractures in rock, *Internat. Jour. Rock Mechanics and Mining Sci.* 7, No. 1, 23-40 (1970).

- [68] Oliveira, R., An example of the influence of lithology on slope stability (Internat. Geol. Cong., 24th, Montreal, 1972, Proc. Eng. Geology, sec. 13, 142-149, 1972).
- [69] Nasmith, H., Landslides and Pleistocene deposits in the Meikle River valley of northern Alberta, Canadian Geotech. Jour. 1, No. 3, 155-166 (1964).
- [70] Hamel, J. V., and Flint, N. K., Failure of colluvial slope (Am. Soc. Civil Engineers Proc., Jour. Soil Mechanics and Found. Div. 98, No. SM2, 167-180, 1972).
- [71] Gray, R. E., Ferguson, H. F., and Hamel, J. V., Slope stability in the Appalachian Plateau of Pennsylvania and West Virginia (GAI Consultants, Inc., Pittsburgh, Pa., 1974).
- [72] Conlon, R. J., Landslide on the Toulmoustouc River, Quebec; Canadian Geotech. Jour. 3, No. 3, 113-144 (1966).
- [73] Lo, K. Y., An approach to the problem of progressive failure, Canadian Geotech. Jour. 9, No. 41, 407-429 (1972).
- [74] Morgenstern, N. R., and Tchalenko, J. S., Microstructural observations on shear zones from slips in natural clays (Geotechnical Conf., Oslo, Proc. 1, 147-152, 1967).
- [75] Broms, B. B., Landslides, chap. 11, Book, Winterkorn, H. F., and Fang, H. Y., eds., Foundation Engineering Handbook, pp. 373-401 (Van Nostrand Reinhold, New York, 1975).
- [76] Haug, M. D., Bauer, E. K., and Fredlund, D. G., Retrogressive slope failures at Beaver Creek, south of Saskatoon, Saskatchewan, Canada; Canadian Geotech. Jour. 14, No. 3, 288-301 (1977).
- [77] Leighton, F. B., Landslides and hillside development, Book, Lung, R., and Proctor, R., eds., Engineering Geology in Southern California, pp.149-207 (Assoc. Eng. Geologists, Los Angeles Sec. Spec. Pub., 1966).
- [78] Dodds, R. K., Rock movement along fractures during failure (Internat. Soc. Rock Mechanics Cong., 1st, Lisbon, 1966, Proc. Lisbon, Lab. Nac. Engenharia Civil 1, 133-137, 1966).

- [79] Wahlstrom, E. E., and Nichols, T. C., Jr., The morphology and chronology of a landslide near Dillon Dam, Dillon, Colorado, Eng. Geology--Internat. Jour. 3, No. 2, 149-174 (1969).
- [80] Barton, N., The shear strength of rock and rock joints, Internat. Jour. Rock Mech. and Mining Sci. 13, No. 9, 255-279 (1976).
- [81] Bell, D. H., Slope evolution and slope stability, Kawarau Valley, central Otago, New Zealand; Internat. Assoc. Eng. Geology Bull. 14, 5-16 (1976).
- [82] Deere, D. U., Hendron, A. J., Jr., Patton, F. D., and Cording, E. J., Design of surface and near-surface construction in rock (Failure and Breakage of Rock, Symposium on Rock Mechanics, 8th Minneapolis, Minn., 1966, Proc. Am. Inst. Mining, Metall., and Petroleum Engineers, 237-302; 1967).
- [83] Fookes, P. G., and Wilson, D. D., The geometry of discontinuities and slope failures in Siwalik clay, Geotechnique 16, No. 4, 305-320 (1966).
- [84] Henkel, D. J., and Yudhbir, The stability of slopes in the Siwalik rocks in India (Internat. Soc. Rock Mechanics Cong., 1st, Lisbon, 1966, Proc. Lisbon, Lab. Nac. Engenharia Civil, 161-165, 1966).
- [85] Early, K. R., and Skempton, A. W., Investigations of the landslide at Walton's Wood, Staffordshire; Quart. Jour. Eng. Geology 5, 19-41 (1972).
- [86] Skempton, A. W., Long-term stability of clay slopes, Geotechnique 14, No. 2, 77-101 (1964).
- [87] Broili, L., Rock slides and security problems in the face of hillside quarries (Internat. Soc. Rock Mechanics Cong., 1st, Lisbon, 1966, Proc. Lisbon, Lab. Nac. Engenharia Civil, 187-191, 1966).
- [88] Stout, M. L., Slip surface geometry in landslides, southern California and Norway, Assoc. Eng. Geologists Bull. 8, No. 1, 59-78 (1971).
- [89] Cooksley, J. W., Jr., Geological investigation of a landslide employing seismic exploration technique (Symposium on Engineering Geology and Soils Engineering, 2d Ann., Pocatello, Idaho, 1964, Proc. Boise, Idaho Dept. Highways, 97-103, 1964).

- [90] Slosson, J. E., and Cilweck, B. A., Parson's Landing landslide--A case history including the effects of eustatic sea level change on stability, Eng. Geology--Internat. Jour. 3, Nos. 1-2, 1-9 (1966).
- [91] Clark, S. P., Jr., ed., Handbook of Physical Constants [revised ed.] (Geol. Soc. America Memoir 97, 1966).
- [92] Wuerker, R. G., Annotated tables of strength and elastic properties of rocks, Am. Inst. Mining, Metall. and Petroleum Engineers, Paper 663-G (1956).
- [93] Kulhawy, F. H., Stress deformation properties of rock and rock discontinuities, Eng. Geology 9, No. 4, 327-350 (1975).
- [94] Coulson, J. H., Shear strength of flat surfaces in rock (Stability of Rock Slopes, Symposium on Rock Mechanics, 13th, Urbana, Ill., 1971, Proc. Am. Soc. Civil Engineers, 77-105, 1972).
- [95] Coates, D. F., and Parsons, R. C., Experimental criteria for classification of rock substances, Internat. Jour. Rock Mechanics and Mining Sci. 3, No. 3, 181-189 (1966).
- [96] D'Andrea, D. H., Fischer, R. L., and Fogelson, D. E., Prediction of compressive strength from other rock properties, U.S. Bureau of Mines Rept. 6702 (1965).
- [97] Ward, W. H., Marsland, A., and Samuels, S. G., Properties of the London Clay at the Ashford common shaft: In situ and drained strength tests, Geotechnique 15, No. 4, 321-344 (1965).
- [98] Fleming, R. W., Spencer, G. S., and Banks, D. C., Empirical study of behavior of clay shale slopes, U.S. Army Engineers Nuclear Cratering Group Tech. Rept. NCG 15 1, No. 2 (1970).
- [99] Paeth, R. C., Harward, M. E., Knox, E. G., and Dyrness, C. T., Factors affecting mass movement of four soils in the western Cascades of Oregon, Soil Sci. Soc. America Proc. 35, No. 6, 943-947 (1971).
- [100] Skopek, J., Rybar, J., and Dobr, J., Pore-water pressure observations in a landslide (Internat. Geological Congress, 24th, Montreal, 1972, Proc. Engineering Geology, sec. 13, 150-159, 1972).

- [101] McGown, A., and Radwan, A., Cutting slopes in fissured Scottish boulder clay (Internat. Assoc. Eng. Geology Cong., 2d, San Paulo, 1974, Proc. 2, paper pV8.1-v8.9, 1974).
- [102] Keller, G. V., and Frischknecht, F. C., Electrical Methods in Geophysical Prospecting (Pergamon Press, New York, 1966).
- [103] Dobrin, M. B., Introduction to Geophysical Prospecting [3d ed.] (McGraw-Hill, New York, 1976).
- [104] Bogoslovsky, V. A., and Ogilvy, A. A., Geophysical methods for the investigation of landslides, Geophysics 42, No. 3, 562-571 (1977).
- [105] Brooke, J. P., Geophysical investigations of a landslide near San Jose, California, Geoexploration 11, No. 2, 61-73 (1973).
- [106] Schwarz, S. D., Geophysical measurements related to tunneling (North American Rapid Excavation and Tunneling Conf., Proc. 1, 195-208, 1972).
- [107] Telford, W. M., Geldart, L. P., Sheriff, R. E., and Keys, D. A., Applied Geophysics (Cambridge Univ. Press, 1976).
- [108] Redpath, B. B., Seismic refraction exploration for engineering site investigations, U.S. Army Engineers Waterways Experiment Station, Explosive Excavation Research Lab Tech. Rept. E-73-4 (1973).
- [109] a) Mooney, H. M., Handbook of Engineering Geophysics (Bison Inst., Inc., Minneapolis, Minn., 1976).
b) Mooney, H. M., Shallow Reflection Seismology (Minneapolis, University of Minnesota, Privately printed, 1976).
- [110] DaGama, C. D., Studying rock fractures by wave attenuation methods (Rock Fracture: Internat. Symposium on Rock Mechanics, Nancy, France, 1971, Proc. Theme 1, paper 2, 10 p., 1971).
- [111] Knill, J. L., Geotechnical significance of some glacially induced rock discontinuities, Assoc. Eng. Geologists Bull. 5, No. 1, 49-62 (1968).

- [112] Knill, J. L., and Price, D. G., Seismic evaluation of rock masses (Internat. Geol. Cong., 24th, Montreal, 1972, Proc., 176-182, 1972).
- [113] Coon, R. F., and Merritt, A. H., Predicting in situ modulus of deformation using rock quality indexes, Determination of the in situ modulus of deformation of rock, Am. Soc. Testing Materials Spec. Tech. Pub. 477, 154-173 (1970).
- [114] Oberste-Lehn, and Deane, Phenomena and properties of geologic materials affecting microwaves, Stanford University Remote Sensing Laboratory, Technical Report 70-10 (1970).
- [115] Barron, K., Detection of fracture friction in rock specimens by the use of a simple ultrasonic listening device, Int. J. of Rock Mechanics and Mining Sciences 8, 55-59 (1971).
- [116] Mearns, R., and Hoover, T., Subaudible rock noise as a measure of slope stability, State of California, Department of Transportation, Division of Highways, Transportation Laboratory, Research Report CA-DOT-TL-2537-1-73-24 (Aug. 1973).
- [117] Soland, D. E., et al., Excavation seismology, AD 755 211 (Dec. 1972).
- [118] Dechman, G. H., and Oudenhoven, M. S., Velocity-based method for slope failure detection, U. S. Bur. of Mines, Report of Investigations 8194 (1976).
- [119] Barringer, A. R., and McNeill, J. D., Radiophase - a new system of conductivity mapping (Proc. of the 5th Symposium on Remote Sensing of the Environment, 1968).
- [120] Inouye, G. T., Bernstein, H., and Goal, R. A., Electromagnetic depth sounder, IEEE Transactions on Geoscience Electronics GE-8 (Oct. 1970).

- [121] Stan, R. L., Detection and determination of faults by surface resistivity measurements, Bur. of Mines, Report of Investigations No. 7975 (1975).
- [122] Jakosky, J. J., Exploration Geophysics (Triga Publishing Co., Los Angeles, California, 1950).
- [123] Takeuchi, A., Fractured zone type landslide and electrical resistivity survey, Bull. Disas. Prev. Res. Inst., Kyoto Univ., 21, Part 1, No. 185 (Sept. 1971).
- [124] Moffat, D. L., and Puskar, R. J., A subsurface electromagnetic pulse radar, Geophysics 41, No. 3 (June 1976).
- [125] Gates, D. C., and Armistead, R. A., The use of advanced technologies for locating underground obstacles, EPRI 78-20-0 Final Report, DOI Contract No. (Aug. 1974).
- [126] Cook, J. C., Radar transparencies of mine and tunnel rocks, Geophysics 40, No. 5, 865-885 (Oct. 1975).
- [127] Ellerbruch, D. A., and Adams, J. W., Microwave measurement of coal layer thickness, Nat. Bur. Stan., NBSIR 74-387 (Sept. 1974).
- [128] a) Ellerbruch, D. A., and Belsher, D. R., Electromagnetic technique of measuring coal layer thickness, IEEE Trans., on Geoscience Electronics GE-16, 126-133 (April 1978).
- b) Ellerbruch, D. A., and Belsher, D. R., FM-CW electromagnetic technique of measuring coal layer thickness, NBSIR 76-840 (May 1976).
- [129] Lundien, J. R., Determining presence, thickness, and electrical properties of stratified media using swept frequency radar, Technical Report M-72-4, Office, Chief of Engineers, U.S. Army (Nov. 1972).
- [130] Graham, J. R., Jr., Gallagher, R. V., and Alongi, A. V., Advanced investigation of high-resolution soil-penetrating radar, Cornell Aeronautical Laboratory for U.S. Army Mobility Equipment Command, Ft. Belvoir, Va., Contract DAAK02-69-C-0043 (1969).
- [131] Robinson, L. A., Weir, W. B., and Young, L., Location and recognition of discontinuities in dielectric media using synthetic rf pulses, Proc. IEEE 62, No. 1 (Jan. 1974).

- [132] Wittman, R. C., Simulated pulse techniques for measuring coal layer thickness, Final Technical Report, U.S. D.O.E. ET-75-G-01-8972 (formerly U.S. B.M. G0155054) (1978).
- [133] a) Yue, O. C., Rope, E. L., and Tricoles, G., Two reconstruction methods for microwave imaging of buried dielectric anomalies, IEEE Trans. on Computers C-24, 381-390 (April 1975).
- b) Tricobes, G., Rope, E. L., and Yue, O. C., Microwave techniques for imaging objects buried below the surface of the ground, Final Report to USMERDC, Ft. Belvoir, VA, Contract DAAK02-71-C-0264 (July 1973).
- [134] Silverman, D., Mapping the earth with elastic holography, IEEE Trans. Geoscience Electronics GE-7, No. 4, 190-199 (Oct. 1969).
- [135] a) Kerns, D. M., and Dayhoff, E. S., Theory of diffraction in microwave interferometry, J. Res. Nat. Bur. Stan. 64B, 1-13 (Jan.-Mar. 1960).
- b) Kerns, D. M., Plane-wave scattering-matrix theory of antennas and antenna-antenna interactions: formulation and applications, J. Res. Nat. Bur. Stand. 80B, 5-51 (Jan. - Mar. 1976).
- c) Newell, A. C., Baird, R. C., and Wacker, P. F., Accurate measurement of antenna gain and polarization at reduced distances by an extrapolation technique, IEEE Trans. Antenna Prop. AP-21, 418-431 (July 1973).
- d) Kerns, D. M., Scattering-matrix description and nearfield measurements of electroacoustic transducers, J. Acoustic Soc. Am. 57, 497-507 (Feb. 1975).
- e) Yaghjian, A. D., Upper-bound errors in far-field antenna parameters determined from planar near-field measurements, part 1: analysis, NBS Technical Note 667 (Oct. 1975).
- f) Newell, A. C., and Crawford, M. L., Planar near-field measurements on high performance array antennas, NBS Internal Report 74-380 (July 1974).
- [136] a) Mitchel, R. E., A realistic approach to shallow geophysical investigations through complementary usage (Proc. of the 57th Annual Engineering Geology and Soils Engineering Symposium, Pocatello, Idaho, 157-172, April 1967).

b) Barringer, A. R., Exploration in the North helped by new techniques, West Miner 47, 13-19 (Feb. 1974).

- [137] Belsher, D. R., Detection of lost oil well casings and unknown water filled voids in coal mines through development of a microwave antenna system, NBS Report to U.S. Bureau of Mines H0272007 (Jan. 1978).
- [138] Graham, J. R., Jr., Gallagher, R. V., and Alongi, A. V., Advanced investigation of high-resolution soil-penetrating radar, Final Technical Report, Cornell Aeronautical Laboratory (May 1969).
- [139] Moffatt, D. L., Puskar, R. J., and Peters, L., Jr., Electromagnetic pulse sounding for geological surveying with application in rock mechanics and the rapid excavation program, Final Technical Report 3408-2, The Ohio State University Electro-Science Laboratory (Sept. 1973).
- [140] Robinson, L. A., Weir, W. B., and Young, L., Location and recognition of discontinuities in dielectric media using synthetic rf pulses, Proc. IEEE 62, 36-44 (Jan. 1974).
- [141] a) Reference [103].
b) Special issue on geophysical data processing, Geoscience Electronics GE-15, No. 1 (Jan. 1977).
- [142] Reference [103], Chapters 11-16.
- [143] a) Zissis, C. J., Infrared technology fundamentals, Opt. Engr. 15, 484-497 (Nov.-Dec. 1976).
b) Reference [147], Chapter 6.
- [144] Tomiyasu, K., Remote sensing of the earth by microwaves, Proc. IEEE 62, 86-92 (Jan. 1974).
- [145] a) Palacky, G. T., and Jagodits, F. L., Computer data processing and quantitative interpretation of airborne resistivity surveys, Geophysics 40, 818-830 (Oct. 1975).
b) Reference [103], Chapter 17.
- [146] Reference [147], Chapter 7.

- [147] Gates, D. C., and Armistead, R. A., The use of advanced technologies for locating underground obstacles, EPRI Report 78-20-0 prepared by Stanford Research Institute, Menlo Park, California (Aug. 1974).
- [148] a) Reference [103], Chapter 17.
- b) Fountain, L. S., Herzig, F. X., and Owen, T. E., Detection of subsurface cavities by surface remote sensing techniques, FHWA Report (FHWA-RD-75-80) prepared by Southwest Research Institute (June 1975).
- c) Stahl, R. L., Detection and delineation of faults by surface resistivity measurements, Bureau of Mines, Report of Investigations No. 7975 (1974).
- [149] a) Cook, J. C., Status of ground-probing radar and some recent experience (Proc. Engineering Foundation Conference on Subsurface Exploration for Underground Excavation and Heavy Construction, Henniker, N.H., Aug. 1974).
- b) Daniels, D. J., The use of radar in geophysical prospecting (Proc. of the International Conference, Radar - 77 sponsored by IEEE, Savoy Place, London, Oct. 1977).
- c) Rubin, L. A., and Fowler J. C., Ground-probing radar for delineation of rock features (Proc. of the 17th U.S. Symposium on Rock Mechanics, Snowbird, Utah, Aug. 1976).
- [150] a) Ultrasound in Medicine (series) (Plenum Press, New York, 1977-1978).
- b) Proceedings of the 23rd Annual Meeting of the American Institute of Ultrasound in Medicine, San Diego, California (Oct. 1978).
- c) Iinuma, K., Kidokoro, T., and Takemura, High resolution real time ultrasonic imaging systems for medical use, Toshiba Review 114, 13-17 (Mar.-Apr. 1978).
- [151] Price, T. O., Demonstration of acoustical underground survey system in the Washington metropolitan area, FHWA Report (FHWA-RD-75-82) prepared by Holosonics (June 1975).
- [152] Goodman, J. W., Introduction to Fourier Optics (McGraw-Hill, New York, 1968).

- [153] a) Metherell, A. F., et al., Introduction to acoustic holography, *Acoust. Soc. Am.* 42, 733-742 (April 1967).
- b) Thurstone, F. L., Holographic imaging with ultrasound, *J. Acoust. Soc. Am.* 45, 895-899 (May 1968).
- [154] Kujoory, M. A., and Farhat, N. H., Microwave holographic subtraction for imaging of buried objects, *Proc. IEEE* 66, 94-96 (Jan 1978).
- [155] a) Sondhi, M. M., Reconstruction of objects from their sound-diffraction patterns, *J. Acoust. Soc. Am.* 46, 1158-1164 (Nov. 1969).
- b) Boyer, A. L., et al., Computer reconstruction of images from ultrasonic holograms, *Book, Acoustical Holography 2*, Ch. 15 (Plenum, New York, 1970).
- c) Farr, J. B., Acoustical holography experiments using digital processing, *Book, Acoustical Holography 2*, Ch. 16 (Plenum, New York, 1970).
- d) Powers, J. P., Computer simulation of linear acoustic diffraction, *Book, Acoustical Holography 7*, pp. 193-205 (Plenum, New York, 1977).
- e) Hoover, G. H., Acoustical holography using digital processing, *Geophysics* 37, 1-19 (Feb. 1972).
- [156] Stoke, G. W., *An Introduction to Coherent Optics and Holography* (Academic Press, New York, 1966).
- [157] Hildebrand, B. P., and Brenden, B. B., *An Introduction to Acoustic Holography* (Plenum, New York, 1972).
- [158] a) Jensen, H., et al., Side-looking airborne radar, *Scientific American* 237, 84-95 (Oct. 1977).
- b) Tomiyasu, K., Tutorial review of synthetic aperture radar (SAR) with applications to imaging of the ocean surface, *Proc. IEEE* 66, 563-583 (May 1978).
- c) Larson, R. W., Zelenka, J. S., and Johansen, E. L., Results obtained from the University of Michigan microwave hologram radar (*Proc. 7th Inter. Symp. on Remote Sensing of Environment II*, 809-842 (May 1971)).

- [159] Whipp, E., and Horne, D. A., Digitising of side-scan sonar signals, *Ultrasonics* 14, 201-204 (Sept. 1976).
- [160] a) Scudder, H. J., Introduction to computer aided tomography, *Proc. IEEE* 66, 628-637 (June 1978).
 b) Horn, B. K. P., Density reconstruction using arbitrary ray-sampling schemes, *Proc. IEEE* 66, 551-562 (May 1978).
 c) Lytle, R. J., et al., Electromagnetic cross-borehold survey of a site proposed from an urban transit station, Lawrence Livermore Laboratory Report UCRL-52484 (June 5, 1978).
 d) Lytle, R. J., Geophysical characterization using advanced data processing, Lawrence Livermore Laboratory Preprint UCRL-81294 (July 28, 1978).
- [161] Nishimura, M., Takiyama, K., and Shigesawa, H., Reconstructed image in microwave holography, *Digest of 1978 ISAP at Sendai, Japan*, 397-400 (Aug. 1978).
- [162] Bleistein, N., and Cohen, J.K., Nonuniqueness in the inverse source problem in acoustics and electromagnetics, *J. Math, Phys.* 18, 194-201 (Feb. 1977).
- [163] Bojarski, N. N., A survey of electromagnetic inverse scattering, Syracuse University Research Corp, Special Projects Lab. Rep. (Oct. 1966).
- [164] Cohen, J. K., and Bleistein, N., An inverse method for determining small variations in propagation speed, *SIAM* 32, 784-799 (June 1977).
- [165] Tsien, D. S., and Chen, Y. M., A pulse spectrum technique for remote sensing of stratified media, *Radio Science* 13, 775-783 (Sept-Oct. 1978).
- [166] Stratton, J. A., *Electromagnetic Theory* (McGraw-Hill, New York, 1941).
- [167] Stubenrauch, C. S., and Yaghjian, A. D., Efficient computation of coupling between co-sited antennas, NBS report under preparation, Boulder, Colorado.
- [168] Harris, J. L., Diffraction and resolving power, *J. Opt. Soc. Am.* 54, 931-936 (July 1964).

- [169] McMahon, B. K., Indices related to the mechanical properties of jointed rock (Chapter 6, Status of Practical Rock Mechanics-Symposium on Rock Mechanics, 9th Golden, Colorado, 1967, Proc. Am. Inst. Mining, Metal, and Petroleum Engineers, 117-133, 1968).
- [170] Deere, D. U., Technical description of rock cores for engineering purposes, Rock Mechanics and Eng. Geology 1, No. 1, 16-22 (1964).
- [171] Clayton, J. L., and Arnold, J. F., Practical grain size, fracturing density and weathering classification of intrusive rock of Idaho Batholith, U.S. Forest Service Gen. Tech. Rept. INT-2. (1972).
- [172] Ramo, S., Whinnery, J. R., and Van Duzer, T., Fields and Waves in Communication Electronics (John Wiley and Sons, Inc., New York, 1965).
- [173] Kerr, J. L., Short axial length broadband horns (Proc. of the 22nd Annual Symposium on USAF Antenna Research and Development, University of Illinois, Oct. 11-13, 1972).
- [174] Deere, D. U. and Miller, R. P., Engineering classification and index properties for intact rock, Tech. Rept. No. AFWL-TR-65-116, University of Illinois, Urbana, Illinois, 300 pp. (1966).
- [175] Judd, W. R., and Huber, C., Correlation of rock properties by statistical methods, Book, International Symposium Mining Research 2, pp. 621-648, G. Clarke, ed. (Oxford, Pergamon Press, 1962).
- [176] Johnson, R. B., Factors that influence the stability of slopes--a literature review, FHWA-RD-79-54 (Jan. 1979).

APPENDIX

Contained in this appendix are summaries of physical tests run on intact core samples which document the physical characteristics of the site. Included are measurements of dielectric constants by the NBS. The USGS measured unconfined compressive strength, static elastic moduli, sonic velocities, dynamic elastic moduli, and Schmidt hardness values.

Measurements of Dielectric Constants

Drill core samples of the granite that were representative of subsurface conditions at site 2 were selected and cut by the USGS for laboratory experiments. Some samples were sent to the NBS High Frequency Immittance Laboratory at Boulder, Colorado. Measurements were taken of the granite samples by bridge techniques to obtain values of 5.635 and 5.459 for ϵ' at 100 and 200 MHz respectively. These are plotted in Fig. 24 along with the other NBS value obtained by Clark [91] for table 6 section 3.2. This plot shows a good correlation of the values of ϵ' obtained at different frequencies by different measurement techniques. In particular, the plot shows the degree of accuracy for the field value.

Laboratory Determination of Physical Properties

Unconfined compressive strengths, sonic velocities, elastic properties and Schmidt hardness values were determined from the core samples obtained in the four boreholes. Selection of the core for testing was limited to samples above and below fractures, whenever possible, with controls being both selected near the weathered surface material and in sound rock at depth. The location and number of each sample is shown on Figs. 25-28 which are graphic logs of the four drill holes. RQD, Schmidt hammer data, compressional or P-wave sonic velocity, and shear or S-wave velocity values are given at appropriate depths on the figures.

Samples selected from the standard NX-size cores from the boreholes were sawed into 125 mm segments for lab testing. Additional 50 mm specimens were cut and given to the NBS for determination of dielectric constants. The sawed edges of the selected cores were ground within the acceptable tolerance limits for testing. The lab tests were performed to obtain exact values for comparison of the different physical properties.

Unconfined Compressive Strength

The unconfined compressive strength of the cores is the ratio of the maximum load at failure to the cross-sectional area of the specimen before testing.

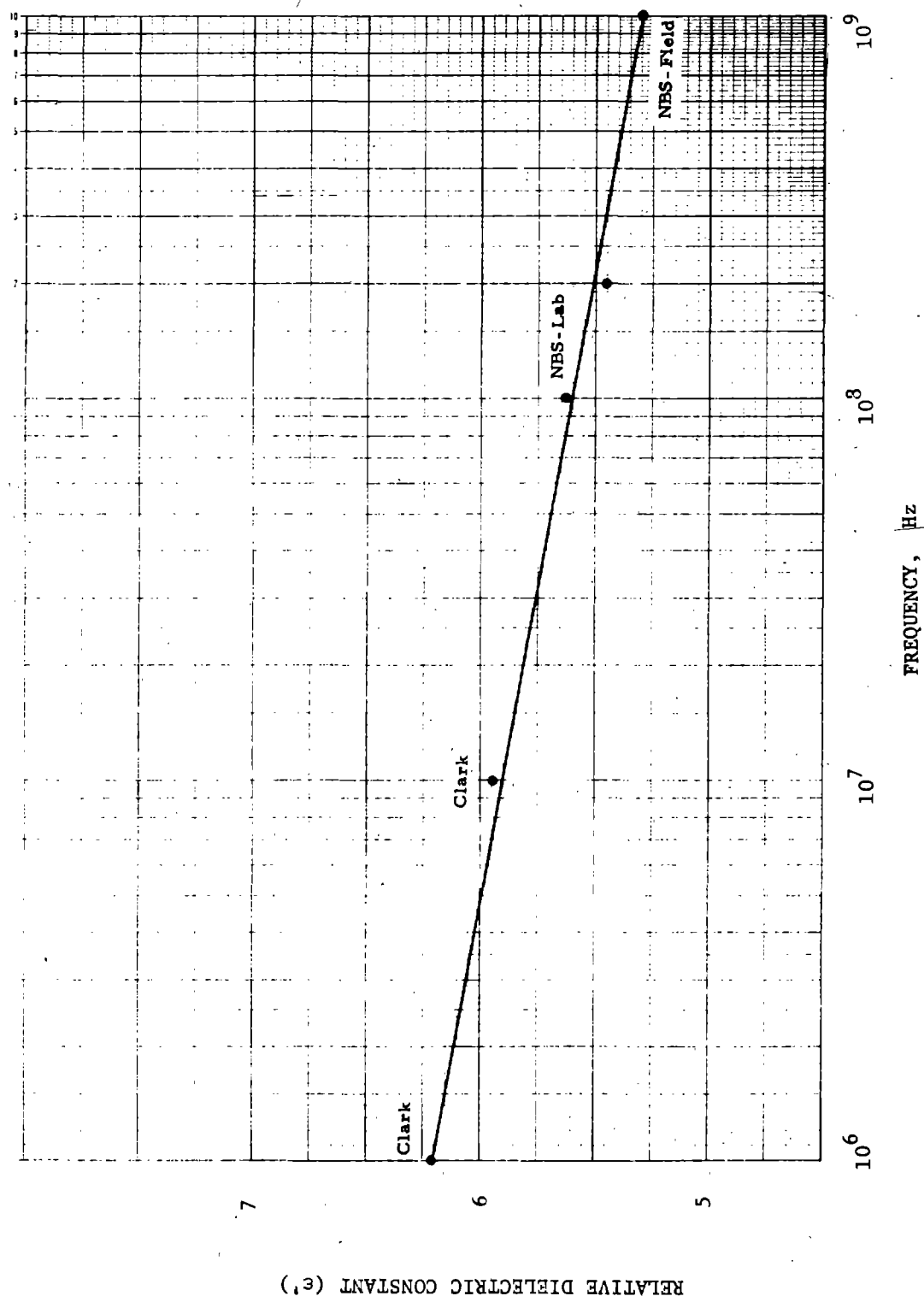


Figure 24. Plot of relative dielectric constant as a function of frequency.

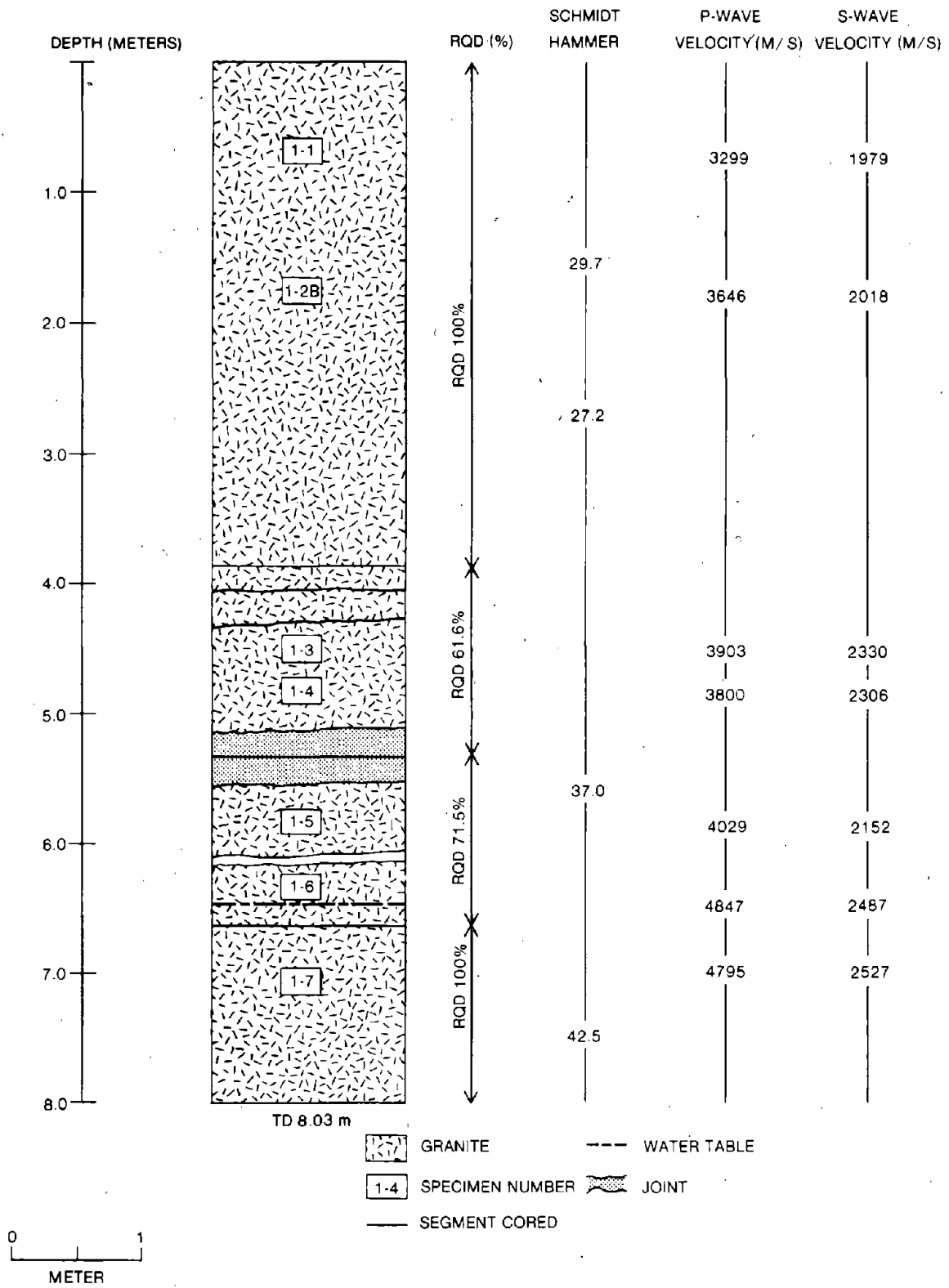


Figure 25. Graphic log of borehole 1.

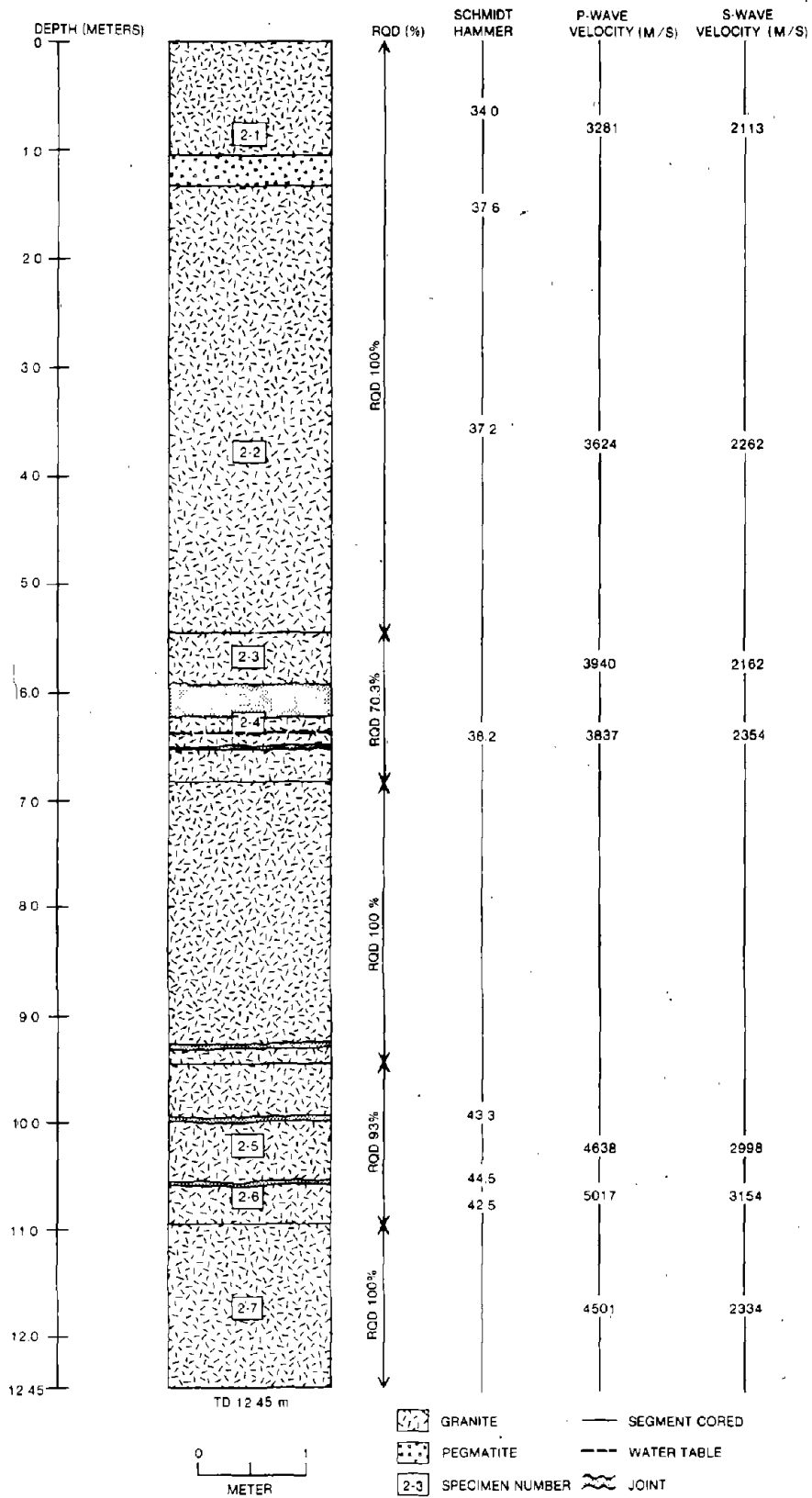


Figure 26. Graphic log of borehole 2.

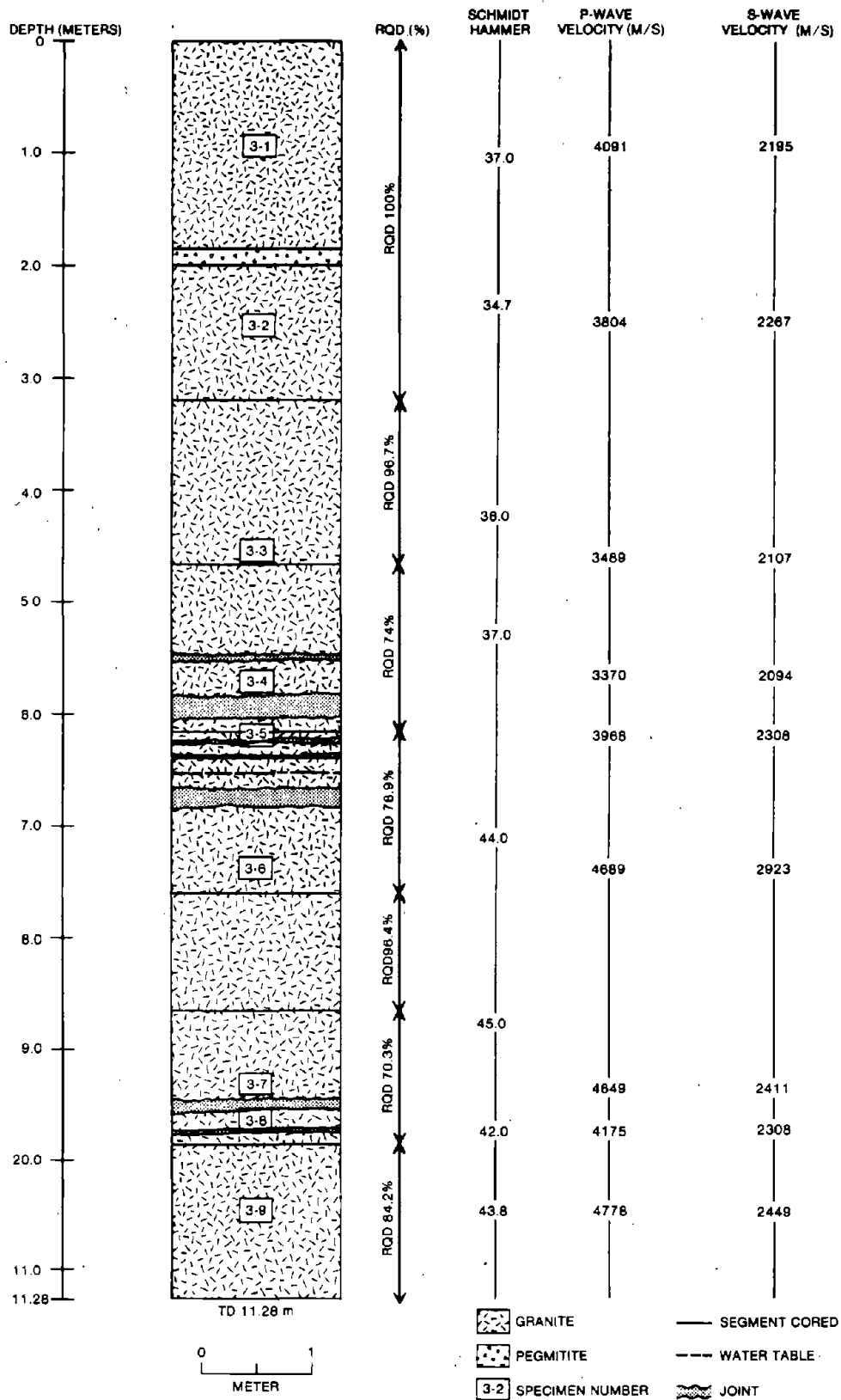


Figure 27. Graphic log of borehole 3.

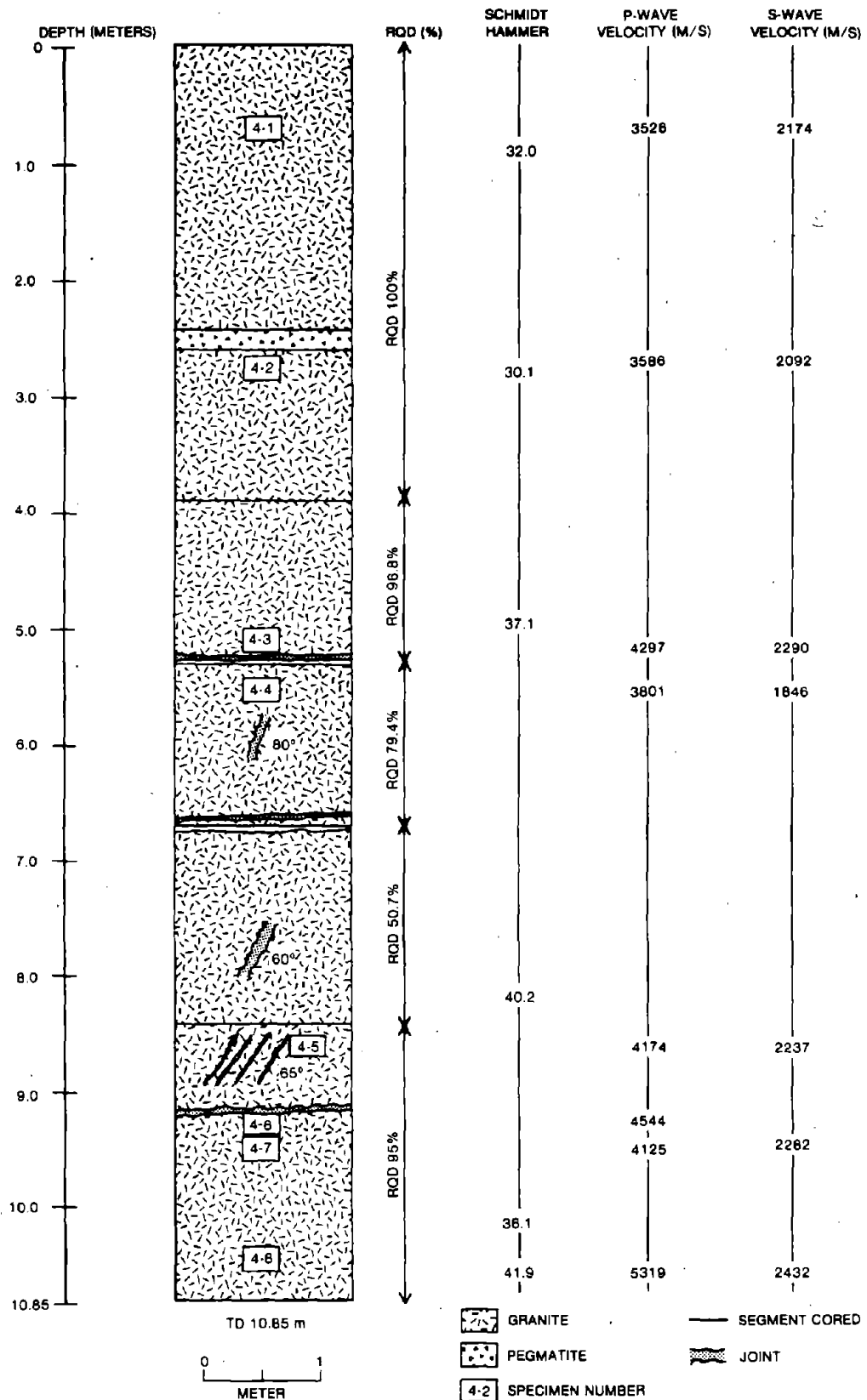


Figure 28. Graphic log of borehole 4.

Determination of Static Elastic Moduli

The static elastic moduli, Young's Modulus, Poissons ratio, shear modulus, and bulk modulus were determined on 10 samples as defined below and listed in table 14.

$$\text{Young's Modulus (E)} = \frac{\text{Unit Stress}}{\text{Unit Strain}}$$

$$\text{Poisson's Ratio } (\nu) = \frac{\text{Lateral Unit Strain}}{\text{Longitudinal Unit Strain}}$$

$$\text{Shear Modulus (G)} = \frac{E}{2(1 + \nu)}$$

$$\text{Bulk Modulus (K)} = \frac{E}{3(1 - 2\nu)}$$

The 10 samples selected for testing were chosen from cores in boreholes 1, 2, and 3 which were drilled in the same granite block. The samples selected are in sound and weathered rock, above and below joints, providing a representative sample of the entire drill site.

Sonic Velocities

An SBEL 1007H Seismic Analyzer with combined compressive and shear-wave velocity platens was used to measure sonic velocities in the core samples. The instrument incorporates a high-energy pulsing circuit with a sensitive receiving circuit. The unit is used to measure the travel time through the cores in micro-seconds. As indicated by the operating instructions, 120 mm cores were used to measure P-wave velocity while 50 mm cores were used to measure S-wave velocity.

Determination of Dynamic Elastic Moduli

The dynamic elastic moduli for 10 samples were determined by using the compressional and shear velocities for each sample along with an average dry bulk density of 2.643 g/cm³ (table 15).

Table 16 presents the formulas used to calculate four important **dynamic** elastic moduli, Young's Modulus, Poisson's ratio, shear modulus, and bulk modulus.

Table 14. Static Modulus and Poisson's Ratio

CORE IDENTIFICATION AND ROCK TYPE	STRESS RANGE (psi)	POISSON'S RATIO (ν)	STATIC SECANT MODULUS				
			YOUNG'S MODULUS (E) ($\times 10^9$ N/M ²) ($\times 10^6$ Psi)	SHEAR MODULUS (G) ($\times 10^9$ N/M ²) ($\times 10^6$ psi)	BULK MODULUS (K) ($\times 10^9$ N/M ²) ($\times 10^6$ psi)		
1-7 Granite	0-6250	0.17	53.641	22.890	3.32	27.096	3.93
2-1 Granite	0-6250	0.16	32.750	14.134	2.05	16.065	2.33
2-7 Granite	0-5300	0.21	56.812	23.442	3.40	32.681	4.74
3-1 Granite	0-6200	0.31	37.093	14.134	2.05	32.543	4.72
3-9 Granite	0-6150	0.24	66.603	26.889	3.90	42.678	6.19
2-2 Granite	0-6200	0.18	39.37	16.69	2.42	20.48	2.97
2-3 Granite	0-5600	0.15	39.37	17.10	2.48	18.75	2.72
2-4 Granite	0-6400	0.20	37.09	15.44	2.24	20.62	2.99
2-5 Granite	0-6400	0.23	64.33	26.15	3.79	39.71	5.76
2-6 Granite	0-6200	0.27	64.33	25.33	3.67	46.61	6.86
			MEASURED VALUES			CALCULATED VALUES	

$$G = \frac{E}{2(1+\nu)}$$

$$K = \frac{E}{3(1-\nu)}$$

Table 15. Determination of Density

<u>Core No.</u>	<u>Dry Wt.</u> (as received)	<u>Dry Wt.</u> (16 hrs. at 105°C)	<u>Wt. Loss</u>	<u>% Loss</u>
3-2	686.38 g	686.51 g	0.87 g	.001
3-7	695.80 g	695.10 g	0.70 g	.001

Caliper Volume

3-2	259.758 cc
3-7	262.604 cc

Dry Bulk Density

2.639 g/cc
2.647 g/cc

average 2.643 g/cc

<u>Core No.</u>	<u>Sat. Wt.</u>	<u>Susp. Wt.</u>	<u>Vol. Bulk</u>	<u>Vol. Grain</u>
3-2	688.00 g	428.28 g	259.72 cc	257.23 cc
3-7	696.78 g	433.11 g	263.67 cc	261.99 cc

Dry Bulk Density

3-2	2.639 g/cc
3-7	2.636 g/cc

Grain Density

Porosity

0.75%	2.665 g/cc
0.64%	2.653 g/cc

Saturated for \approx 120 hrs. under vacuum after 16 hrs. initial vacuum.

Table 16. Elastic Moduli Expressed in V_p and V_s .

$$\text{Young's Modulus} = E = \rho \frac{V_s^2 (3V_p^2 - 4V_s^2)}{V_p^2 - V_s^2}$$

$$\text{Poisson's Ratio} = \nu = \frac{V_p^2 - 2V_s^2}{2(V_p^2 - V_s^2)}$$

$$\text{Bulk Modulus} = K = \rho \left(V_p^2 - \frac{4}{3} V_s^2 \right)$$

$$\text{Shear Modulus} = G = \rho V_s^2$$

where:

ρ = density

V_p = P or compressional wave propagation velocity

V_s = S or shear wave propagation velocity

Schmidt Hammer Test

A Type L Concrete Schmidt Hammer was used to test the core samples obtained from the drill site to determine a quantitative value of hardness. The Schmidt Hammer is a portable unit and its use constitutes a nondestructive test. It has been used to predict the unconfined compressive strengthened rock [174].

The hammer consists of a cylinder approximately 50 mm (2 in.) in diameter and 250 mm (10 in.) in length. The spring-loaded hammer within the cylinder contains 0.075 m/kg (0.54 ft/lbs) of impact energy which is released upon impact. A marker and a scale are attached to the hammer indicating the amount of rebound of the hammer after the initial impact.

Before use on the cores, the Schmidt hammer was calibrated with a special 16 kg (35 lbs) testing anvil. The testing anvil has a steel-hardened test surface of Brinell hardness equal 500 kg/mm². The core specimens were placed longitudinally in a special cradle and

three separate readings were taken at equal spacings along the core sample. The core was then rotated 45° and three more readings were taken, repeating the procedure until 25 readings had been obtained. Finally, an average value for the hardness was determined by taking the median value of the 25 separate readings.

Summary of Laboratory Test Data (USGS)

The determination of unconfined compressive strength and the static elastic moduli, i.e., Poisson's ratio, Young's modulus, shear modulus, and bulk modulus, for 10 core samples provided the data base for comparison with dynamic elastic moduli and Schmidt hammer data. This has permitted extrapolation of the various parameters which were not obtained on all samples taken from the cores. Of primary interest is the physical state of the rock mass overlying the first major discontinuity. It is through this material that the FM-CW method has been field tested. Similar comparisons of rock physical properties have been reported in the literature [96,175].

Sonic velocities, V_p and V_s , where V_p is compressional velocity and V_s is shear velocity, were used to compute the dynamic elastic moduli. For prediction purposes, only values for dynamic Young's modulus (E), and Poisson's ratio (ν), were calculated and compared with static data for the same samples. These data are in table 17.

Plots of unconfined compressive strength vs. Poisson's ratio derived both statically and dynamically have shown such scatter that Poisson's ratio has not been used for prediction purposes. Similar scatter has been noted in plots of static and dynamic Poisson's ratio vs. static and dynamic Young's modulus.

A plot of unconfined compressive strength vs. static Young's modulus, E_s , strength is shown as Fig. 29. While the clustering of the points may not justify fitting a linear regression line to the data, this has been done on the basis of published literature which dealt with a greater number of samples [96]. A plot of the dynamic Young's modulus, E_D , on the same figure displays a greater amount of scatter.

Figure 30 illustrates the relationship between unconfined compressive strength and the compressional velocity, V_p . The expected increase in velocity with increasing strength is shown. In both figures, note the position of sample 1-7. In evaluating all other static data and corresponding calculated dynamic data including velocities, it appears that the uncompressive strength value for the sample is in error. All other values are predictable within static parameters, within dynamic parameters and in cross comparisons. The sample, therefore, has been

Table 17. Selected Sonic, Static and Dynamic Test Data for 10 Test Samples

Sample	V_p m/s	V_s m/s	Unconfined Compressive Strength MPa	E_s GPa	E_D GPa	ν_s	ν_D
1-7	4795	2527	90.03	53.64	42.49	0.17	0.31
2-1	3281	2113	108.63	32.75	26.03	0.16	0.15
2-2	3624	2262	106.52	39.37	30.75	0.18	0.18
2-3	3940	2162	110.11	39.37	30.55	0.15	0.28
2-4	3837	2354	95.28	37.09	33.77	0.20	0.20
2-5	4638	2997	130.59	64.33	52.19	0.23	0.14
2-6	5017	3154	127.62	64.33	59.36	0.27	0.17
2-7	4501	2335	124.08	56.81	36.50	0.21	0.32
3-1	4091	2195	99.89	37.09	31.81	0.31	0.30
3-9	4778	2449	124.08	66.60	40.33	0.24	0.32

V_p = Velocity of Compressional Wave

V_s = Velocity of Shear Wave

E_s = Static Young's Modulus

E_D = Dynamic Young's Modulus

ν_s = Static Poisson's Ratio

ν_D = Dynamic Poisson's Ratio

MPa = MegaPascal

GPa = GigaPascal

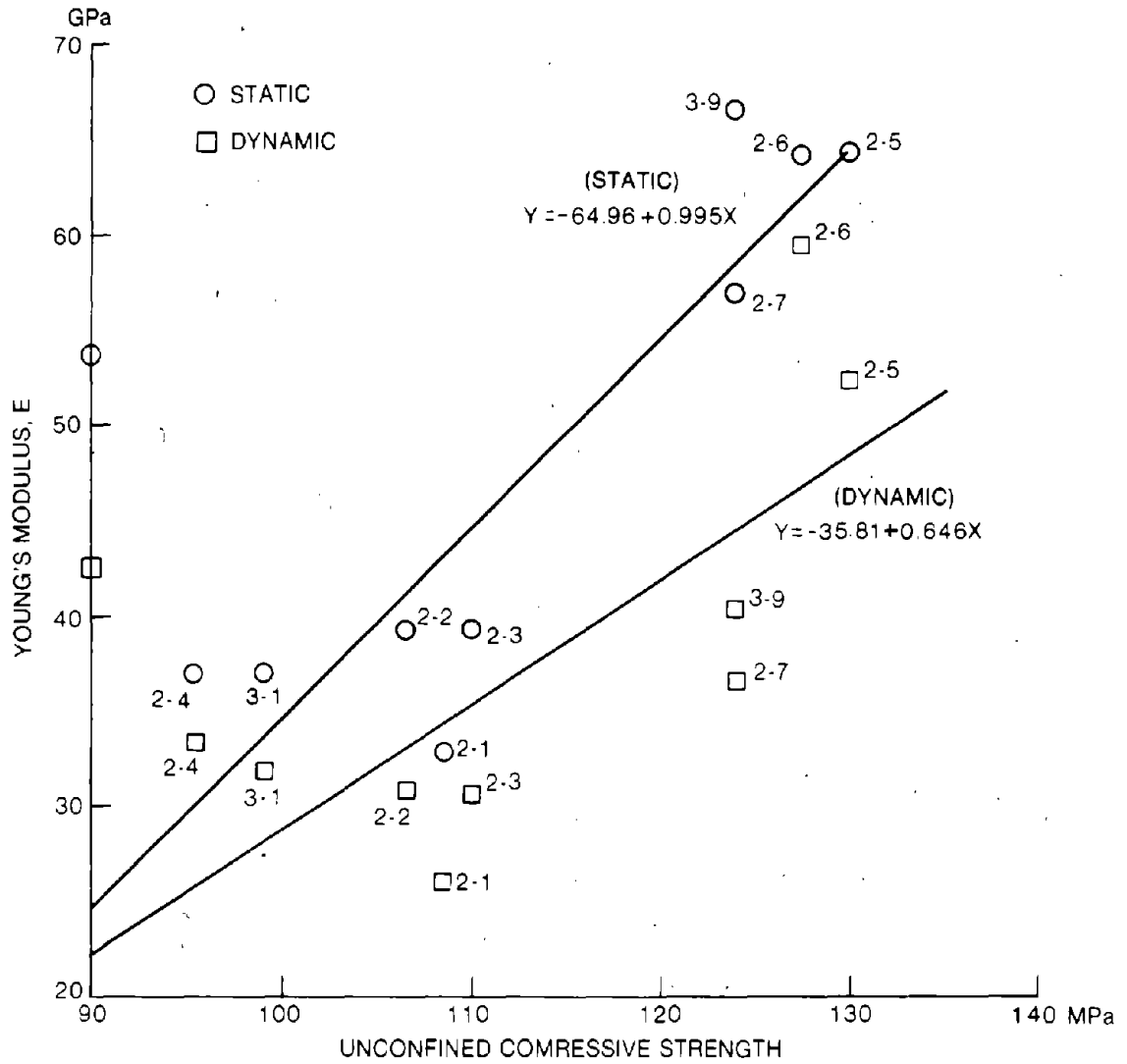


Figure 29. Plot of unconfined compressive strength and Young's modulus.

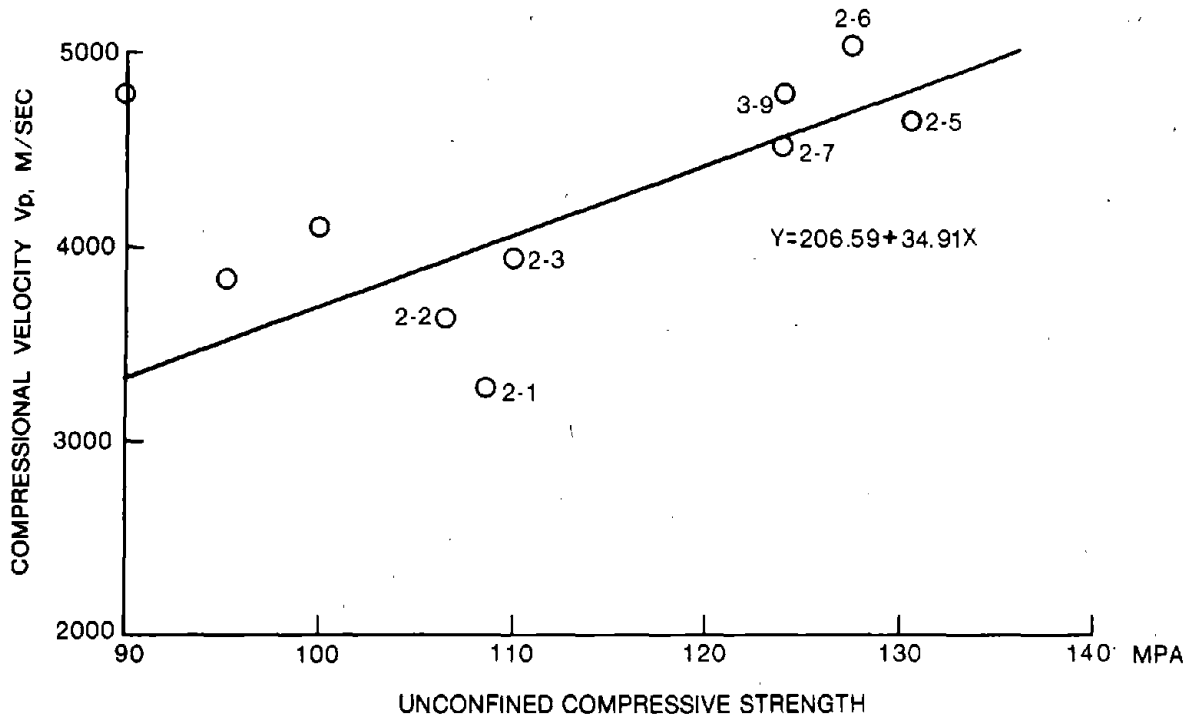


Figure 30. Plot of unconfined compressive strength and compressional velocity for 10 samples.

left out when fitting regression lines to data involving unconfined compressive strength. Figure 31 is a plot of all strength and V_p data, including the 10 points used in the previous figure.

Plots of static and dynamic Young's modulus, E_s , and E_D , vs. compressional velocity, V_p , are shown on Fig. 32. Good linear regression line fits are obtainable for both parameters. Both permit estimation of E_s and E_D for untested samples from values of V_p for those samples.

The shear wave velocity, V_s , also may be used for prediction of Young's modulus (Fig. 33). However, there is greater scatter of V_s for higher values of E_s than when using V_p . The better fit of both V_p and V_s with dynamic parameters is to be expected because the velocities are used in calculating the dynamic moduli.

The plot of compressional velocity, V_p , with shear velocity, V_s , is quite compatible with the literature [7,96]. The velocity of the shear wave typically is about $2/3 V_p$ or $0.67 V_p$. The regression line fitted to the data in Fig. 34 indicates that $V_s = 0.63 V_p$ for the 30 samples plotted.

Schmidt hammer data obtained on sections of core adjacent to seven of the ten samples on which complete testing was done have been compared with unconfined compressive strength as shown in Fig. 35. The scatter of points about the regression line indicates Schmidt hammer data permit adequate estimation of unconfined compressive strength for the test site specimens.

The Schmidt hammer data in turn may be either predicted by the compressional velocity, V_p , or they may be used to predict V_p (Fig. 36). The positive slope of the regression line is compatible with the positive response of V_p with unconfined compressive strength shown on an earlier figure.

The data used in this section are summarized in table 18. From the foregoing discussion, it is obvious that several routes are open in predicting parameters that were not obtained directly. The selection of the appropriate parameters and corresponding regression equations may be made by comparing the graphs.

Distinct clustering of data may be noted in several of the preceding figures which utilized both static and dynamic data for the 10 samples on which all tests were run. Table 19 summarizes the strength, modulus, and Schmidt hammer data for the two consistent sample clusters. It will be seen that the mean values of all parameters for cluster 1 are lower than

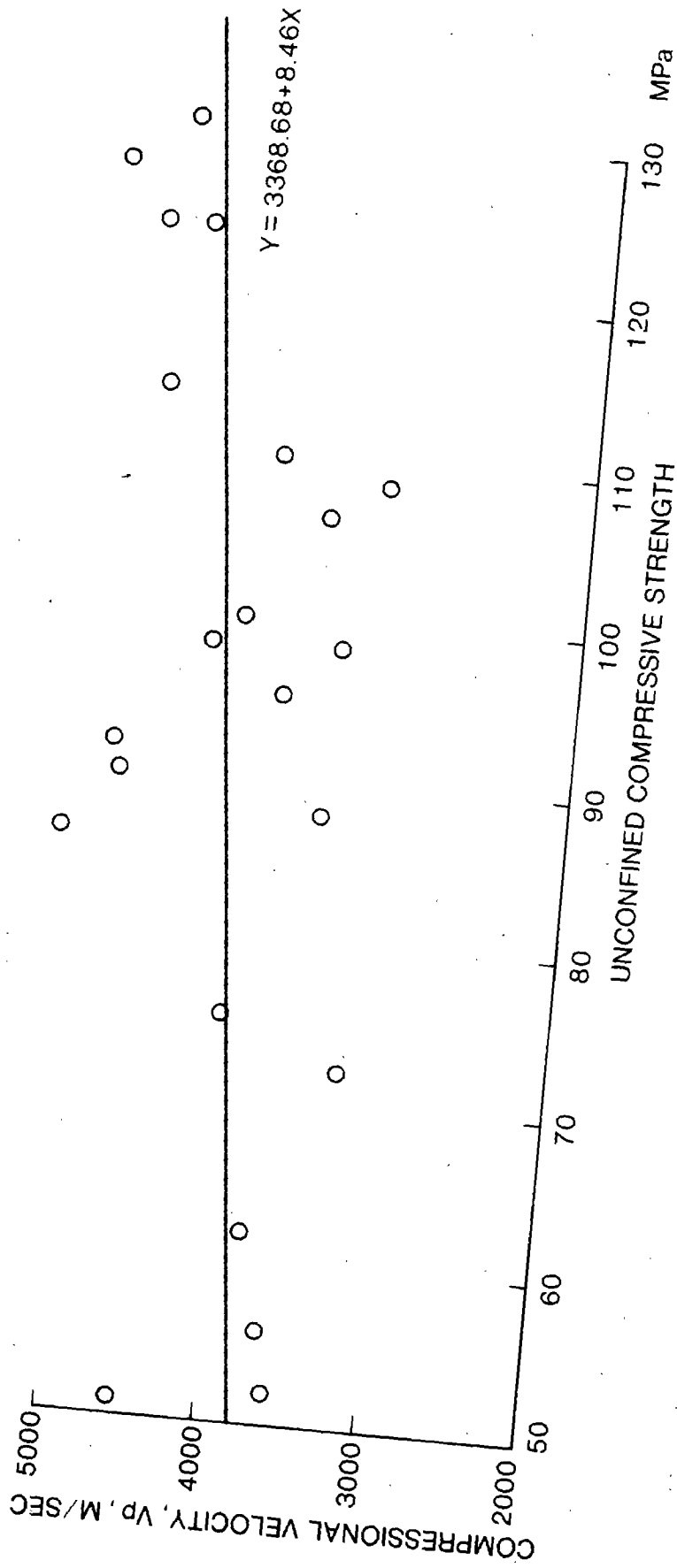


Figure 31. Plot of all compressional strength and compressional velocity data.

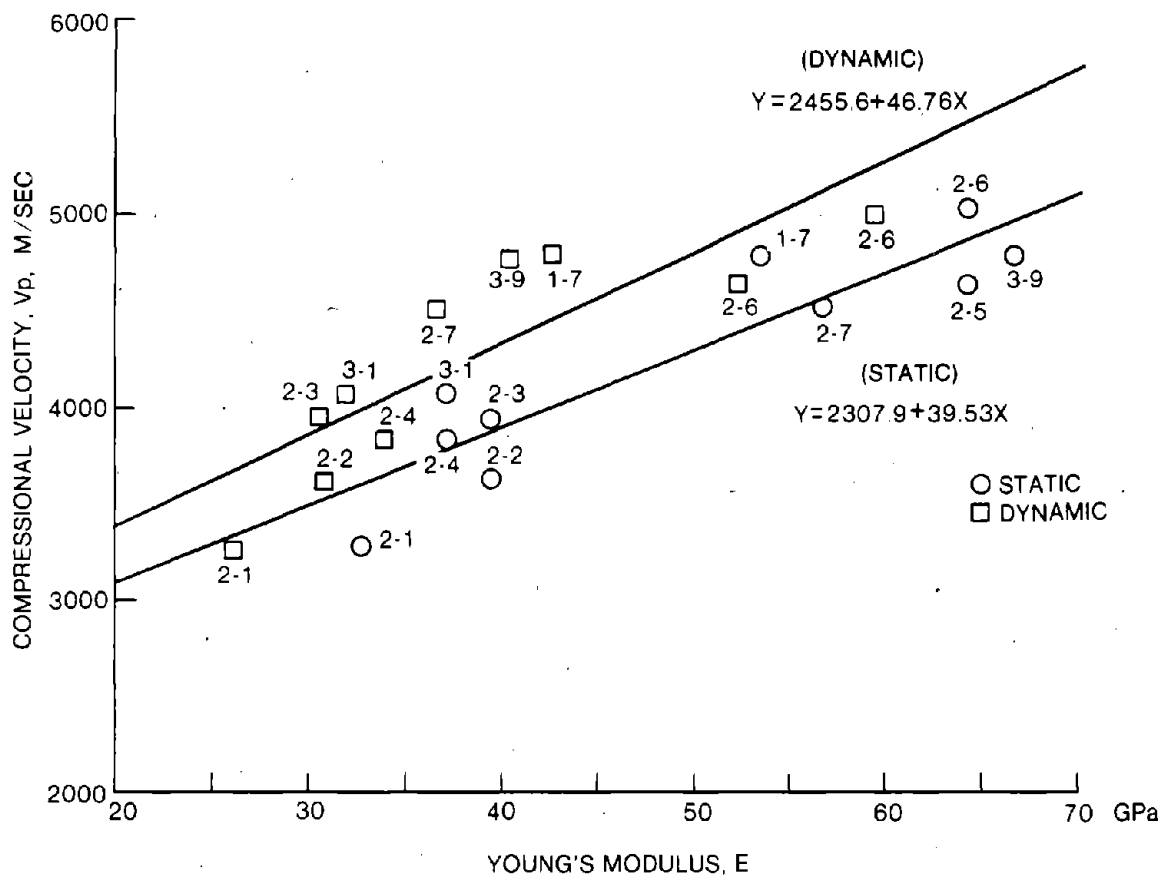


Figure 32. Plot of Young's modulus and compressional velocity.

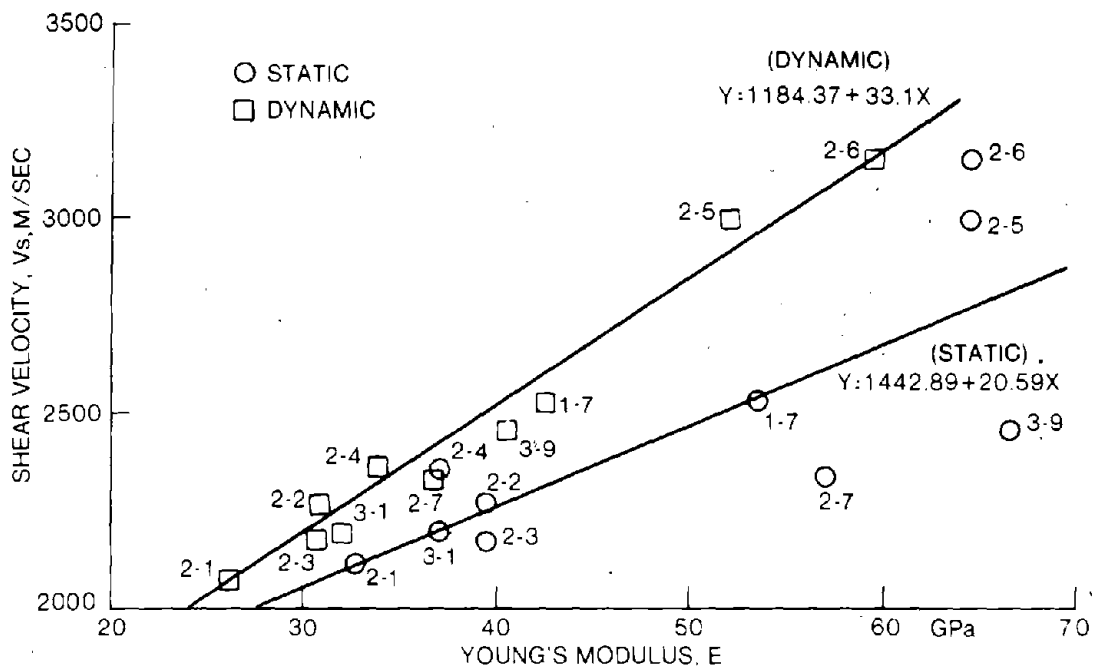


Figure 33. Plot of Young's modulus and shear velocity.

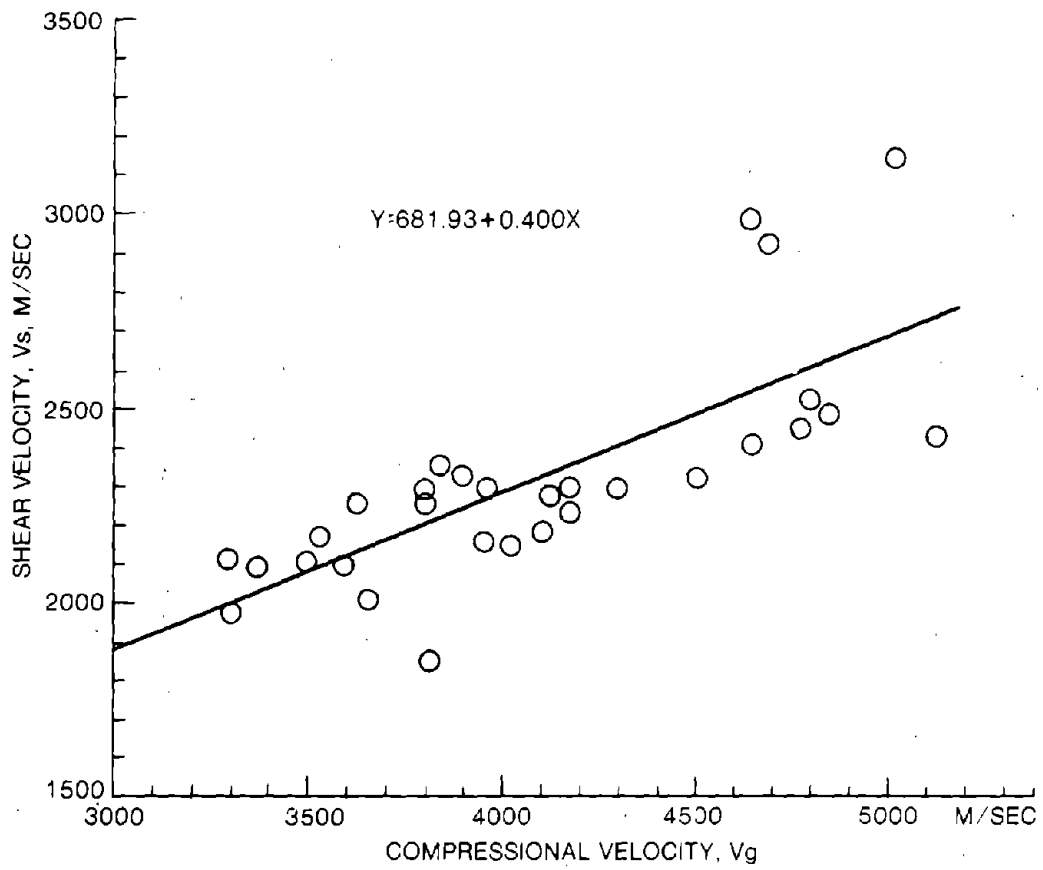


Figure 34. Plot of compressional velocity and shear velocity.

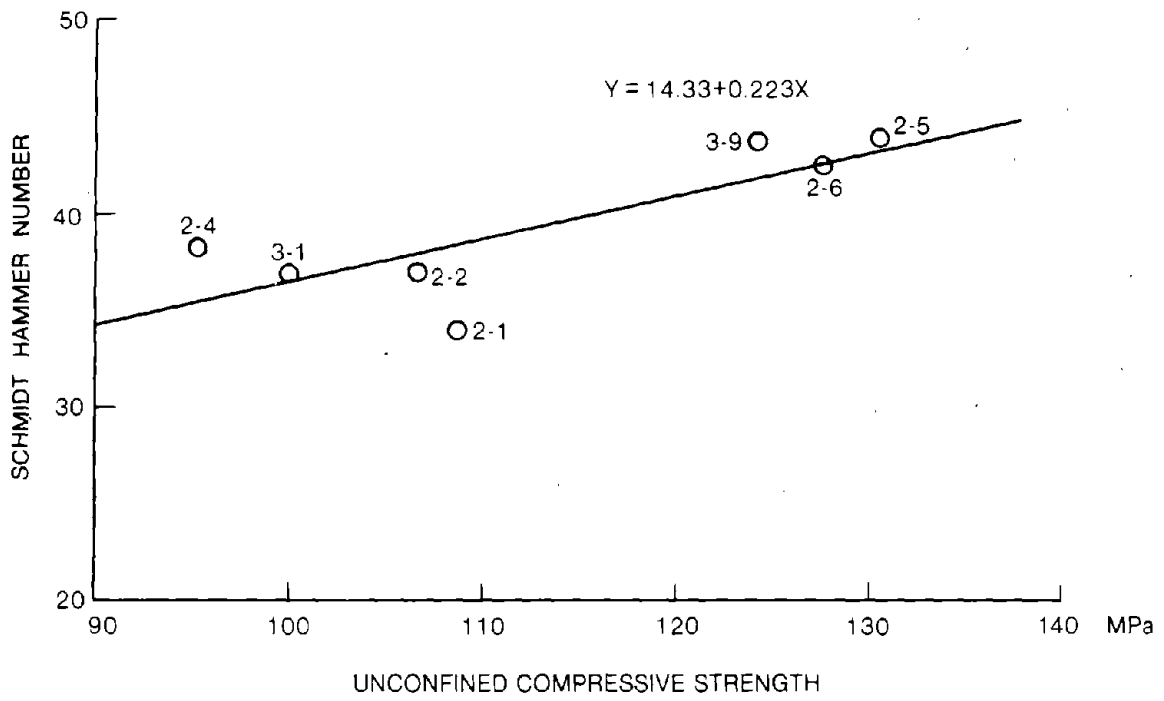


Figure 35. Plot of unconfined compressive strength and Schmidt rebound number.

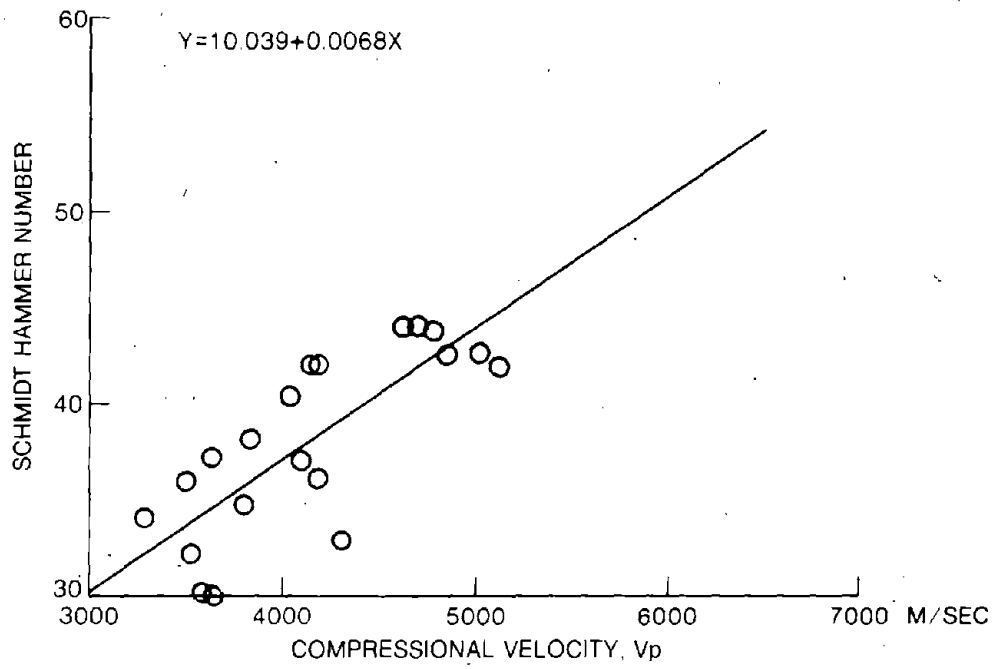


Figure 36. Plot of compression velocity and Schmidt rebound number.

Table 18. Selected Test Data for All Samples

Sample	Compressional Velocity, V_p		Shear Velocity, V_s	Unconfined Compressive Strength		Schmidt Rebound Number	Young's Modulus, E		Poisson's Ratio, ν
	m/s	m/s		MPa	MPa		static/dynamic	static/dynamic	
1-1	3299	1979	71.74	---	---	---	---	---	---
1-2B	3646	2018	55.71	29.7	---	---	---	---	---
1-3	3903	2330	45.30	---	---	---	---	---	---
1-4	3800	2306	---	---	---	---	---	---	---
1-5	4029	2152	75.22	37.0	---	---	---	---	---
1-6	4847	2487	91.70	42.5	---	---	---	---	---
1-7	4795	2527	90.03	---	---	---	53.64/42.49	0.17/0.31	---
2-1	3281	2113	108.63	34.0	---	---	32.75/26.03	.16/.15	---
2-2	3624	2262	106.52	37.2	---	---	39.37/30.75	.18/.18	---
2-3	3940	2162	110.11	---	---	---	39.37.30.55	.15/.28	---
2-4	3837	2354	95.28	38.2	---	---	37.09/33.77	.20/.20	---
2-5	4638	2998	130.59	44.0	---	---	64.33/52.19	.23/.14	---
2-6	5017	3154	127.62	42.5	---	---	64.33/59.36	.27/.17	---
2-7	4501	2334	124.08	---	---	---	56.81/36.50	.21/.32	---
3-1	4091	2195	99.89	37.0	---	---	37.09/31.81	.31/.30	---
3-2	3804	2267	---	34.7	---	---	---	.31/.30	---
3-3	3489	2107	98.59	36.0	---	---	---	---	---
3-4	3370	2094	---	---	---	---	---	---	---
3-5	3968	2308	---	---	---	---	---	---	---
3-6	4689	2923	114.04	44.0	---	---	---	---	---
3-7	4649	2411	---	---	---	---	---	---	---
3-8	4175	2308	---	42.0	---	---	---	---	---
3-9	4798	2449	124.08	43.8	---	---	66.60/40.33	.24/.32	---
4-1	3526	2174	87.98	32.0	---	---	---	---	---
4-2	3586	2092	51.85	30.1	---	---	---	---	---
4-3	4297	2290	98.46	37.1	---	---	---	---	---
4-4	3801	1846	61.85	---	---	---	---	---	---
4-5	4174	2237	---	36.1	---	---	---	---	---
4-6	4544	---	51.16	---	---	---	---	---	---
4-7	4125	2282	---	42.1	---	---	---	---	---
4-8	5124	2432	86.25	41.9	---	---	---	---	---

Table 19. Clustered Data Above and Below First Joint

Sample	V_p m/s	V_s m/s	Strength MPa	E GPa	Static GPa	E GPa	Dynamic GPa	ν Static	ν Dynamic	Schmidt No.	Depth m
Cluster 1 - above joint											
2-1	3281	2113	108.6	32.75	26.03	0.16	0.15	0.16	0.15	34.0	0.80
2-2	3624	2262	106.5	39.37	30.75	0.18	0.18	0.18	0.18	37.2	3.75
2-3	3940	2162	110.1	39.37	30.55	0.15	0.28	0.15	0.28	----	5.70
2-4*	3837	2354	95.3	37.09	33.77	0.20	0.20	0.20	0.20	38.2	6.30
3-1	4091	2195	99.9	37.09	31.81	0.31	0.30	0.31	0.30	37.0	1.00
mean	3755	2217	104.1	37.1	30.6	0.20	0.22	0.20	0.22	36.6	3.51
Cluster 2 - below joint											
1-7	4795	2527	90.0**	53.64	42.49	0.17	0.31	0.17	0.31	----	7.10
2-5	4638	2998	130.6	64.33	52.19	0.23	0.14	0.23	0.14	44.0	10.25
2-6	5017	3154	127.6	64.33	59.36	0.27	0.17	0.27	0.17	42.5	10.60
2-7	4501	2334	124.1	56.81	36.50	0.21	0.32	0.21	0.32	----	11.7
3-9	4778	2449	124.1	66.60	40.33	0.24	0.32	0.24	0.32	43.8	10.5
mean	4746	2692	126.6	61.1	46.2	0.22	0.25	0.22	0.25	43.4	10.03

* Immediately below joint

** Not used in calculating mean

those for cluster 2. The least difference is seen for values of Poisson's ratio as might be expected for the scattered data.

A comparison of the samples in each cluster with sample position relative to the first major joint on the graphic core logs was made. It shows that, with one exception, cluster 1 samples lie above the joint and those in cluster 2 lie below. Only sample 2-4 is an exception and it lies immediately below the discontinuity. The samples were originally taken so that they would be representative of both depth and closeness to joints or discontinuities with accompanying weathering. There is no apparent correlation of sample depth and parameter value nor is there any apparent correlation between position relative to a joint. Rather the specimens from the apparently intact rock mass above the first joint exhibit lower values for all measured parameters in comparison with those below. There also is indication that chemical alteration adjacent to the joints must be limited to a very narrow zone as the standard deviations of the clustered parameters are low indicating relative independence from weathering. An exception is sample 2-4 which lies immediately below the joint and also possibly within an altered zone associated with the thick, clay-filled joint. The lower parameter values are interpreted as resulting primarily from stress relief in the rock mass.

All samples lying above the first joint were examined for a comparison with the clustered sample data. The average values of the various selected parameters are given in table 20. The mean values for 14 samples are all similar to and lower than those for the five samples making cluster 1.

The mean values may be used to describe the mass physical properties of the rock mass through which the FM-CW energy has been transmitted. While there is variation, it appears to be random rather than systematic.

Table 20. Tabulation of Selected Data for Zone Above Joint for All Samples

Sample	V _p m/s	V _s m/s	Strength MPA	Schmidt no.
1-1	3299	1979	71.79	---
1-2B	3646	2018	55.71	29.7
1-3	3903	2330	45.30	---
1-4	3800	2306	---	---
2-1	3281	2113	108.6	34.0
2-2	3624	2262	106.5	37.3
2-3	3940	2162	110.1	---
3-1	4091	2195	99.9	37.0
3-2	3804	2267	---	34.7
3-3	3489	2107	98.59	36.0
3-4	3370	2094	---	---
4-1	3526	2174	87.98	32.0
4-2	3586	2092	51.85	30.1
4-3	4297	2290	98.46	37.1

mean	3690	2171	83.76	34.2